AN ABSTRACT OF THE DISSERTATION OF

Brian M. Wing for the degree of Doctor of Philosophy in Forest Engineering presented on June 8, 2012.
Title: Examination of Airborne Discrete-Return Lidar in Prediction and Identification of Unique Forest Attributes.

Abstract approved:

_____
Kevin D. Boston

Airborne discrete-return lidar is an active remote sensing technology capable of obtaining accurate, fine-resolution three-dimensional measurements over large areas. Discrete-return lidar data produce three-dimensional object characterizations in the form of point clouds defined by precise x, y and z coordinates. The data also provide intensity values for each point that help quantify the reflectance and surface properties of intersected objects. These data features have proven to be useful for the characterization of many important forest attributes, such as standing tree biomass, height, density, and canopy cover, with new applications for the data currently accelerating. This dissertation explores three new applications for airborne discrete-return lidar data.

The first application uses lidar-derived metrics to predict understory vegetation cover, which has been a difficult metric to predict using traditional explanatory variables. A new airborne lidar-derived metric, understory lidar cover

density, created by filtering understory lidar points using intensity values, increased the coefficient of variation (R^2) from non-lidar understory vegetation cover estimation models from 0.2-0.45 to 0.7-0.8. The method presented in this chapter provides the ability to accurately quantify understory vegetation cover (± 22%) at fine spatial resolutions over entire landscapes within the interior ponderosa pine forest type.

In the second application, a new method for quantifying and locating snags using airborne discrete-return lidar is presented. The importance of snags in forest ecosystems and the inherent difficulties associated with their quantification has been well documented. A new semi-automated method using both 2D and 3D local-area lidar point filters focused on individual point spatial location and intensity information is used to identify points associated with snags and eliminate points associated with live trees. The end result is a stem map of individual snags across the landscape with height estimates for each snag. The overall detection rate for snags DBH ≥ 38 cm was 70.6% (standard error: ± 2.7%), with low commission error rates. This information can be used to: analyze the spatial distribution of snags over entire landscapes, provide a better understanding of wildlife snag use dynamics, create accurate snag density estimates, and assess achievement and usefulness of snag stocking standard requirements.

In the third application, live above-ground biomass prediction models are created using three separate sets of lidar-derived metrics. Models are then compared using both model selection statistics and cross-validation. The three sets of lidar-derived metrics used in the study were: 1) a 'traditional' set created using the entire plot point cloud, 2) a 'live-tree' set created using a plot point cloud where points associated with dead trees were removed, and 3) a 'vegetation-intensity' set created using a plot point cloud containing points meeting predetermined intensity value criteria. The models using live-tree lidar-derived metrics produced the best results, reducing prediction variability by 4.3% over the traditional set in plots containing filtered dead tree points.

The methods developed and presented for all three applications displayed promise in prediction or identification of unique forest attributes, improving our ability to quantify and characterize understory vegetation cover, snags, and live above ground biomass. This information can be used to provide useful information for forest management decisions and improve our understanding of forest ecosystem dynamics. Intensity information was useful for filtering point clouds and identifying lidar points associated with unique forest attributes (e.g., understory components, live and dead trees). These intensity filtering methods provide an enhanced framework for analyzing airborne lidar data in forest ecosystem applications.

©Copyright by Brian M. Wing
June 8, 2012
All Rights Reserved

Examination of Airborne Discrete-Return Lidar in Prediction and Identification of Unique Forest Attributes

by
Brian M. Wing

A DISSERTATION

submitted to

Oregon State University

in partial fulfillment of
the requirements for the
degree of

Doctor of Philosophy

Presented June 8, 2012
Commencement June 2013

Doctor of Philosophy of Brian M. Wing presented on June 8, 2012.

APPROVED:

_____

Major Professor, representing Forest Engineering

_____

Head of the Department of Forest Engineering, Resources and Management

_____

Dean of the Graduate School

I understand that my dissertation will become part of the permanent collection of Oregon State University libraries. My signature below authorizes release of my dissertation to any reader upon request.

_____

Brian M. Wing, Author

ACKNOWLEDGEMENTS

This dissertation represents many hours of arduous but rewarding work. During the process I've grown both scholarly and emotionally. This growth would not have been possible without the help and support of many individuals. The completion of this dissertation represents their success as well as mine, so it is only proper to acknowledge these fine people.

I first want to offer my sincerest gratitude to my major professor Dr. Kevin Boston for all of his encouragement, guidance and support. Without his careful guidance, his constant support, and his unfailing confidence in me, this work would not have been possible. I also extend my greatest thanks to my doctoral committee composed of Drs. Alix Gitelman, Michael Olsen, Warren Cohen, and Martin Ritchie, who were always available when I needed their expertise. A special thanks to Martin Ritchie who spearheaded much of the research in this dissertation. Martin has been a tremendous mentor and friend that has helped me both professionally and personally. Without his support this dissertation would never have been possible. Thank you all for your help, guidance, patience, and encouragement.

I also would like to thank the field crew who collected data for this dissertation. The quality of any research project is heavily dependent upon the quality of the data collected. David McClung, Thomas Fisher, Travis Springer and a number of others helped ensure the field data for this project was of the highest quality of which I'm very grateful. They also made the data collection process enjoyable and I have many great memories from those summers.

Many thanks to my fellow Forestry graduate students including Donald Gagliasso, Bianca Eskelson, Jacob Strunk, Rebecca Hamner, Cody Hale and many other fellow Peavy basement-dwellers for their advice, support and friendship over the past few years.

I am most grateful for the love and support of my family and friends who have encouraged me in all my decisions and who have always been available for much needed support through this process. Special loving thanks to my wife Valerie who has been on the frontline with me during this process and shown tremendous patience and support in every way that I needed. She knows more than anyone what this process has required, and I love her tremendously for being my true partner.

Lastly, I want to thank my Lord and Savior Jesus Christ for granting me this opportunity and being my rock through this process. Psalms 23:4 & Proverbs 3: 4-6.

This research was supported by funding from a cooperative agreement with the US Forest Service, Pacific Southwest Research Station and Lassen National Forest. The views described here are those of the author alone and do not represent those of the US Forest Service.

CONTRIBUTION OF AUTHORS

Drs. Kevin Boston, Martin Ritchie, Warren Cohen, Mike Olsen, and Alix Gitelman provided extensive comments and professional expertise for chapters 1-5.

Dr. Martin Ritchie also provided help with field data collection.

TABLE OF CONTENTS

Page

CHAPTER 1: INTRODUCTION 1

CHAPTER 2: PREDICTION OF UNDERSTORY VEGETATION COVER WITH AIRBORNE LIDAR IN AN INTERIOR PONDEROSA PINE FOREST 7

Abstract 8

Introduction 9

Materials and Methods 15

Results 33

Discussion and Conclusions 36

CHAPTER 3: INDIVIDUAL SNAG DETECTION USING AIRBORNE LIDAR DATA AND 3D LOCAL-AREA POINT-BASED INTENSITY FILTRATION. 60

In review: Forest Science 60

Abstract 61

Introduction 62

Materials and Methods 70

Results 96

Discussion 105

Conclusions 117

CHAPTER 4: IMPROVING PLOT-BASED PREDICTION OF LIVE ABOVE GROUND BIOMASS USING POINT-FILTERED AIRBORNE LIDAR DATA. 135

Abstract 136

TABLE OF CONTENTS (Continued)

Page

Introduction 137

Materials and Methods 142

Results 153

Discussion 156

Conclusions 161

CHAPTER 5: CONCLUSIONS 171

BIBLIOGRAPHY 177

APPENDIX A 191

LIST OF FIGURES

Figure Page

Figure 2.1: Geographic location of the Blacks Mountain Experimental Forest and layout of the Blacks Mountain Long-Term Ecological Research Project in northeastern California. 46

Figure 2.2:. Standing live tree (DBH > 9 cm) attributes from all plots per treatment type (LoD, HiD, RNA) at BMEF. 47

Figure 2.3: Field sampling design for understory shrub cover. 48

Figure 2.4: ArcGIS understory vegetation cover layer created from field-measured shrub data. 49

Figure 2.5: Procedure for creation of the understory lidar cover density (ULCD) metric. sd = standard deviation, UP_F = number of understory points remaining after filtering, RGP = relative ground points. 50

Figure 2.6: Frequency histogram for average and maximum shrub heights and depiction of how understory layer height range is determined. n = number of shrubs sampled. 51

Figure 2.7: Depiction of possible understory components that airborne lidar pulses can intersect. Artwork derived from Dunning (1928). 52

Figure 2.8: Depiction of the ArcGIS layer created to derive the lidar effective plot coverage (EPC) metric using 0.3 x 0.3 m grid cells. 53

Figure 2.9: Percent canopy cover (determined by the proportion of first returns over 1.5 m in height) versus WR2 understory vegetation cover model prediction errors for the 40.5 m^2 circular plots (n = 154). 54

Figure 2.10: Understory point density versus WR2 understory vegetation cover model prediction errors for the 40.5 m^2 circular plots (n = 154). 55

Figure 2.11: Field-measured understory vegetation cover versus understory lidar cover density and the reference one to one ratio line. 56

LIST OF FIGURES (Continued)

Figure Page

Figure 2.12: Field-measured understory vegetation and coarse woody debris cover combined versus understory lidar cover density and the reference one to one ratio line. 57

Figure 3.1: Geographic location of the Blacks Mountain Experimental Forest and the Storrie Fire with study design depictions. 119

Figure 3.2: Visual depiction of snag condition stages used for the study. Derived from Thomas et al. (1979). Stage 8 and 9 snags were not sampled in the study. 120

Figure 3.3: Depiction of a individual plot lidar cloud and the stage one 3D local-area robust elimination filter. Lidar points are colored by intensity values. 121

Figure 3.4: Depiction of a fine-scale 2D local-area used in the second reinstitution filter and how SPR was calculated for each grid cell. 122

Figure 3.5: Overall detection rate summaries and trends for the various forest types at BMEF and SF under different DBH and height scenarios. >= DBH snag detection rates are defined as all snags with DBHs greater than or equal to the DBH listed (i.e., >= DBH 25 cm = detection rate for all trees with DBHs ≥ 25 cm). 123

Figure 3.6: Detection rate summaries and trends for the three treatment groups at BMEF under different DBH scenarios (LoD = low diversity; HiD = high diversity; RNA = research natural area). All summaries are for the height ≥ 3 m scenario. >= DBH snag detection rates are defined as all snags with DBHs greater than or equal to the DBH listed (i.e., >= DBH 25 cm = detection rate for all trees with DBHs ≥ 25 cm). 124

LIST OF FIGURES (Continued)

Figure Page

Figure 3.7: Overall detection rate summaries and trends for the two grouped fire severity strata at SF under different DBH and height scenarios. >= DBH snag detection rates are defined as all snags with DBHs greater than or equal to the DBH listed (i.e., >= DBH 25 cm = detection rate for all trees with DBHs ≥ 25 cm). 125

Figure 3.8: Canopy cover snag detection rate trends for different >= DBH scenarios combining data from both study locations (≥ 3 m height threshold). Data points represent the detection rates for the various canopy cover classes. Trend lines are based on the detection rate data points..... 126

Figure 3.9: Lidar point density snag detection rate trends for different >= DBH scenarios combining data from both study locations (≥ 3 m height threshold). Data points represent the detection rates for the various canopy cover classes. Trend lines are based on the detection rate data points..... 127

Figure 3.10:. Lidar derived snag heights versus field measured snag heights, categorized by snag condition. 128

Figure 4.1: Geographic location of the Blacks Mountain Experimental Forest and layout of the Blacks Mountain Long-Term Ecological Research Project in northeastern California..... 163

Figure 4.2: Live tree (DBH > 9 cm) oven dry weight above ground biomass summary from all plots per treatment type (LoD, HiD, RNA) at BMEF. 164

Figure 4.3: Lidar canopy volume (VolCov) versus field estimated live above ground biomass for the three different sets of lidar-derived metrics (Traditional, Live-Tree, and Vegetation-Intensity)..... 165

LIST OF TABLES

Table Page

Table 2.1: Final statistical model summaries. WR = Weighted Regression; BR = Beta regression; BIC = Bayesian Information Criterion. Regression parameters and BIC values have different interpretations for BR and WR. 58

Table 2.2: Leave-one-out cross-validation results for prediction of understory vegetation cover using individual models. RMSPE = Root mean square prediction error; AB = Absolute bias. 59

Table 3.1: Standing live tree (DBH ≥ 9 cm; Heights ≥ 3 m) attributes from all plots per strata at SF and treatment type (LoD, HiD, RNA) at BMEF (n_s = number of snags; n_p = number of plots; sd = standard deviation). 129

Table 3.2: Standing dead tree (DBH ≥ 9 cm; Heights ≥ 3 m) attributes from all plots per strata at SF and treatment type (LoD, HiD, RNA) at BMEF (n_s = number of snags; n_p = number of plots; sd = standard deviation). 130

Table 3.3: Snag species detection rates and summary for BMEF and SF (n = number of snags; sd = standard deviation). 131

Table 3.4: Snag detection rates for snag decay conditions for all snags combined (n = number of snags). Standard errors are given in parenthesis. Some snags were missing snag conditon information and were excluded from the table analysis. 132

Table 3.5: Categorized omission error summary combining both study locations. Standard errors are given in parenthesis. 133

Table 3.6: Summary of commission error rates for each forest type. Standard errors are given in parenthesis. 134

Table 4.1: Standing live and dead tree (DBH ≥ 9 cm; Heights ≥ 3 m) attributes from all plots per treatment type (LoD, HiD, RNA) at BMEF (n_s = number of snags; n_p = number of plots; sd = standard deviation). 166

LIST OF TABLES (Continued)

Table Page

Table 4.2: Parameter values used for the biomass equation (Jenkins et al., 2003). R^2 is the coefficient of variation model statistic calculated using the number of data points generated from the published equations for parameter estimation. 167

Table 4.3: Plot-level lidar-derived explanatory variables (metrics) used in regression analysis (h subscript stands for height). 168

Table 4.4: Final regression model parameters with fit and selection statistics for the two datasets (all plots and detected snag plots). Model T = traditional lidar point cloud metrics; Model LT = live-tree point cloud metrics; Model V = vegetation-intensity point cloud metrics; a = final model; b = single variable model; VIF = variance inflation factor. 169

Table 4.5: Live above ground biomass leave-one-out cross validation summary statistics for all models using both datasets (all plots (n = 154), and detected snag plots (n = 53)). Model T = traditional lidar point cloud metrics; Model LT = live-tree point cloud metrics; Model V = vegetation-intensity point cloud metrics; a = final model; b = single variable model; RMSE (%) = normalized root mean square for plot estimated biomass. 170

EXMANINATION OF AIRBORNE DISCRETE-RETURN LIDAR IN PREDICTION AND IDENTIFICATION OF UNIQUE FOREST ATTRIBUTES.

CHAPTER 1: INTRODUCTION

Airborne discrete-return lidar (Light Detection And Ranging) remote sensing is an established technology for obtaining accurate, fine-resolution three-dimensional data over large areas, and provides the ability to increase the accuracy and efficiency of large-scale forest inventories (Næsset, 2002; Maltamo et al., 2006). Since the technology's inception, its use for quantifying forest biophysical characteristics has increased rapidly. It has been used to successfully estimate and predict many important forest attributes, such as above ground biomass, tree height and density, and canopy cover, with new attributes being explored at an accelerated pace.

Airborne lidar is an active remote sensing technology employing an aircraft mounted laser capable of simultaneously mapping terrain and vegetation heights with sub-meter accuracy. Lidar data produce three-dimensional characterizations of objects in the form of point clouds that are defined by precise x, y and z coordinates. The data can also help characterize the reflectance and surface properties of intersected objects by providing intensity values, which are a measure of return-signal strength, for each point. These attributes are useful for forest inventory and characterization, because in theory, every object in a forest with a vertical dimension

can be detected if adequate lidar point densities are collected within all forest canopy layers (e.g., understory, overstory) (Pesonen et al., 2008).

Airborne lidar has been used successfully to estimate many standing tree characteristics such as biomass and volume (Heurich et al., 2004; Hyyppä et al., 2001; Næsset, 2002; Maltamo et al., 2006; Packalén & Maltamo, 2006), as well as canopy cover and height profiles (Coops et al., 2007, Goetz et al. 2007; Lim et al., 2003). It has also been incorporated into assessments of biodiversity (Clawges et al., 2008; Goodwin et al., 2007; Hill & Broughton,2009; Maltamo et al., 2005; Zimble et al., 2003), fire behavior models (Andersen et al., 2005; Mutlu et al., 2008; Riaňo et al., 2003), and wildlife habitat modeling (Goetz et al., 2007; Vierling et al., 2008). The majority of research exploring the ability of the technology to characterize forest attributes has focused on standing trees. Analysis methods can be separated into individual-tree and plot-based assessment (Reutebuch et al., 2005).

Individual-tree assessments attempt to identify and measure characteristics of individual trees using automated detection methods. Most methods to date have located individual trees by identifying local maxima in a lidar-derived canopy height model (CHM). A tree location typically corresponds with a peak in the CHM, and the corresponding crown area is delineated using some form of edge-detecting segmentation algorithm (Kaartinen & Hyyppä, 2008; Vauhkonen et al., 2011). Successful detection rates vary depending on CHM interpolation, crown delineation

methods, and forest type and conditions. The detection algorithms are generally inadequate in their ability to locate intermediate and suppressed trees, trees in tight clusters, and trees located in stands with dense canopies; which has limited the use of these assessments (Reitberger et al., 2009). Newer methods, attempting to overcome these limitations have recently been developed (Wang et al., 2008; Reitberger et al., 2009), but they still are unable to adequately identify individual trees located beneath the upper canopy layer. Nonetheless, the individual-tree approach still has appeal both statistically and for management implications, and will continue to see a concerted research effort.

Plot-based airborne lidar assessments have been more commonly used, because they have proven to accurately estimate and predict plot-level forest attributes in a diversity of forest types and conditions. These methods derive a myriad of plot-level point cloud metrics that quantify the height and density characteristics of individual plot point clouds. These metrics are then used as explanatory variables in a linear or nonlinear regression analysis to estimate plot-level field measured attributes, such as biomass, mean tree height, and tree density (Lim et al., 2003). Results have been promising in almost all cases using this method (Kim et al., 2009; Lefsky et al., 1999; Lim & Treitz, 2004; Næsset, 2002; Means et al., 2000; Nelson et al., 2004). After model validation, the regression models are applied

to the remainder of the lidar dataset to predict the attribute across the landscape using a simple two-stage procedure outlined in Næsset (2002).

More recently, the ability of discrete-return airborne lidar data to characterize understory components has received attention. Martinuzzi et al. (2009) studied the presence and absence of understory shrub cover (cover > 25%) on 20 m x 20 m pixels using airborne discrete-return lidar and found presence accuracies of 83% using two airborne lidar understory metrics along with a transformed slope aspect variable. Hill et al. (2009) examined the presence and absence of understory vegetation using two separate airborne discrete-return lidar datasets collected at the same location; one collected in leaf-on and one collected in leaf-off conditions. They found accuracies of 77% using a combination of both lidar datasets and 72% using only the leaf-off lidar on 20 m x 20 m plots. In another recent study, Morsdorf et al. (2010) used airborne discrete-return lidar height and intensity information to identify individual vegetation strata on 5 m x 5 m pixels in various forest conditions and had some success detecting the presence of the understory vegetation strata. Detection of coarse woody debris (CWD) with airborne lidar has also been studied with some promising results (Pesonen et al., 2008; Seielstad & Queen, 2003). These studies all point to the possibility of using airborne lidar to accurately predict understory components across the landscape.

Airborne discrete-return lidar provide information on the reflectance and surface properties of intersected objects in the form of intensity values. Intensity values are an often underexploited feature of lidar data, due to difficulty and variability associated with acquisition settings and calibration. Intensity is the ratio of the power returned to the power emitted by a laser pulse. It is primarily a measure of surface reflectance and is a function of the wavelength of the source energy, path distance, and the composition and orientation of the surface or object which the laser pulse intersects (Boyd & Hill, 2007). The usefulness of intensity data is dependent upon its quality, which is a function of various acquisition parameters. Laser beam divergence, type of source energy, path lengths and variable gain settings all affect the quality of the intensity information. These attributes have limited the use of intensity data, due to variability associated with intensity values from different acquisitions. As vendor calibration and acquisition techniques become more standardized and end user calibration becomes possible, the use of intensity information is likely to increase.

Despite these difficulties, intensity information has already been used successfully in many forestry applications to differentiate between tree species, estimate live and dead biomass, and predict basal area (Donoghue et al., 2007; Holmgren & Persson, 2004; Hudak et al., 2006; Kim et al., 2009; Lim et al., 2003; Morsdorf et al., 2010). Lim et al. (2003) used an intensity threshold to remove lower

NIR intensity returns when estimating live biomass of a northern hardwood forest in Ontario, Canada. In that study, the mean height of the higher intensity returns (> 200) was the best predictor of basal area, biomass and volume. More recently, Kim et al. (2009) used intensity value threshold filtering to successfully estimate live and dead standing tree biomass. All of these studies point toward the great potential of intensity information to help characterize many forest attributes.

The goal of this dissertation is to explore the use of airborne discrete-return lidar to both predict and identify important forest attributes. The use of intensity information to help characterize and identify individual forest attributes is explored in detail. The specific objectives are to: 1) create useful lidar-derived metrics for prediction of understory vegetation cover and examine prediction accuracy, 2) create a semi-automated method to detect individual snags across the landscape using an individual lidar point filtering algorithm based on local-area intensity information and assess its detection rate accuracy, and 3) create new plot-level lidar-derived canopy metrics and compare them with traditional lidar-derived canopy metrics in their ability to estimate and predict live above ground biomass. Objectives 1-3 of the dissertation are addressed in Chapters 2-4, respectively.

CHAPTER 2: PREDICTION OF UNDERSTORY VEGETATION COVER WITH AIRBORNE LIDAR IN AN INTERIOR PONDEROSA PINE FOREST

Brian M. Wing

Martin W. Ritchie

Kevin Boston

Warren B. Cohen

Alix Gitelman

Michael J. Olsen

In review: Remote Sensing of Environment

Abstract

Forest understory communities are important components in forest ecosystems providing wildlife habitat and influencing nutrient cycling, fuel loading, fire behavior and tree species composition over time. A widely utilized understory component metric is understory vegetation cover, often used as a measure of vegetation abundance. To date, understory vegetation cover estimation has proven to be inherently difficult using traditional explanatory variables such as: leaf area index, basal area, slope, and aspect. We introduce airborne lidar-derived metrics into the modeling framework for understory vegetation cover. A new airborne lidar metric, understory lidar cover density, created by filtering understory lidar points using intensity values; increased traditional explanatory power from non-lidar understory vegetation cover estimation models (non-lidar R^2-values: 0.2-0.45 vs. lidar R^2-values: 0.7-0.8). Beta regression analysis, a relatively new modeling technique, is compared with a traditional weighted linear regression modeling procedure. Model validation and comparison was performed using a leave-one-out cross validation procedure. Both models provided similar understory vegetation cover accuracies (± 22%) and biases (~ 0%) from a leave-one-out cross validation procedure using 40.5 m^2 circular plots (n = 154). The method provides the ability to predict understory vegetation cover over large areas at fine spatial resolutions for the interior

ponderosa pine forest type. Additional model enhancement and the extension of the method into other forest types warrant further investigation.

Introduction

Forest understory communities play many important roles in forest ecosystems (Suchar & Crookston, 2010). They provide habitat and forage for wildlife, are important factors in nutrient cycling and fire behavior, and help determine overstory species composition and structure over time (Falkowski et al., 2009; Legare et al., 2002; Scott & Reinhardt, 2001). Thus, understory communities are often considered good ecological indicators of forest health (Kerns & Ohmann, 2004; Tremblay & Larocque, 2001). To properly utilize understory components in the assessment of the above criteria, predictive models are needed for these characteristics (Suchar & Crookston, 2010). Unfortunately, most of the significant variables found to be useful for prediction of the above criteria have been limited in explanatory power and spatial extent (Eskelson et al., 2011; Kerns & Ohmann, 2004; Russell et al., 2007; Suchar & Crookston, 2010; Venier & Pearce, 2007).

Understory vegetation cover, often used as an abundance measure, is an important metric used for wildlife habitat and fuel load characterization, fire behavior modeling, and understanding forest competition dynamics (Chen et al., 2008a). It is often laborious and costly to measure, which has resulted in it being sampled in a variety of ways (Eskelson et al., 2011). Traditional sampling methods

include ocular estimation, line-intercept sampling, and fixed plot sampling (Bonham, 1989). All of these result in a percentage estimate for a unit area covered by understory vegetation.

Estimation and prediction of understory vegetation cover using field-derived explanatory variables has proven to be inherently difficult. To date, there have been two types of explanatory variables used in the estimation and prediction of understory vegetation cover; 1) topographically-derived (e.g., slope, aspect, digital terrain synthesis (DTS)), and 2) overstory-derived (basal area (BA), trees per hectare, leaf area index (LAI), canopy cover). The explanatory power associated with these models has been relatively poor (R^2 - values ranging from 0.2 to 0.45) and their spatial extents often limited to local study areas (e.g., Eskelson et al., 2011; Kerns & Ohmann, 2004; Russell et al., 2007; Suchar & Crookston, 2010; Venier & Pearce, 2007).

Traditional remote sensing techniques have shown potential for providing information on forest characteristics, such as wildlife habitat, over broad areas at lower costs than traditional field inventories (Cohen & Goward, 2004; Kerr & Orstrovsky, 2003; Schroeder et al., 2007). In terms of estimation or prediction of understory vegetation cover, traditional remote sensing methods have been used to derive useful explanatory variables in cover modeling. Unfortunately, these methods are not sufficiently sensitive to 3D vegetation structure, which restricts their ability in

the direct assessment of smaller areas or objects (Kerr & Orstrovsky, 2003; McDermid et al., 2005; Pesonen et al., 2008; Wulder & Franklin, 2003). They also have coarse spatial resolutions (> 20 m), which can often constrain their usefulness.

A very promising fine spatial resolution remote-sensing technology for increasing the accuracy and efficiency of large-scale forest inventories is airborne discrete-return lidar (Næsset, 2002; Maltamo et al., 2006). Airborne lidar can be used to directly measure the three-dimensional structure of terrestrial and aquatic ecosystems across large spatial extents (Lefsky et al., 2002a). Airborne lidar data produce three-dimensional characterizations of objects in the form of point clouds that are defined by precise x, y and z coordinates. They also help characterize the reflectance and surface properties of intersected objects by providing intensity values, which are a measure of return-signal strength, for each point. These attributes are useful for forest inventory and characterization, because in theory, every object in a forest with a vertical dimension can be detected if adequate lidar point densities are collected within all forest canopy layers (e.g., understory, overstory) (Pesonen et al., 2008).

In recent years, airborne lidar has been used successfully to estimate many standing tree characteristics such as biomass and volume (Heurich et al., 2004; Hyyppä et al., 2001; Næsset, 2002; Maltamo et al., 2006; Packalén & Maltamo, 2006), as well as canopy cover and height profiles (Coops et al., 2007, Goetz et al., 2007; Lim

et al., 2003). Airborne lidar has also been incorporated into assessments of biodiversity (Clawges et al., 2008; Goodwin et al., 2007; Hill & Broughton,2009; Maltamo et al., 2005; Zimble et al., 2003), fire behavior models (Andersen et al., 2005; Mutlu et al., 2008; Riaňo et al., 2003), and wildlife habitat models (Goetz et al., 2007; Vierling et al., 2008). Estimation and prediction of understory components such as vegetation cover with airborne lidar has received less study. Martinuzzi et al. (2009) studied the presence and absence of understory shrub cover (cover > 25%) on 20 m x 20 m pixels using airborne discrete-return lidar. They found presence accuracies of 83% using two airborne lidar understory metrics along with a transformed slope aspect variable. Hill et al. (2009) examined the presence and absence of understory vegetation using two separate airborne discrete-return lidar datasets collected at the same location; one collected in leaf-on and one collected in leaf-off conditions. They found accuracies of 77% using a combination of both lidar datasets and 72% using only the leaf-off lidar on 20 m x 20 m plots. In another recent study, Morsdorf et al. (2010) used airborne discrete-return lidar height and intensity information to identify individual vegetation strata on 5 m x 5 m pixels in various forest conditions and had some success detecting the presence of the understory vegetation strata. Detection of coarse woody debris (CWD) with airborne lidar has also been studied with some promising results (Pesonen et al., 2008; Seielstad & Queen, 2003).

Intensity is the ratio of the power returned to the power emitted by a laser pulse. Intensity values are an often underexploited feature of lidar data, due to difficulty and variability associated with acquisition settings and calibration. It is primarily a measure of surface reflectance and is a function of the wavelength of the source energy, path distance, and the composition and orientation of the surface or object which the laser pulse intersects (Boyd & Hill, 2007). Currently, airborne lidar sensors use variable gain controls to compensate for variations in ground brightness and surface object reflectance to help ensure the sensor is adequately detecting returns. They affect the quality and the usefulness of intensity values. Variable gain settings can either be manually or automatically adjusted throughout an acquisition (automatic more prevalent), which can result in intensity values that lack calibration or normalization into the same reference scale (often referred to as radiometric calibration). Gain settings are currently proprietary, thus they are unavailable to end users making radiometric calibration dependent on vendors (Boyd & Hill, 2007; Donoghue et al., 2007; Kaasalainen et al., 2007). At the time of this study, the majority of lidar vendors do not calibrate intensity values; thus they rely solely on variable gain and acquisition settings to provide useful intensity information. The quality of the intensity data is also dependent upon additional lidar acquisition parameters. Laser beam divergence, type of source energy, and path lengths all affect the quality of the intensity information and thus must be adjusted for different

acquisition scenarios to ensure useful intensity information is obtained. These attributes have resulted in a broad range of quality and limited the use of intensity data. As vendor calibration and acquisition techniques become more robust and end user calibration becomes possible, the use of intensity information will likely increase.

Even with these difficulties, intensity information has been used successfully in many forestry applications to differentiate between tree species, estimate biomass, and predict basal area (Donoghue et al., 2007; Holmgren & Persson, 2004; Hudak et al., 2006; Kim et al., 2009; Lim et al., 2003; Morsdorf et al., 2010). Lim et al. (2003) used an intensity threshold to remove lower NIR intensity returns when estimating live biomass of a northern hardwood forest in Ontario, Canada. In that study, the mean height of the higher intensity returns (> 200) was the best predictor of basal area, biomass and volume. More recently, Kim et al. (2009) used intensity value threshold filtering to successfully estimate live and dead standing tree biomass. All of these studies point toward the great potential of intensity information to help characterize many forest attributes. In this study, we explored the ability of intensity information to filter lidar points associated with various understory components.

This study seeks to expand on previous work and exploit the additional information available in airborne lidar data to predict understory vegetation cover. The primary objectives of this study are to: 1) analyze the potential of airborne lidar-

derived metrics to estimate and predict understory vegetation cover; 2) explore the use intensity values to filter understory component lidar points, 3) compare two modeling approaches for prediction of understory vegetation cover using the airborne lidar-derived metrics; and 4) develop a practical method that utilizes airborne lidar-derived metrics to predict understory vegetation cover. New understory airborne lidar metrics are introduced and explored.

Materials and Methods

Study Area

The study was conducted at Blacks Mountain Experimental Forest (BMEF) in northeastern California (Figure 2.1). The experimental forest (40°40´N, 10 121°10´W), managed by the USDA Forest Service Pacific Southwest Research Station, is located approximately 35 km northeast of Mount Lassen Volcanic National Park and ranges between 1700 and 2100 m elevation. Stands are dominated by ponderosa pine (*Pinus ponderosa* Dougl. ex P. & C. Laws) with some white fir (*Abies concolor* (Gord. & Glend.) Lindl.) and incense-cedar (*Calocedrus decurrens* (Torr.) Florin) at higher elevations. At lower elevations, Jeffrey pine (*Pinus jeffreyi* (Grev. & Balf.); Oliver, 2000) can also be found in some stands. Classified as an interior ponderosa pine forest type (Forest Cover Type 237) (Eyre, 1980), the 4,358 ha forest has a wide range of stand conditions as a result of past research and management activities, as well as disturbance events (Ritchie et al., 2007).

As part of a large-scale, long-term interdisciplinary experimental design at BMEF initiated in 1991, two contrasting stand structures were created: low structural diversity (LoD) and high structural diversity (HiD) (Oliver, 2000). LoD stands were thinned to maintain a single canopy layer of intermediate trees, with the goal of simplifying forest tree structure. At the time of treatment implementation (1996 - 1998), stands were thinned to a uniformly spaced density of approximately 40 trees ha^{-1}, maintaining trees with heights ranging from 12 to 30 m and crown ratios generally greater than 50%. At the time of our study, LoD stand densities ranged from 25 to 430 trees ha^{-1} based on plot-level data (DBH > 9 cm). In contrast, the HiD units retained all canopy layers, which resulted in stands that feature multiple age classes and varying crown structures (Oliver, 2000). All large old trees were maintained with one smaller tree retained within the larger tree's crown circumference. Tree densities ranged from 60 to 95 trees ha^{-1} at initial implementation and ranged from 90 to 1400 trees ha^{-1} at the time of our study based on plot-level data (DBH > 9 cm). Plots with higher tree densities are associated with a few spatially scattered dense thickets (0.4-0.8 ha) containing smaller trees that were left as part of the HiD prescription.

Six research units each were randomly assigned from both the LoD and HiD treatments ranging in size from 77 to 144 ha. Each unit was then split in half with one randomly assigned half receiving prescribed fire treatments (Figure 2.1). Due to the

large unit size, treatment implementation took several years. The three individual treatment blocks, each with four units, were created in 1996, 1997, and 1998, respectively.

Also included at BMEF, are four research natural areas (RNA) each approximately 40 ha in size (RA, RB, RC, RD). The RNAs were set aside to serve as unmanaged, qualitative controls representative of the interior ponderosa pine type. They have never received mechanical treatment, but fire exclusion has greatly increased their understory tree densities. Two of the four RNAs (RB & RC) received one application of prescribed fire in the late 1990's. RNA stand densities ranged from 420 to 1220 trees ha^{-1} for trees ≥ 9 cm DBH at the time of our study.

As part of the experimental design, all 16 research units at BMEF have permanently monumented grid markers located within them on a 100 x 100 m lattice pattern. The permanent grid markers serve as the center points for the plot level research being conducted on the forest. Each grid was located by conventional survey methods and placed within 15 cm of their predetermined UTM coordinates using the High Precision Geodetic Network along with survey grade GPS (Oliver, 2000). These provide a solid foundation to conduct airborne lidar research, because plot location errors are minimized.

Field Data

Field data were collected on five of the LoD units, six of the HiD units and 2 randomly selected RNAs in July of 2009 (RC & RD). Standing live tree (DBH ≥ 9 cm) stand attributes for all three structure types at the time of our study are summarized in Figure 2.2. Using the BMEF permanent grid system, plot locations were assigned systematically with a random start within each unit on every other grid point in all intercardinal directions (282 m spacing). At each selected grid point location two nested circular plots were established: 1) a 40.5 m^2 circular plot to measure understory vegetation, and 2) a 805 m^2 circular plot to measure standing trees and coarse woody debris (CWD). A total of 154 plots were measured (LoD = 65, HiD = 79, RNA = 10). Every shrub with a height greater than 0.3 m was measured for crown dimensions and stem mapped (Figure 2.3). These measurements included the azimuth and distance from the plot center to the center of the shrub, two perpendicular crown width measurements, and two height measurements (maximum height and average height). Maximum height was defined as the top height of the shrub, and average height was determined by ocular estimation measured with a tape measure. Shrub species found in our study included (listed in order of abundance): greenleaf manzanita (*Arctostaphylos patula* Green), antelope bitterbrush (*Purshia tridentate* (Pursh)), snowbrush (*Ceanothus veluntinus* Dougl. Ex Hook.), wax current (*Ribes cereum*), Pacific serviceberry (*Amelanchier alnifolia* Nutt.),

rabbitbrush (species) (*Chrysothamnus sp*.), common snowberry (*Symphoricarpos albus (*L.) S.F. BLake), and Sierra gooseberry (*Ribes rozelii* Regel). Greenleaf Manzanita and snowbrush exhibit denser foliage with larger leaf areas, more branching complexity, and tend to grow taller and wider than the other shrub species.

A geographically registered shrub cover layer was then constructed using shrub locations coupled with crown dimensions (Figure 2.4). For each shrub, the arithmetic mean of the two perpendicular crown widths was used as the average shrub diameter. Next, a circle was assumed for the general two-dimensional shrub shape and each shrub's circular area was incorporated into the layer. Lastly, the circular shrub areas were merged to create one shrub cover layer for each plot. This technique accounts for overlapping shrub crowns, edge effects, and should result in a more accurate estimation of shrub cover when compared to many traditional sampling methods.

Seedlings over 0.3 m in height and all saplings were tallied for each plot. Saplings were tallied into two diameter at breast height (DBH) classes (2.54 & 5.08 cm). For seedling and sapling cover estimates, predetermined cover values were used (seedlings = 0.15 m^2; saplings (2.54 cm class) = 0.5 m^2; saplings (5.08 cm class) = 1 m^2). These cover values were based on average values from a subsample of seedling and sapling crown dimensions. Saplings greater than 6.35 cm in DBH were considered to have crowns above the understory layer based on field observations. Total

understory vegetation cover was determined by summing all three of the cover areas and dividing by the total plot area. This method does not account for overlapping seedling and sapling crowns which could slightly affect the accuracy of the plot measured understory vegetation cover values where multiple seedlings and saplings were present.

In addition to the understory vegetation measured, all coarse woody debris with at least one end height above 0.3 m and one end diameter greater than 0.3 m were measured at every understory vegetation plot location only using a larger plot size (809 m^2 circular). Azimuth and distance was measured to the middle of each end from plot center and each end's width and height were also measured for cover and volume estimation. The spatial characteristics of the data enable direct determination of the geographic spatial arrangement associated with each piece of CWD. These attributes provided the ability to determine the quantity, cover and volume of CWD located within the 40.5 m^2 circular understory vegetation plots. In addition, prominent stumps (height > 0.5 m) were located using azimuth and distance from plot center.

Standing live and dead trees ≥ 9 cm DBH were also measured on the 809 m^2 circular plots. All trees were stem mapped from plot center and measured for height, DBH, crown width, and height to live and dead crown. These data were used for verification of plot locations and to create overstory lidar metrics.

Lidar Data

Discrete multiple return airborne lidar data were provided by Watershed Sciences Inc. in LAS file format (version 1.1). The lidar data were acquired over the entire BMEF study area in late July 2009 using a Leica ALS50 Phase II laser system mounted on a fixed wing aircraft. The aircraft was flown at 900 m above ground level following topography. Data were acquired using an opposing flight line side-lap of 50% and a sensor scan angle 14-degrees from nadir to provide good penetration of laser shots through the canopy layers. On-ground laser beam diameter was approximately 25 cm (narrow beam divergence setting), which resulted in a low percentage of multiple returns (higher order than first returns: 9.2%) and a high percentage of first and single returns (first: 9.4%; single: 81.4%). The high ratio of first and single returns helped provide better quality intensity information, because calibration problems associated with laser pulse energy are reduced for these returns (for review: Morsdorf et al., 2010). An average of 6.9 points m^{-2} was obtained for the entire study area, with a standard deviation of 5.6 points m^{-2}. Ground survey data were collected to enable the geo-spatial correction of the aircraft positional coordinate data collected throughout the flight, and to allow for quality assurance checks on final LiDAR data products. Simultaneous with the airborne data collection mission, multiple static (1 Hz recording frequency) ground surveys were conducted over monuments with known coordinates to enable geo-spatial data correction.

Indexed by time, these GPS data were used to correct the continuous onboard measurements of aircraft position. To enable assessment of LiDAR data accuracy, ground truth points were collected using GPS based real-time kinematic (RTK) surveying.

The vendor post-processed lidar data utilized proprietary software (TerraScan) coupled with manual methods to identify ground points for development of the digital terrain model (DTM). Vertical DTM accuracy for BMEF was approximately 15 cm at a 95% confidence level. The vendor used an automatic variable gain setting during acquisition and did not calibrate the intensity values post-acquisition. In past acquisitions, where the vendor used similar acquisition methods, the intensity information was successfully used to differentiate between live and dead biomass (Kim et al., 2009).

Data Analysis

An important step in any airborne lidar data analysis for forestry applications is verification of geo-registered plot locations. Inaccurate plot locations can be one of largest sources of model error found in many types of airborne lidar analysis. Even though the permanent grid system at BMEF helps to minimize the need for this step, every plot location was manually inspected using the standing tree stem maps for each 809 m^2 circular plot. Every 809 m^2 circular plot point cloud was compared to the field-measured standing tree stem map to assess the validity of the plot location. All

plot locations were found to be highly accurate (0.2 m) based on the manual inspection.

Once plot locations were verified, the lidar point cloud heights were normalized using the DTM and points corresponding to the 40.5 m^2 circular plots were extracted from the normalized lidar dataset. These plot point clouds were used to derive all potential explanatory lidar metrics used in the understory vegetation cover modeling analysis.

Understory Lidar Metrics

Martinuzzi et al. (2009) found the use of two understory airborne lidar metrics along with a common slope-aspect transformation variable could accurately estimate the presence of shrub cover (accuracy: 83%). The two understory lidar metrics utilized in their study were the percentage of ground points and percentage of points between 1 and 2.5 m compared to all plot points. We introduce a new understory lidar metric that combines inherent information found in these two metrics.

The new metric, understory lidar cover density (ULCD), can be derived using a series of standardized steps that can be semi-automated (Figure 2.5). First, the height range for the understory layer is determined from the average and maximum shrub height data collected from field measurements. The minimum height for the understory layer was determined by rounding the field-measured minimum average

shrub height value downward to the nearest 0.1 m. The maximum height for the understory layer for each plot was determined by rounding the field-measured maximum shrub height upper 99th percentile value to the nearest 0.1 m. By using the 99th percentile value of the maximum height range the maximum height threshold for the understory layer was reduced by 0.4 m and was determined to better represent the overall shrub crown height distributions for the site. The maximum height for the understory layer also served as the cut-off level between understory and overstory points.

For this study, average shrub heights ranged from 0.25 to 1.45 m and maximum heights ranged from 0.5 to 1.85 m (Figure 2.6). This resulted in an understory layer that ranged from 0.2 to 1.5 m. There were a total of 8 shrubs (shrub sample size: n = 821) measured that had portions of their crowns above the maximum understory layer height threshold. All lidar points located within the understory layer were then extracted from the plot point cloud for further analysis. The average plot-level percentage of first and single returns in this layer was similar to that of the entire acquisition (first: 6.7%; single: 83.4%). Theoretically, points in this layer can intersect one of eight understory components for this forest type: shrubs, the base of standing tree boles, seedlings, saplings, CWD, taller herbaceous vegetation, low hanging tree branches, and stumps (Figure 2.7). Other intersected components were considered too rare to be significant in this study area.

We explored the use of intensity values to filter points associated with unwanted understory components (e.g., non-vegetation and herbaceous points) from the understory layer point cloud. It was hypothesized that the intensity values would differ for the various understory components, thus providing a technique to identify the points associated with understory vegetation. For each plot, all points below the understory threshold (< 1.5 m) were used to calculate understory intensity mean and standard deviation values. It was determined from manual inspection of understory lidar point clouds, that points associated with live vegetation typically contained intensity values within one standard deviation of the mean intensity value, and points associated with other understory components were often outside this range. Based on this observation, all points with intensity values beyond one standard deviation from the plot's mean intensity value were removed from the understory point cloud. The understory lidar cover density metric is then obtained using the formula:

(1)

where is the number of remaining understory points after applying the intensity filter, and is the number of relative ground points (points under 0.2 m).

Two additional understory lidar metrics derived from the understory point cloud (heights < 1.5 m) were understory point density (UPD) and effective plot

coverage (EPC). Understory point density was defined as the number of lidar points per square meter under 1.5 m, and ranged from 1.5 to 24.2 points m^{-2} with a mean of 5.4 points m^{-2} and a standard deviation of 3.1 points m^{-2}. Typically, point densities are used to assess the adequacy of plot point cloud coverage. High point densities for a plot are often associated with adequate point coverage over the entire plot. In an understory context, it is possible to obtain high point densities while areas within the plot have no representative points because of scanning attributes (e.g., scan angle and path distance) and overstory obstructions. In attempt to overcome this problem, the EPC metric was derived to measure the amount of the plot area that received adequate point coverage. This metric contains inherent information from overstory characteristics (e.g., canopy cover and structure, species composition, etc.) and acquisition methodologies (e.g., point densities, scan angles, pulse rate and pattern). Two assumptions must be made to derive the metric. First, how much area an individual point should represent, and second, what the significant minimum shrub cover area is (i.e., the minimum cover area associated with a shrub that would meet sampling requirements). A balance between these two assumptions must be determined. After initial exploration, it was assumed that an area of 0.09 m^2 was a good representative area in the determination of EPC, because it coincided with the smallest shrub crown area sampled. To derive the metric, plots were gridded into 0.3 x 0.3 m cells and each grid cell was evaluated to determine if it contained an

understory point. Grid cells containing at least one point were summed up to determine the effective area covered by understory lidar points (Figure 2.8). EPC was then determined by dividing the effective area covered by the total plot area. The effective plot coverage ranged from 0.12 to 0.88 with a mean of 0.38.

Overstory Lidar Metrics

Many previous understory vegetation cover studies found variables associated with the overstory (e.g., standing basal area, tree density, species composition) to be significant in the estimation of understory vegetation cover (Eskelson et al., 2011; Kerns & Ohmann, 2004; Suchar & Crookston, 2010; Venier & Pearce, 2007). From previous lidar studies, the following overstory metrics were derived from first, last and combined return overstory point clouds (heights > 1.5 m): 1) the quantiles corresponding to the 01, 10,…, 90 percentiles of the canopy heights ; 2) the maximum height values; 3) the mean height values; 4) the standard deviation and coefficient of variation of height values; 5) the proportion of points above the 01, 10,…, 90 quantiles to the total number of points; 6) the proportion of points located within six predetermined canopy height intervals (s1 = 1.5-5 m, s2 = 5-10 m, s3 = 10-20 m, s4 = 20-30 m, s5 = 30-40 m, s6 > 40 m), and 7) overstory canopy cover determined by the proportion of first returns over the 1.5 m understory height threshold (Falkowski et al., 2009; Hudak et al., 2008; Næsset, 2002).

Topographic and Stand Attribute Variables

Topographic variables are often used for estimation and prediction of understory cover (Eskelson et al., 2011; Martinuzzi et al., 2009). Five independent topographic variables and two stand attribute variables were used in the model selection procedure. Topographic variables were derived from the airborne-lidar-generated DTM for each plot: elevation, slope, aspect, and two commonly used slope aspect transformations [slope · cosine(aspect); slope · sin(aspect)] (Stage & Salas, 2007). Stand attribute variables included the research unit number and strata (LoD, HiD, RNA).

Estimation and Prediction Modeling

Although cover is frequently sampled in vegetation surveys, the theoretical and statistical basis underlying cover measures are not well understood (Chen et al., 2006). Understory vegetation cover data, including data used in this study, are characterized by two key distributional features that do not conform to the assumptions of standard statistical procedures (Damgaard, 2009). They are bounded between 0 and 1, and have heteroscedastic error variances. In ordinary least squares (OLS), parameter estimates are unbiased but are inefficient when heteroscadastic error variances are present; in addition the usual parameter estimate variance-covariance estimators are biased. There are a number of alternative adjustment methods to deal with the unequal error variance problem in the OLS linear regression

setting. The two most common adjustment methods are applying independent and dependent variable transformations and the use of weighted regression (WR) (Kmenta, 1986).

A theoretically correct way to model cover data is by using the properties of the beta distribution, a flexible and useful tool for modeling continuous random variables that assume values in the standard unit interval (0, 1), such as rates, percentages and proportions (Kieschnick & McCullough, 2003). Thus, it can be appropriate for modeling vegetation cover data because it adequately describes the frequency distribution of cover for various individual plant species or plant communities (Bonham, 1989; Chen et al., 2006; Damgaard, 2009; Pielou, 1997). While most of the work with the beta distribution has been completed for grasslands and crop fields (Chen et al., 2006, 2008a, 2008b), it has recently been applied in forestry applications. For example, Eskelson et al. (2011) used beta regression (BR) in the estimation of riparian understory vegetation cover and found that it performed better than the OLS model. Korhonen et al. (2007) also successfully estimated forest canopy cover with beta regression.

Based on the characteristics of the study's understory vegetation cover data (i.e., heteroscedastic error variance), weighted and beta regression models were specified for the estimation and prediction of understory vegetation cover using the airborne lidar-derived metrics. All three treatment strata (LoD, HiD, RNA) were

grouped together to test the models' robustness to varying forest structure and canopy densities.

Model Specification

Weighted least squares regression can be used when the unequal error variance assumption of the linear regression model is violated. The theory behind this method is based on the assumption that the weights are known exactly (Kmenta, 1986). This is rarely the case, so estimated weights must be used instead. For this study, the equally sized group iterative procedure described in Kmenta (1986) to stabilize and determine final model parameter estimates was followed (5 iterations). Five groups of size approximately 31 were used in the procedure. Fitting this model is equivalent to minimizing:

(2)

where are weights = for from the 5 weighted groups, is a vector of dependent variables, and is from the OLS linear model: .

Using a parameterization of the beta distribution, Ferrari & Cribari-Neto (2004) introduced a beta regression model similar to the approach for generalized linear models (McCullagh & Nelder, 1989), except that the distribution of the

response is not a member of the exponential family. In the extended generalized linear model approach, are independent random variables with each a parameterization of the beta probability density function with mean and variance . The beta regression model is specified:

(3)

where is a vector of explanatory variables, is a vector of unknown regression parameters, is a linear predictor, $g(\cdot)$ is a strictly increasing and twice differentiable link function that maps (0, 1) into the real line, and indicates the transpose of the vector. A variety of link functions $g(\cdot)$ are available, but the logit link is particularly useful, because is obtainable in closed form (Espinheira et al., 2008).

Model Selection

Weighted and beta multiple regression models were fit for estimation and prediction of understory vegetation cover. The models were fit to all strata grouped together into one dataset to test the robustness of the models to varying forest structures and canopy densities.

Selection of significant independent variables was completed via a two-stage procedure. First, a forward and backward stepwise model selection procedure was performed using OLS linear regression to reduce the field of explanatory variables to

twenty based on Bayesian information criterion (BIC) model performance. Twenty was used as the cut-off level to help ensure significant variables ($P < 0.05$) would not be eliminated in this step. In the second step, BR models were fit using different sets and combinations of the twenty explanatory variables to identify the most significant variables based on BIC model performance. Because understory shrub cover data included zero values, the following commonly used transformation was applied to the understory vegetation cover dependent variable (Smithson & Verkuilen, 2006):

(4)

where is field-measured estimate of understory vegetation cover and is the number of sample plots (= 154). Independent predictor variables with associated p-values greater than 0.05 were removed after this step. The final models were selected based on the lowest BIC value while assessing variable interactions. Variable interactions were assessed using a standard principal component analysis procedure (Weisberg, 1985). Two models were selected for further analysis with both WR and BR; one containing only the most significant variable based on lowest partial F-statistic value and one containing all significant variables.

Model Comparison

No independent data were available to assess the accuracy of the regression equations used for prediction. Therefore, leave-one-out cross-validation was used to

assess the prediction accuracy of the models. For each step in the validation procedure, one sample plot was removed from the dataset at a time and the selected models were fitted to the remaining plots ( ). Understory vegetation cover was then predicted for the removed plot. This procedure was repeated until predicted values were obtained for all plots. Two reliability figures were used to determine the accuracy of predictions. The absolute bias (AB), and root mean squared prediction error (RMSPE) were reported:

(5)

(6)

Results

The final selected model contained three variables: 1) 2) the standard deviation of overstory lidar first return point heights ( ); and 3) the density of overstory lidar first return points in the predetermined fifth height stratum ( ) (Table 2.1). The signs of the coefficients correspond to the responses between understory vegetation cover and the independent variables. Understory vegetation cover had a slightly negative relationship with and a positive relationship

with . While predictions from the two model types are directly comparable, the regression parameters and BIC values are not, due to different model fitting techniques.

explained the greatest amount of variability for understory vegetation cover followed by the standard deviation of overstory first return point heights ( ) and then the density of overstory first return points in the predetermined fifth height strata ( ). The WR model containing only ULCD had a BIC value of (-382.3), while inclusion of the two significant overstory estimators decreased the value to (-396.6). For the BR model the BIC value went from (-530.0) to (-543.3) with the inclusion of the two overstory estimator variables. BIC values for the two model families (WR and BR) can only be used to compare within model performance. According to Raferty (1995) and Kass and Raferty (1995), a difference in BIC values (ΔBIC) of ≤ 2 between models is “not worth more than a bare mention” and a ΔBIC > 10 implies very strong evidence that the models are different.

Prediction accuracy was similar for both the WR and the BR models. Overall, RMSPE was 0.003 larger for BR2 compared to WR2, which equates to an average understory vegetation cover prediction difference of approximately 0.3% (Table 2.2). Absolute bias was virtually zero for both models with the BR models displaying a slightly lower AB (BR2 0.001 vs. WR2 0.005). RMSPE increased slightly for the models containing only the ULCD variable. Both models performed well in the prediction of

understory vegetation cover with root mean square prediction errors ranging from 0.0640 to 0.0735, which translates to average understory vegetation cover prediction errors of approximately ± 7%. The overall prediction accuracy for understory vegetation cover was ± 22% for all model forms. AB was not significantly different from zero for any of the model forms. No trends were found between understory vegetation cover prediction errors and canopy cover for any of the models (Figure 2.9). A small trend, which should be viewed with caution, was found between understory vegetation cover prediction errors and understory point densities. The errors decreased with increasing understory point densities, although as point densities increased the sample size diminished (Figure 2.10).

Residuals for WR models were normally distributed and centered on zero with no obvious dependencies or patterns that might reveal improper model specification besides the unequal error variance issue in the linear model, which was dealt with by using the WR procedure. BR residuals displayed similar traits, except the residual errors displayed a more equal variance across all values. The BR residual distribution also displayed a slightly more pronounced negative tail. Larger residual errors from both the WR and BR models were most often associated with plots that contained CWD.

Discussion and Conclusions

Understory vegetation cover has been difficult to estimate and predict, especially over large spatial extents. The method presented in this paper greatly increases the ability to estimate and predict understory vegetation cover in interior ponderosa pine forests. Both the WR and BR models produced satisfactory errors for prediction of understory vegetation cover. Only a simple independent variable transformation was necessary for the beta regression modeling framework, which did not result in any prediction bias. Theoretically the BR model seems the most appropriate choice; however the WR model performed equally well. This is most likely due to the most significant variable (ULCD) being a proportion bounded between 0 and 1, which essentially measures the same metric (i.e., the proportion of an area covered by shrub crowns). In theory, there should be a one-to-one type of relationship between these two variables. To demonstrate this point a simple linear regression model is presented in Figure 2.11 between ULCD and field-measured understory vegetation cover.

The method was robust in terms of applicability to different forest structures in this forest type based on the model performance combining all three BMEF treatment strata (LoD, HiD, RNA). Understory vegetation cover prediction errors did not show any obvious relationships with canopy cover in this forest type (Figure 2.9). This fact seems somewhat counterintuitive, since areas with higher overstory canopy

densities typically occlude laser pulses from reaching the understory. Previous airborne lidar studies have identified this occlusion problem as a significant limiting factor in characterizing understory components (Hill & Broughton, 2009; Morsdorf et al., 2010). The problem was less evident in this forest type and likely resulted from a combination of unique characteristics associated with this study. First, the most significant variable, ULCD, is relative to the number of points that reach the understory. A proportion bounded by 0 and 1 itself, the ratio between the number of understory cover points to the total number of points below the understory maximum height threshold remains relatively stable under different overstory conditions. Even though laser pulses are less likely to intersect understory vegetation in denser canopy conditions, they are also less likely to reach the ground. The second key characteristic is that the likelihood of encountering understory vegetation decreases with increasing overstory cover for this forest type. Therefore, it is less important that a lower number of laser pulses are reaching the understory in these situations, because there is less probability of the area containing understory vegetation. The third key characteristic is associated with the relationship between the overstory and understory layers in this forest type. There tends to be a distinct height difference between overstory and understory layers in this forest type, which makes it easier to identify and analyze the understory vegetation cover layer separately.

Although as yet untested, we hypothesize that this method will not perform as well in forest types that contain an abundance of understory vegetation under dense overstory cover conditions, or where the understory and overstory layers intermix. Obtaining higher understory point densities would help to alleviate these problems, but this is difficult in areas with dense overstory conditions and would also increase acquisition costs. The use of small-footprint full-waveform airborne lidar (SFFW) might also provide more explanatory value in identifying and ultimately predicting understory characteristics, such as cover. SFFW provides more than just coordinate and intensity information, it also provides echo width information. Echo width information has proven to be useful for classifying ground and vegetation returns and warrants investigation (Ducic et al., 2006; Wagner et al., 2008). Costs associated with SFFW acquisition are relatively high, making its use prohibitive for most broad-scale forest inventory applications. These costs will likely decrease over the next decade. In forests with significant proportions of deciduous trees, lidar acquisition completed during overstory leaf-off conditions and understory leaf-on conditions, if and when available, should increase understory lidar point densities and provide better results. In areas with taller herbaceous vegetation, acquisition should be completed while the herbaceous cover has yet to reach the minimum height requirement for the understory layer.

While both models performed well, producing R^2 values that exceeded most other published reports, additional modeling strategies should be investigated for this type of data to help determine the best approach. Two potential models not investigated in this study are the zero-inflated beta regression model (Ospina & Ferrari, 2012), and the Copula model (Nelsen, 2006). The zero-inflated beta regression model is an extension of BR that incorporates the probability of observing a zero value into the model. Copulas are multivariate distribution functions whose one-dimensional margins are uniform on the interval (0, 1) (Nelsen, 2006). Eskelson et al. (2011) had promising results applying a multivariate Gaussian copula model to understory vegetation cover data which also accounted for spatial dependence. Both these models seem well suited for understory vegetation cover data since zero values are likely, but we leave this for future work.

The two overstory explanatory variables selected in the final model (,) indicate that there are significant interactions between overstory and understory vegetation. This trend coincides with previous understory vegetation studies (Eskelson et al., 2010; Martinuzzi et al., 2009). It is also interesting to note that Hopkinson et al. (2006) found the standard deviation of vertical point structure to be the most powerful predictor of canopy height for various forest structures, and concluded it should be used as a universal lidar canopy height metric. This study found the same metric ( ) to be the most significant overstory estimator

variable, thus supporting their hypothesis. The metric replaced a combination of canopy height distribution quantile metrics. When the metric was removed from the model and the model was refit with the remaining estimator variables, two lidar canopy height quantile metrics took its place; one representing the lower portion and one representing the upper portion of the crown profile. This demonstrates the usefulness of in areas containing variable forest structure and its ability to replace multiple lidar derived height metrics.

Plots containing CWD produced the largest residual errors. To demonstrate the effects of CWD, plot-level CWD cover was added to the plot-level understory vegetation cover dependent variable and the simple linear model (Figure 2.11) was refit (Figure 2.12). The explanatory power (R^2) increased from 0.74 to 0.81. This suggests that the filtering method was not successful in filtering out all points associated with CWD. To further solidify this point, the residual errors from the understory vegetation cover models were found to be the most significant estimators in a CWD presence and absence logistic regression estimation model (40.5 m^2 plot-level CWD volume > 1.5 m^3). Theoretically, the understory vegetation cover model residual errors should predominately be associated with the CWD lidar points, since other understory component points were successfully filtered based on visual inspection of the point cloud data. Residual errors coupled with two other significant independent variables, slope · sin(aspect) and the proportion of discarded intensity

filtered points, produced presence accuracies of approximately 70% for estimating cumulative CWD volumes greater than 1.5 m^3 on the 40.5 m^2 circular plots. While the intensity filter successfully removed a portion of the CWD points from the ULCD variable, the understory vegetation cover model residual errors displayed more explanatory power than the proportion of discarded intensity filtered points in the CWD model. This suggests that there were a higher proportion of unfiltered CWD points using the filtering method in this study. If improved lidar point filtering techniques can be created, it might become possible to predict CWD in addition to understory vegetation cover using a similar method to the one outlined in this paper. A linear object recognition filter (Vosselman et al., 2004) coupled with intensity filtering might be successfully utilized.

Even though the intensity filtering method used in the study did not successfully remove all non-vegetation understory component points, it was successful at removing a large portion of them (> 50%). The filter still might be improved in a number of ways. The first resides in the fact that the filtering method used all lidar points associated with each plot's understory and relative ground layers (points < 1.5 m height). The filter might perform better if only understory vegetation layer points are used. This would require a larger plot size or higher understory point densities to ensure enough understory component points are available for creation of the plot-level intensity filtering statistics (e.g., mean & standard deviation). The

use of only first and single understory returns could also provide a way of improving the filtering method, since intensity information associated with these returns has been shown to be of better quality, especially when no post-acquisition radiometric calibration is applied. This theory was tested using the data from this study and the results were neither improved nor diminished, which was likely due to the high percentage of first and single understory returns (90.1%). It was also found that the understory layer intensity data displayed both bi-modal and uni-modal distributions before filtering. A filtering method that treated them separately might provide another way of improving the intensity filter. It is also important to note that the lidar data in this study was acquired during understory leaf-on conditions, which likely made differentiating intensity values associated with understory vegetation and other understory components easier.

The use of intensity information to characterize forest attributes is dependent upon the quality of the intensity information. The intensity data in this study did not receive post-acquisition calibration, if it had, filtration results would likely improve. Even without calibration, it displayed great potential in distinguishing lidar points associated with the various understory components. Currently, airborne lidar vendors are just beginning to develop and apply post-acquisition intensity calibration techniques. As this continues to improve, intensity values will likely become a much more valuable feature of airborne lidar data.

The field sampling design and data analysis steps used to obtain field-measured understory vegetation cover are simple to implement, provide accurate estimates, and fit well into most traditional forest inventory sampling designs. The shrub stem map and crown dimensional measurements provided a good method to estimate shrub cover accurately by accounting for overlapping crowns and incorporated well with the traditional airborne lidar plot-based standing tree inventory sampling design. The method can be improved by stem mapping and dimensionally measuring seedlings and saplings. Then seedlings and saplings can be incorporated into the field based spatial understory shrub cover layer for more accurate field estimation of understory vegetation cover. Matching the actual shrub, seedling, and sapling crown shapes could also provide for more accurate estimation. Although a circle seems like an appropriate assumption for shrub, seedling, and sapling cover shapes, the two perpendicular crown width measurements could be used to better match the actual crown shape of individual shrubs spatially. This might result in more accurate understory vegetation cover estimates. Plot size, sampling efficiency and costs associated with this sampling design should also be examined in further detail. Understanding the effects of increasing plot size on model variability would help to determine the most efficient sampling design. The use of terrestrial lidar scanning could also provide a good method in the future for obtaining accurate understory vegetation cover field measurements.

Application of the prediction model to entire forested stands can be completed following the traditional airborne lidar two-stage plot-based gridding procedure outlined in Næsset (2002). In this procedure, stands of interest are first divided into grid cells that match the prediction model's plot size. Then significant independent variable values are obtained for each grid cell and the prediction model is applied using weights for each grid cell to minimize edge bias associated with the smaller boundary-edge grid cells. The end result can be used to: 1) identify areas that meet understory vegetation cover habitat criteria and create habitat maps over entire forest stands, 2) determine understory fuel loadings over entire stands, which can then be used to refine fire behavior models, 3) accurately estimate and predict understory vegetation biomass and carbon stocks, 4) help assess forest health and biodiversity, and 5) assess competition dynamics between understory vegetation and standing trees.

The characteristics of this study's sampling design, airborne lidar acquisition and intensity value calibration provided a unique opportunity to examine the capability of airborne lidar to predict understory vegetation cover. The method presented in this paper was practical and efficient, and showed promise for predicting understory vegetation cover at fine spatial resolutions over large spatial extents in the interior ponderosa pine forest type. Incorporating airborne lidar with other remote sensing techniques such as aerial photography, or utilizing small-

footprint full-waveform airborne lidar could also enhance the ability to characterize and predict understory components such as vegetation cover. The new ULCD metric displayed a strong relationship with understory vegetation cover and was robust to various forest structures and densities in this forest type. The filtering of lidar points using intensity information helped to remove a portion of understory component points not associated with understory vegetation cover (i.e., CWD, stumps, live tree boles). The extension of the method to additional forest types warrants further investigation.

Acknowledgements

This study was funded through a cooperative agreement between Oregon State University and the U.S. Forest Service Pacific Southwest Research Station. The authors gratefully acknowledge the field work and additional help of Thomas Fisher, David McClung and Travis Springer.

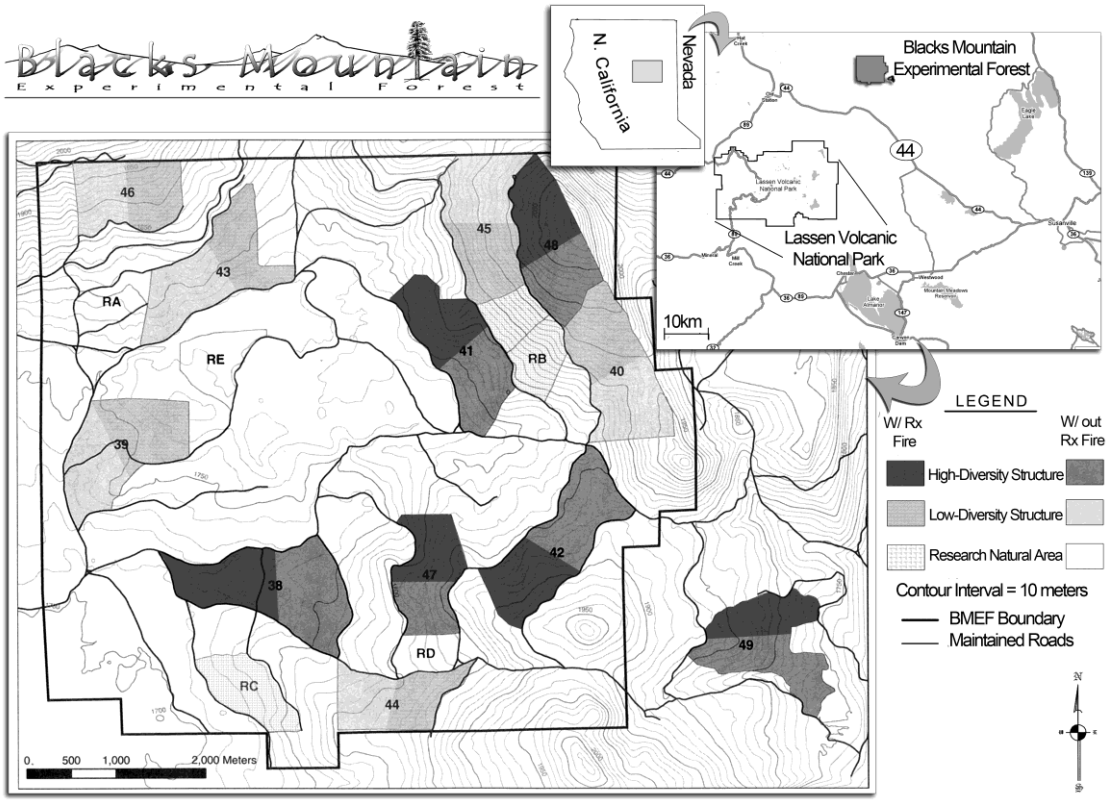

Figure 2.1: Geographic location of the Blacks Mountain Experimental Forest and layout of the Blacks Mountain Long-Term Ecological Research Project in northeastern California

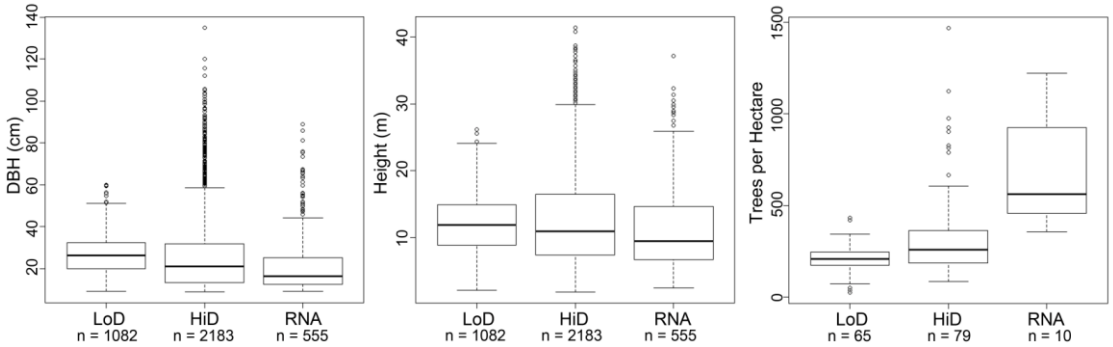

Figure 2.2:. Standing live tree (DBH > 9 cm) attributes from all plots per treatment type (LoD, HiD, RNA) at BMEF.

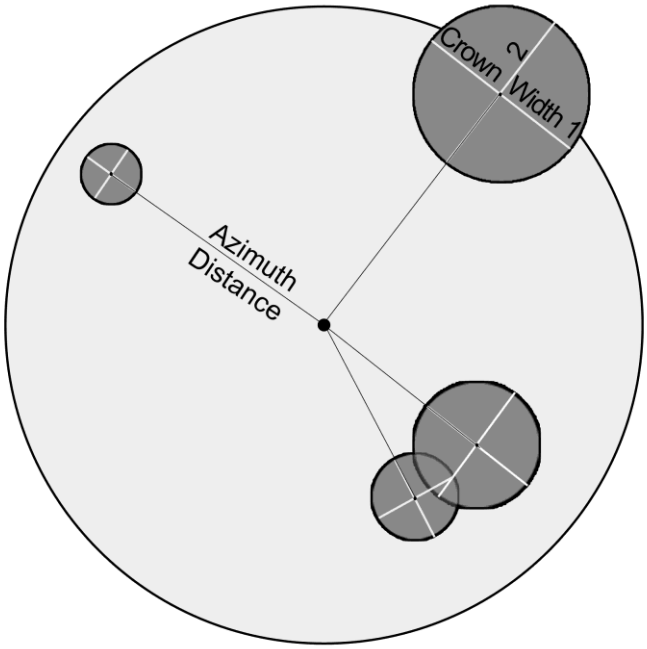

Figure 2.3: Field sampling design for understory shrub cover.

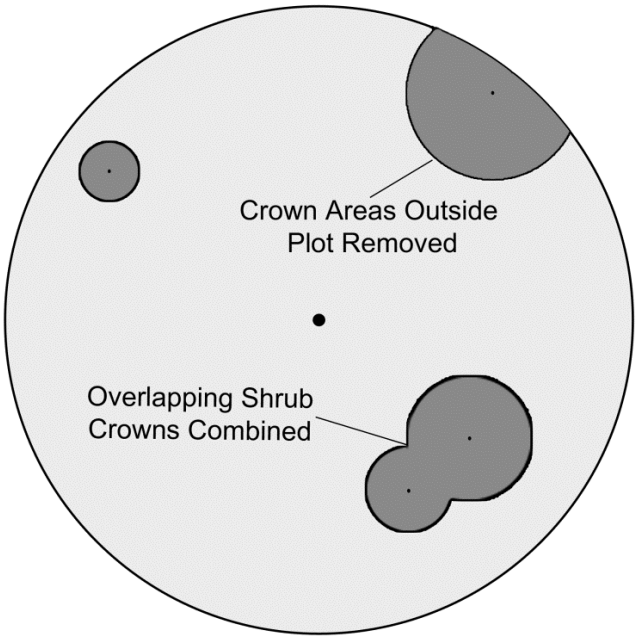

Figure 2.4: ArcGIS understory vegetation cover layer created from field-measured shrub data.

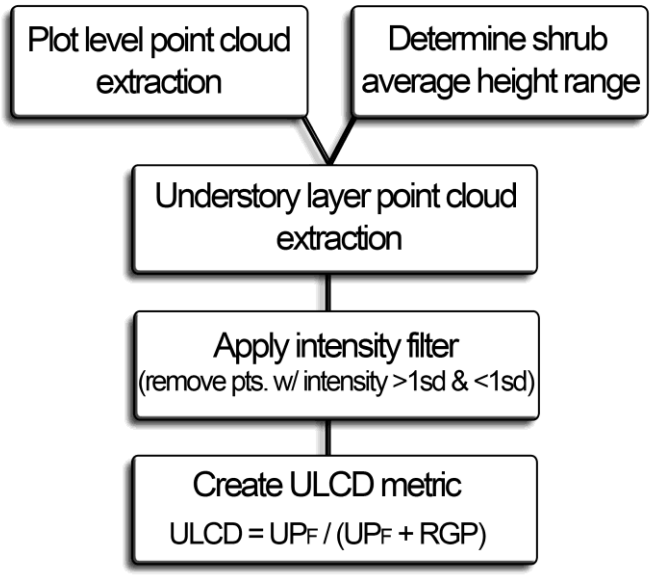

Figure 2.5: Procedure for creation of the understory lidar cover density (ULCD) metric. sd = standard deviation, UP_F = number of understory points remaining after filtering, RGP = relative ground points.

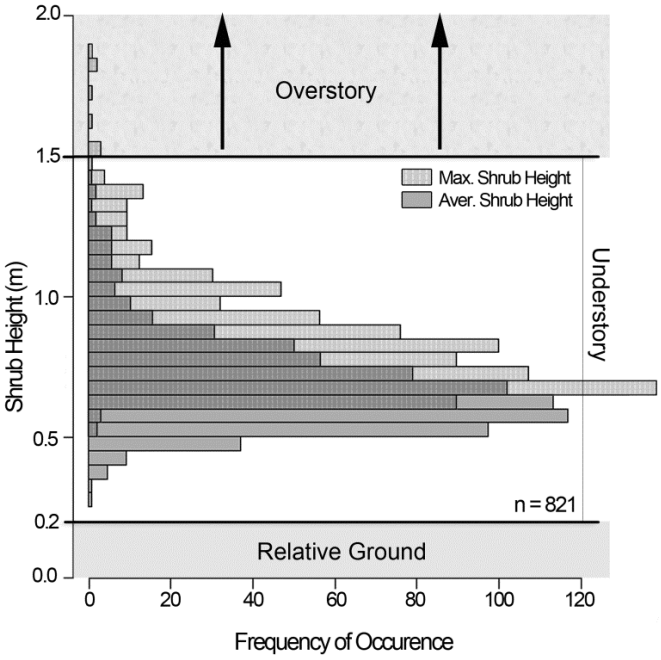

Figure 2.6: Frequency histogram for average and maximum shrub heights and depiction of how understory layer height range is determined. n = number of shrubs sampled.

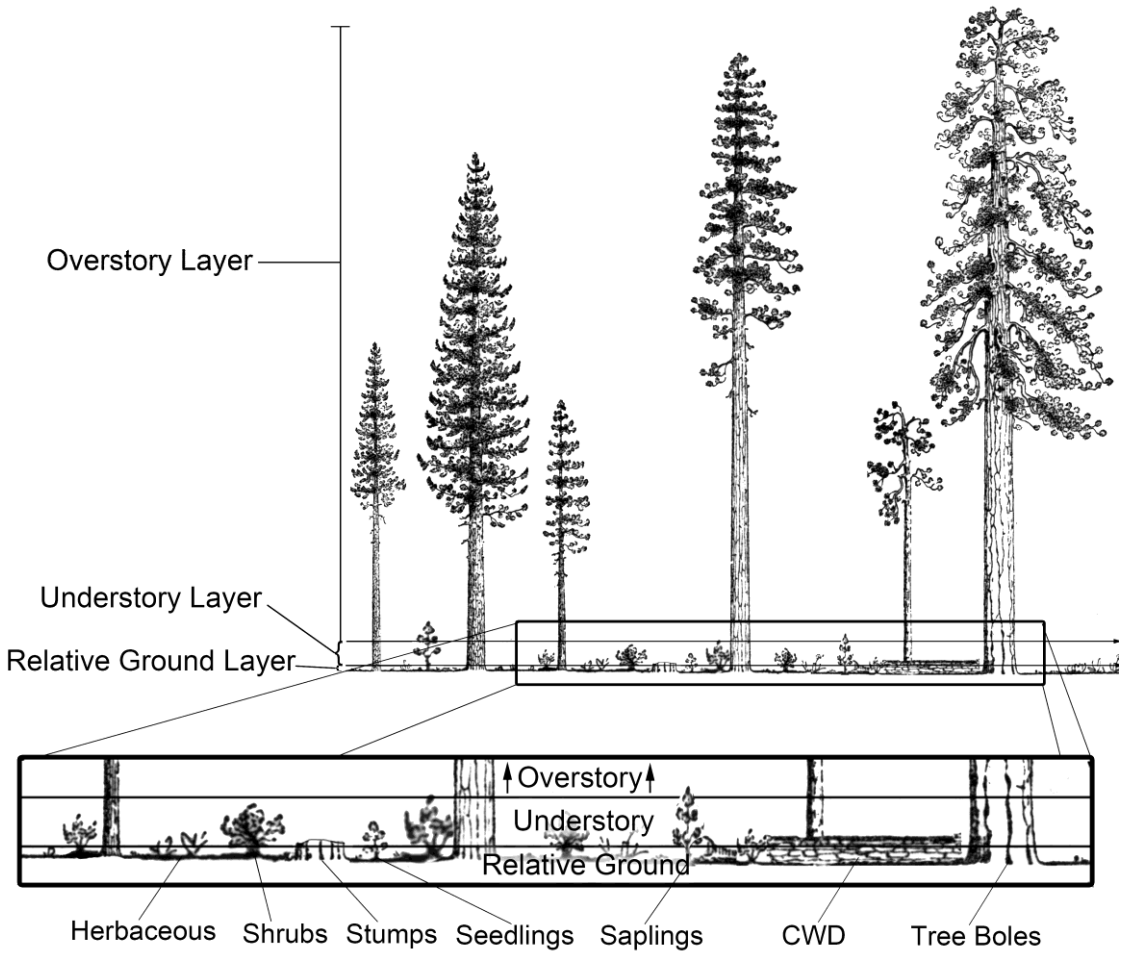

Figure 2.7: Depiction of possible understory components that airborne lidar pulses can intersect. Artwork derived from Dunning (1928).

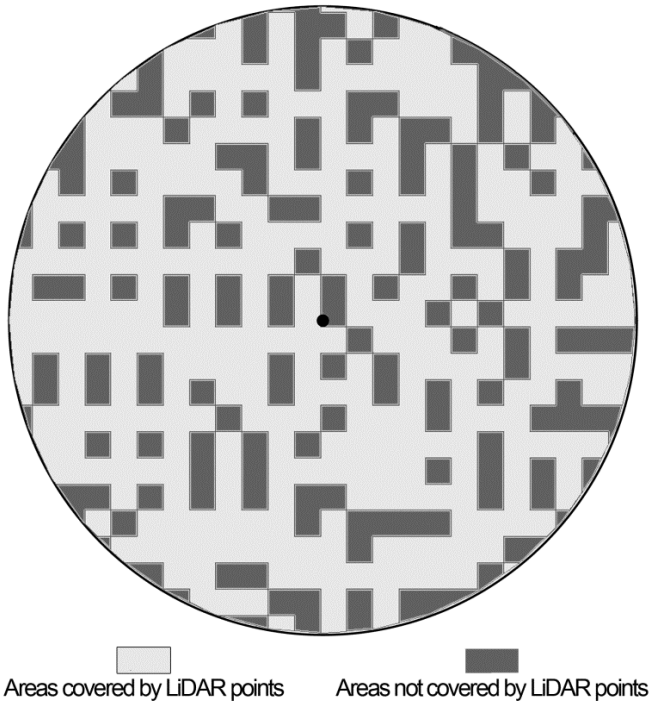

Figure 2.8: Depiction of the ArcGIS layer created to derive the lidar effective plot coverage (EPC) metric using 0.3 x 0.3 m grid cells.

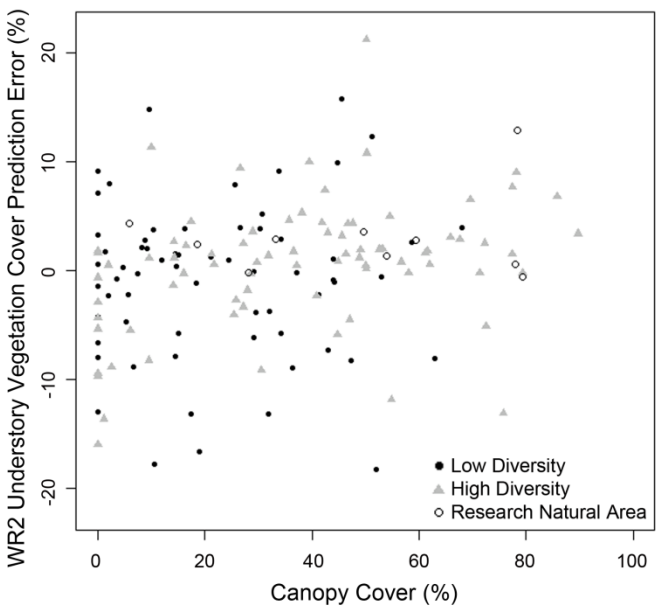

Figure 2.9: Percent canopy cover (determined by the proportion of first returns over 1.5 m in height) versus WR2 understory vegetation cover model prediction errors for the 40.5 m^2 circular plots (n = 154).

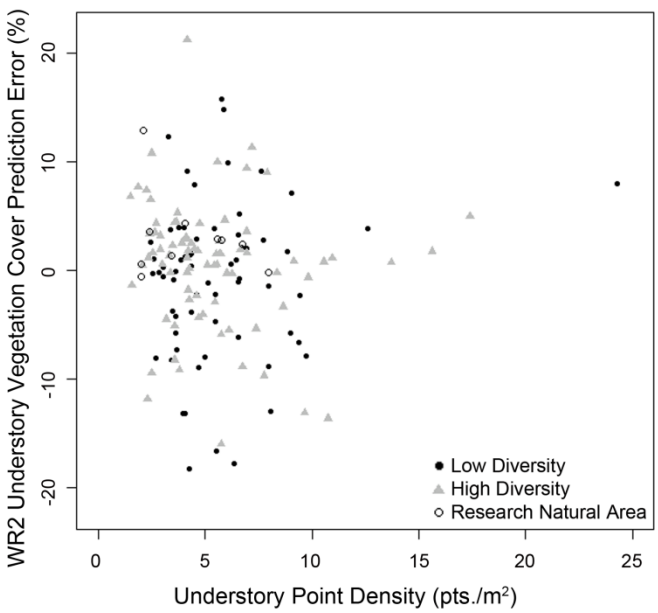

Figure 2.10: Understory point density versus WR2 understory vegetation cover model prediction errors for the 40.5 m^2 circular plots (n = 154).

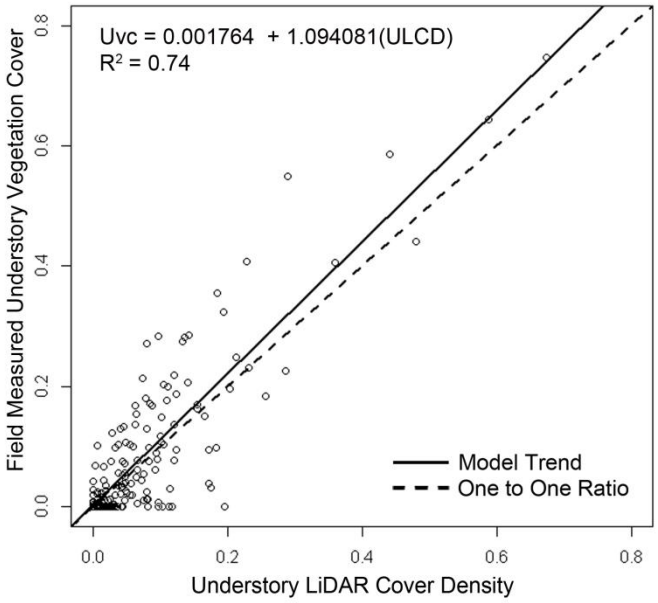

Figure 2.11: Field-measured understory vegetation cover versus understory lidar cover density and the reference one to one ratio line.

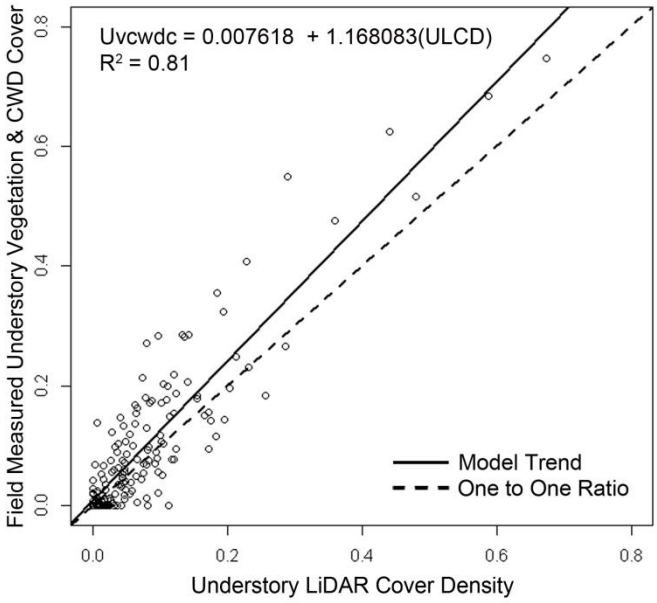

Figure 2.12: Field-measured understory vegetation and coarse woody debris cover combined versus understory lidar cover density and the reference one to one ratio line.

Table 2.1: Final statistical model summaries. WR = Weighted Regression; BR = Beta regression; BIC = Bayesian Information Criterion. Regression parameters and BIC values have different interpretations for BR and WR.

			Independent Variables			
Model	**Dependent Variable**	**Intercept**	$ULCD$	OH_{sdf}	OD_{s5f}	**BIC**
WR1	Understory Vegetation Cover	0.0048 (0.004)	1.0537 (0.066)			-466
WR2	Understory Vegetation Cover	0.0251 (0.006)	1.0260 (0.063)	-0.0064 (0.001)	0.1559 (0.031)	-488
BR1	Understory Vegetation Cover	-3.0847 (0.109)	7.2843 (0.562)			-530
BR2	Understory Vegetation Cover	-2.5740 (0.141)	6.4823 (0.537)	-0.1719 (0.033)	2.6719 (0.868)	-543

* Independent variable standard errors are given in parenthesis

Table 2.2: Leave-one-out cross-validation results for prediction of understory vegetation cover using individual models. RMSPE = Root mean square prediction error; AB = Absolute bias.

Model	RMSPE	AB
WR1	0.0678	0.0004 (*P* = *0.957*)
WR2	0.0640	0.0005 (*P* = *0.946*)
BR1	0.0735	0.0000 (*P* = *0.997*)
BR2	0.0671	-0.0001 (*P* = *0.988*)

* *P value* for *t* test; testing whether the bias is significantly different from 0.

CHAPTER 3: INDIVIDUAL SNAG DETECTION USING AIRBORNE LIDAR DATA AND 3D LOCAL-AREA POINT-BASED INTENSITY FILTRATION.

Brian M. Wing

Martin W. Ritchie

Kevin Boston

Warren B. Cohen

Michael J. Olsen

In review: Forest Science

Abstract

Standing dead trees (snags) play many essential roles in forested ecosystems at various scales. This has resulted in forest regulatory bodies and forest certification programs creating snag stocking standards to help ensure biodiversity is maintained or restored over time. The quantification and monitoring of snags across the landscape has been difficult due to their irregular and sparse distribution, often requiring intensive sampling methods to obtain statistically significant estimates. This study presents a new method for quantifying and locating snags using airborne discrete-return lidar. The semi-automated method uses both 2D and 3D local-area lidar point filters focused on spatial location and intensity information to identify individual lidar points associated with snags and eliminate points associated with live trees. The end result is a stem map of individual snags across the landscape with height estimates for each snag. The method was tested in four different forest types with similar results. Detection rates ranged from 35-100%, increasing as the size of snags increased. The overall detection rate for snags DBH ≥ 38 cm was 70.6% (± 2.7%), with low commission error rates in all forest types. The method provides the ability to quantify snags across the landscape. This information could be used to analyze the spatial distribution of snags over entire landscapes, provide a better understanding of wildlife snag use dynamics, assess achievement of stocking standard requirements, and create more accurate snag stocking standards.

Introduction

In recent years, recognition of the essential roles standing dead trees (snags) play in forest ecosystems has become more apparent at various scales. Snags provide critical nest, roost, and den habitat for a myriad of vertebrate wildlife species while also providing excellent foraging resources (Bate, 1995, Rose et al., 2001; Harmon, 2002; Laudenslayer, 2002; Mellen et al., 2006). Snags have been classified as key habitat components for many threatened and forest health indicator species (Harmon, 2002; Laudenslayer, 2002), and many fungal and invertebrate life cycles are dependent on snags (Boddy et al., 2008; Jonsson et al., 2005). Additionally, they are important for nutrient cycling and provide long-term carbon storage (Harmon, 2002). For all these reasons, snags are often considered to be key indicators of biodiversity and forest health.

As the recognition of the importance of snags has become more apparent, numerous certification programs and forest management regulatory bodies have developed minimum snag stocking requirements to help ensure biodiversity is maintained or restored (Pasher & King, 2009). These most often require a certain density or volume of snags to be maintained over time in order to provide continuous habitat support and ecosystem sustainability (Franklin et al., 1997; Holloway et al., 2007). These standards and regulations are often based on results from snag sampling studies, which estimate the size and quantity of snags from field

sampling methods. One limitation associated with these methods is that the distribution of snags across forest stands is highly variable, even within stands that are similar in many other respects (Fan et al., 2004). Due to this fact, field sampling and monitoring of snags has proven to be inherently difficult; requiring complex, intensive, and often expensive sampling procedures to produce statistically significant estimates (Rose et al., 2001).

Much work has gone into development of robust and efficient field sampling and monitoring methods for snag quantification (Krebs, 1989; Bull et al., 1990; Harmon & Sexton, 1996; Bate et al., 1999; Rose et al., 2001; Ducey et al., 2002; Kenning et al., 2005). Typically, snag data is collected using field sample plots, strips or transects with high intensities. The field work is not only cost- and time-consuming, but often difficult in remote areas with rough terrain and steep slopes (Bütler & Schlaepfer, 2004). The precision of estimates depends largely on the snag spatial patterns. Most standard sampling designs will not be efficient for rare events, such a snags (Yoccoz et al., 2001). Therefore, large sample and plot sizes are required to produce statistically significant snag quantifications (Lämas & Stahl, 1998; Gray, 2003). All of these attributes have led to the exploration of utilizing remote sensing technologies (e.g., aerial and satellite sensors) to better estimate snag quantities and distributions across the landscape (Croft et al., 1982; Bütler & Schlaepfer, 2004; Bater et al., 2009; Martinuzzi et al., 2009).

Using remote sensing techniques to estimate the quantity and distribution of snags can provide a more practical, cost-effective, and reliable method (Bater et al., 2009). However, to date there have been a relatively small number of studies testing the capabilities of remote sensing to quantify snags. While some have used Landsat (Frescino et al., 2001), most have utilized airborne multispectral imagery and have focused on stand-level disturbance events, such as insect outbreaks, disease or windfall (Guo et al., 2007; Hamilton et al., 2010; Kelly et al., 2004). Others have focused on the assessment of individual snags (Croft et al., 1982; Haara & Nevalainen, 2002; Bütler & Schlaepfer, 2004; Leckie et al., 2004; Pasher & King, 2009). Bütler & Schlaepfer (2004) achieved promising results by developing a four-step individual-snag detection method that coupled airborne CIR photos (1:10,000) with a geographic information system (GIS) and produced detection rates of 82% for unbroken snags ≥ 25 cm diameter at breast height (DBH). However this method had many noted limitations; 1) most smaller (DBH < 25 cm) or broken snags were not detected, 2) the method requires high-levels of technology, including special software, and 3) accuracy can be affected by factors such as aspect, surface slope, weather, and hour of flight. Most methods utilizing aerial photography also suffer from time and cost issues, and are prone to operator interpretation bias and subjectivity errors (Bater et al., 2009). As a result, there has been an increased interest in augmenting techniques to estimate and detect snags, which has led to

researching the use of new remote sensing technologies, such as airborne light detection and ranging (lidar).

Airborne lidar is an active remote sensing technology employing an aircraft mounted laser capable of simultaneously mapping terrain and vegetation heights with sub-meter accuracy. It has proven to be a very promising remote-sensing technology for increasing the accuracy and efficiency of large-scale forest inventories for a myriad of important forest inventory and wildlife habitat variables (Næsset, 2002; Maltamo et al., 2006; Martinuzzi et al., 2009). Airborne lidar can be used to directly measure the three-dimensional structure of terrestrial and aquatic ecosystems across large spatial extents (Lefsky et al., 2002a). Lidar data produce three-dimensional characterizations of objects in the form of point clouds that are defined by precise x, y and z coordinates. They also help characterize the reflectance and surface properties of intersected objects by providing intensity values, which are a measure of return-signal strength, for each point. These attributes are useful for forest inventory and characterization, because in theory, every object in a forest with a vertical dimension can be detected if adequate lidar point densities are collected within all vertical layers (e.g., understory & overstory, Pesonen et al., 2008).

The use of airborne discrete-return lidar in the quantification of snags has received increasing attention in the past few years. The methods for estimating snag attributes using airborne lidar can be separated into individual-tree and plot-based

assessment (Reutebuch et al., 2005). Plot-based assessments seek to estimate plot-level snag volume, biomass or abundance measures (Pesonen et al., 2008; Kim et al., 2009; Bater et al., 2009; Martinuzzi et al., 2009). Pesonen et al. (2008) achieved relatively poor results predicting snag volume using plot-based canopy derived lidar-metrics (RMSE 79%). Kim et al. (2009) achieved better results estimating snag biomass using similar plot-based metrics that had been stratified based on intensity values. Bater et al. (2009) found that the coefficient of variation of the lidar height data was a strong predictor of the proportion of snags in different levels of decay.

Individual-tree based snag assessment using airborne lidar data has received less attention. Individual-tree based assessments seek to extract and measure individual trees using segmentation methods. Most methods to date have found individual trees by identifying local maxima in a canopy height model (CHM). A CHM is an interpolated raster surface model with normalized height values and can be thought of as a piece of pliable material laid on top of tree canopies. Tree location typically corresponds with a peak in the CHM, and the corresponding crown area is delineated using some form of edge-detecting segmentation algorithm (i.e., watershed, slope-based, height-crown relationships) (for thorough review: Kaartinen & Hyyppä, 2008; Vauhkonen et al., 2011). Successful extraction rates vary depending on CHM interpolation, crown delineation methods, and forest type and structure. In addition, the methods are most often specialized to unique locales (Kaartinen &

Hyyppä, 2008). The major drawback with these methods is that they all rely on the CHM, which is reconstructed from the lidar data in an interpolation process which smoothes the data to different extents. This can virtually eliminate smaller neighboring trees as they become part of larger tree crowns during the CHM interpolation process. Thus, approaches that solely use the CHM have had restricted success rates, especially in heterogeneous forests where trees grow close together (Reitberger et al., 2009). Newer methods, attempting to overcome these limitations have recently been developed. Some have developed procedures to predict small occluded trees in the understory (Maltamo et al., 2004; Mehtätalo, 2006), while others have focused on three-dimensional (3D) assessment or reconstruction (Morsdorf et al., 2003; Wang et al., 2008; Reitberger et al., 2009). All of these studies have focused on extracting both live and dead trees, with most attention on the former. There have been no studies, to date, that have attempted to identify and extract individual snags using lidar-based individual-tree assessment methods.

Intensity values are an often underexploited feature of lidar data, due to difficulty and variability associated with acquisition settings and calibration (Wing et al., in review (a)). Intensity data are primarily a measure of surface reflectance and are a function of the wavelength of the source energy, path distance, and the composition and orientation of the surface or object which the laser pulse intersects (Boyd & Hill, 2007). The quality of the intensity data is dependent upon adjustable

lidar acquisition parameters. Laser beam divergence, type of source energy, path lengths and variable gain control settings all affect the quality of the intensity information. These attributes have limited the use of intensity data, due to variability associated with intensity values from different acquisitions. As vendor calibration and acquisition techniques become more standardized and end user calibration becomes possible, the use of intensity information is likely to increase.

Intensity has been used successfully in many forestry applications to differentiate between tree species, estimate live and dead biomass, and predict basal area (Donoghue et al., 2007; Holmgren & Persson, 2004; Hudak et al., 2006; Kim et al., 2009; Lim et al., 2003; Wing et al., in review (a)). Kim et al. (2009) used intensity value threshold stratification to successfully estimate live and dead standing tree biomass. They stratified plot point clouds based on intensity values and found metrics created with the lower intensity plot point cloud better estimated standing dead biomass. More recently, Wing et al. (in review (a)) successfully utilized intensity information to filter points in the understory not associated with understory vegetation (e.g.., stumps, coarse woody debris, tree boles). These studies point toward the great potential of intensity information in helping characterize many forest attributes.

Theoretically, lidar points associated with snags should have different reflectance and surface properties (intensity values) than live trees, since they

contain no photosynthetic material and typically lack needles and fine branches. If this is true it could be possible to identify lidar points associated with snags and remove lidar points associated with live trees using an intensity value based filtration algorithm. This study tests this theory by attempting to filter and remove lidar points associated with live trees using a series of individual point-based filters that focus on the spatial location of individual points and intensity attributes of local neighborhood points. After the algorithm is applied, a traditional CHM individual-tree extraction technique is used to extract individual snags and provide height estimates. With this two-step semi-automated method, it could be possible to stem map individual snags across the landscape while also providing accurate snag density estimates. This information could be used to analyze the spatial distribution of snags over entire landscapes, provide a better understanding of wildlife snag use dynamics, and assess and create more accurate snag stocking standards. The objectives of this study are to: 1) create an individual point-based local-area filtering algorithm that removes points associated with live trees, 2) apply an individual-snag detection method to the filtered point cloud and test the detection and error rates associated with the method, and 3) test the method in various forest types and structures to determine applicability in different forest conditions.

Materials and Methods

Study Area

The study was conducted at two sites; Blacks Mountain Experimental Forest (BMEF) and the Storrie Fire restoration area. Both are located in northeastern California (Figure 3.1). BMEF (40°40´N, 10 121°10´W), managed by the USDA Forest Service Pacific Southwest Research Station, is located approximately 35 km northeast of Mount Lassen Volcanic National Park and ranges between 1700 and 2100 m elevation. Stands are dominated by ponderosa pine (*Pinus ponderosa* Dougl. ex P. & C. Laws) with some white fir (*Abies concolor* (Gord. & Glend.) Lindl.) and incense-cedar (*Calocedrus decurrens* (Torr.) Florin) at higher elevations. At lower elevations, Jeffrey pine (*Pinus jeffreyi* Grev. & Balf.; Oliver, 2000) can also be found in some stands. Classified as an interior ponderosa pine forest type (Forest Cover Type 237) (Eyre 1980), the 4,358 ha forest has a wide range of stand conditions as a result of past research and management activities, as well as disturbance events (Ritchie et al., 2007).

As part of a large-scale, long-term interdisciplinary experimental design at BMEF initiated in 1991, two contrasting stand structures were created: low structural diversity (LoD) and high structural diversity (HiD) (Oliver, 2000). LoD stands were thinned to maintain a single canopy layer of intermediate trees, with the goal of simplifying forest tree structure. At the time of treatment implementation, stands

were thinned to a uniformly spaced density of approximately 40 trees ha^{-1}, maintaining trees with heights ranging between 12 to 30 m and crown ratios generally greater than 50%. At the time of study initiation, LoD stand densities ranged from 25 to 430 trees ha^{-1} based on plot-level data (DBH > 9 cm). In contrast, the HiD units retained all canopy layers, which resulted in stands that feature multiple age classes and varying crown structures (Oliver, 2000). All large old trees were maintained with one smaller tree retained within the larger tree's crown circumference. Interstices were thinned to approximately 250 stems ha^{-1}. Tree densities ranged from 60 to 95 trees ha^{-1} at initial implementation and ranged from 90 to 1400 trees ha^{-1} at the time of our study based on plot-level data (DBH > 9 cm). Plots with higher tree densities are associated with a few spatially scattered dense thickets (0.4-0.8 ha) containing smaller trees that were left as part of the HiD prescription.

Six research units each were randomly assigned from both the LoD and HiD treatments ranging in size from 77 to 144 ha. Each unit was then split in half with one randomly assigned half receiving prescribed fire treatments (Figure 3.1). Due to the large unit size, treatment implementation took several years. The three individual treatment blocks, each with four units, were created in 1996, 1997, and 1998, respectively.

Also included at BMEF, are four research natural areas (RNA) each approximately 40 ha in size (RA, RB, RC, RD). The RNAs were set aside to serve as unmanaged, qualitative controls representative of the interior ponderosa pine type. They have never received mechanical treatment, but fire exclusion has greatly increased their understory tree densities. Two of the four RNAs (RB & RC) received one application of prescribed fire in the late 1990's. RNA stand densities ranged from 420 to 1220 trees ha^{-1} for trees ≥ 9 cm DBH at the time of this study.

As part of the experimental design all 16 research units at BMEF have permanently monumented grid markers located within them on a 100 x 100 m lattice pattern. The permanent grid markers serve as the center points for the plot level research being conducted on the forest. Each grid was located by conventional survey methods and placed within 15 cm of their predetermined UTM coordinates using the High Precision Geodetic Network along with survey grade GPS (Oliver, 2000). These provide a solid foundation to conduct aerial lidar research, because plot location errors are minimized.

The Storrie Fire restoration area (SF), managed by the USDA Forest Service Lassen and Plumas National Forests (NF), is located approximately 45 km south of Mount Lassen Volcanic National Park and ranges between 900 and 2100 m elevation. The area was subject to a wildfire in late-August, 2000. The fire was characterized by high spatial complexity with varying levels of low- to high-severity burns on the

predominantly forested landscape, burning approximately 23000 ha (Crotteau, 2011). The fire burned within portions of the Plumas and Lassen NF; this study only focused on the Lassen NF portion, which encompassed 48% of the area (11260 ha). The Lassen NF portion is dominated by forests of white fir, California red fir (*Abies. magnifica* var. *magnifica* Andr. Murray), incense-cedar, Sierra lodgepole pine (*Pinus contorta* Louden var. *murrayana* (Grev. & Balf.) Critchf.), sugar pine (*Pinus lambertiana* Douglas), western white pine (*Pinus monticola* Douglas), ponderosa pine, Jeffrey pine, Douglas-fir (*Pseudotsuga menziesii* (Mirbel) Franco), and California black oak (*Quercus kelloggii* Newb.). The area had three dominant vegetation cover types; Red Fir, White Fir, and Sierra Nevada Mixed Conifer (Forest Cover Types 207, 211, and 243 respectively) (Eyre, 1980).

Variable fire severity created a mosaic of different forest conditions within each of the three forest vegetation cover types. To aid with the sampling design for this and other research projects, the area was stratified into twelve total classes: four levels of fire-severity (high (HS), medium (MS), low (LS), and unchanged (U)) across three levels of forest type (Figure 3.1). Fire severity was determined by using the Relative differenced Normalized Burn Ratio (RdNBR; see Miller et al., 2008) to approximate the Composite Burn Index (CBI) produced from the two Landsat Thematic Mapper post-Storrie Fire images yielding the four nominal categories.

The high-severity stratum can be generally characterized as having no surviving live-tree component and numerous snags at similar decay stages, which were most often broken. The medium-severity stratum has very few live trees and numerous snags at various stages of decay. The low-severity stratum has a higher proportion of live trees with some snags at various stages of decay. The unchanged stratum generally has almost no fire-induced mortality in the overstory. Any snags within the unchanged stratum were unlikely to have been killed by the Storrie Fire.

Field Data

At BMEF, five of the LoD units, six of the HiD units and 2 randomly selected RNAs (RC & RD) were sampled in July 2009. Standing live and dead tree (DBH ≥ 9 cm) stand attributes for all three structure types at the time of the study are summarized in Tables 3.1 and 3.2. Using the BMEF permanent grid system, plot locations were systematically located with a random start within each unit on every other grid point in all intercardinal directions (282 m spacing). At each selected grid point, an 805 m^2 circular plot was established to measure all standing trees ≥ 9 cm DBH. All trees were stem mapped from plot center and measured for height, DBH, crown width, and height to live and dead crown. The stem map data were used for verification of plot locations. Trees were also assigned codes for various tree conditions (i.e., broken, dead or forked top, sweep or lean, mistletoe presence, epicormic branching, etc.). Trees having DBH ≥ 60 cm were also assigned vigor condition class ratings using the

systems developed by Ferrell (1989) for fir and cedar species, and Salman and Bongberg (1942) for pine species. The classification systems resulted in individual tree vigor risk ratings ranging from 1 to 3 for the fir and cedar species and 1 to 4 for pine species, with higher risk ratings associated with declining tree vigor. All snags were given a decay condition class rating using the system developed by Thomas et al. (1979), with an addition of a broken top category for snag conditions 3-5 (Figure 3.2).

At SF, one or two plot clusters were randomly located within each stratum. Each plot cluster was comprised of three evenly spaced (50 m) circular plots (805 m^2). Plot clusters were located by first selecting a location within each stratum for the initial plot's establishment. Next, a randomly selected azimuth was used to determine the location of the two adjacent plots. All standing trees were measured using the same sampling protocol utilized at BMEF. Access to the SF area is limited and due to time constraints six strata only received one cluster. Plots were located and permanently established using high-grade GPS in the field. Due to GPS accuracy errors, all plot locations were manually corrected using the field measured stem map data and corresponding lidar point clouds. Standing live and dead tree (DBH > 9 cm) attributes for both study locations are summarized in Tables 3.1 and 3.2.

Lidar Data

Discrete multiple return airborne lidar data were provided by Watershed Sciences Inc. in LAS file format (version 1.1). The lidar data were acquired over both study areas in late July 2009 using a Leica ALS50 Phase II laser system mounted on a fixed wing aircraft. The aircraft was flown at 900 m above ground level following topography. Data were acquired using an opposing flight line side-lap of ≥ 50% and a sensor scan angle ± 14-degrees from nadir to provide good penetration of laser shots through the canopy layers. On-ground laser beam diameter was approximately 25 cm (narrow beam divergence setting), which resulted in a very low percentage of multiple returns (BMEF: 9.2%; SF: 10.1%) and a very high percentage of single returns (BMEF: 81.4% & SF: 78.2%). The high ratio of first and single returns helped provide better quality intensity information, because calibration problems associated with laser pulse energy are reduced for these returns (Morsdorf et al., 2010). At BMEF, an average of 6.9 points m^{-2} was obtained for the entire study area, with a standard deviation of 5.6 points m^{-2}. At SF, an average of 6.7 points m^{-2} was obtained for the entire study area, with a standard deviation of 5.9 points m^{-2}. Ground survey data were collected to enable the geo-spatial correction of the aircraft positional coordinate data collected throughout the flight, and to allow for quality assurance checks on final LiDAR data products. Simultaneous with the airborne data collection mission, multiple static (1 Hz recording frequency) ground surveys were conducted

over monuments with known coordinates to enable geo-spatial data correction. Indexed by time, these GPS data were used to correct the continuous onboard measurements of aircraft position. To enable assessment of LiDAR data accuracy, ground truth points were collected by the vendor using GPS based real-time kinematic (RTK) surveying.

The vendor post-processed lidar data using automated methods in proprietary software (TerraScan) coupled with manual methods to identify ground points for development of the digital terrain model (DTM). Vertical DTM accuracy for both study locations was approximately 15 cm at a 95% confidence level. The vendor used an automatic variable gain setting during acquisition and did not calibrate the intensity values post-acquisition. In past acquisitions, where the vendor used similar acquisition methods, the intensity information was successfully used to differentiate between live and dead biomass (Kim et al., 2009).

Point clouds corresponding to the 805 m^2 circular plots plus a 3 m circular buffer were extracted and their heights were normalized using the DTM. The 3 m circular buffer was added to each plot to eliminate edge effect problems associated with the CHM interpolation method. All points located above 1.5 m for BMEF plots and 2 m for SF plots were extracted for further analysis, because points located below these thresholds corresponded to the understory for those study areas.

Snag Filtering Algorithm

The snag filtering algorithm seeks to identify individual lidar points that are associated with snags and remove points associated with live trees. A series of point elimination and reinstitution filters focusing on local-area intensity information are implemented to accomplish the task. To properly use the intensity information for this purpose, the dynamics of intensity in relation to live trees and dead trees must first be understood. As previously discussed, the quality of intensity information is dependent upon acquisition and calibration methods. Morsdorf et al. (2010) highlighted that first and single returns provided more accurate intensity information due to difficulties associated with calibrating intensity values for multiple returns. Therefore, only first and single returns were used in this study. The lidar acquisition method used for both study areas resulted in first and single return intensity values ranging from 0 to 255 i (i will act as the intensity value index, since intensity values do not have a known numeric value). For the lidar datasets used in this study the following trends were found based on manual inspection of numerous lidar point clouds associated with live and dead trees in various conditions:

For dead trees:

1) Overall, individual point intensity values were typically low (0-75 i). These points seem to be associated with solid woody material (e.g., bare wood, bark, or charred wood).

2) Some snags contained a relatively small percentage of points (~10%) with very high intensity values (> 135 i). These points are thought to be associated with bare wood that has seasoned, thus creating a light-colored, somewhat reflective surface. This is primarily based on the fact that a majority of these high intensity values were associated with snags with higher levels of bark-off conditions.

3) A small percentage of snags (~20%) had a minute number of points (< 5%) with mid-range intensity values (75-135 i). The reason for these is uncertain, but they tended to be associated with snags that contained witches broom (usually formed from mistletoe), sparse dead needles or leaves, or recently dead trees still displaying fine branches. They might also be associated with lichen, although this was not sampled.

For live trees:

1) Individual point intensity values were typically a mix of low (0-75 i) and mid-range values (75-135 i). The low intensity values seemed to be associated with the tree bole and woody branches as they were most often located in the interior portion of individual tree point clouds. The mid-range intensity values were associated with live vegetation, or possibly dead needles and fine branches.

2) A very small number of points associated with live trees (< 3%) displayed high intensity values (>135 i). The reason for these is uncertain, but they tended to be associated with large old trees which typically exhibit less dense live vegetation and are more likely to contain dead limbs which have lost bark, although this was not sampled.

The lidar point filtering algorithm was developed with the intention of capitalizing on the aforementioned intensity characteristics. The algorithm iteratively applies several elimination and reinstitution filters to individual points. There are two basic stages in the algorithm; in the first stage, robust local-area 3D point elimination filters were applied to identify snag points that are easier to discern (i.e., points associated with snags in the open or large snags with multiple branches), and eliminate points associated with live trees. Points are eliminated by replacing their height information (h-value) with a zero value. By using this method, the point's two-dimensional information is retained. This information is used in the next reinstitution stage.

In the second stage, a series of local-area 2D and 3D reinstitution filters are applied to identify points associated with snags that were eliminated during the first elimination stage. These snags were more difficult to detect for a number of reasons but tended to: 1) be located directly adjacent to or near live trees, 2) have shorter heights resulting in lower point densities, and 3) have a small number (< 5%) of mid-

range intensity values (70-125 i) associated with them. If a point is determined to be a snag point during this stage, the point is reinstituted by reestablishing its original h-value.

The final product is a point cloud where points associated with snags are in their original positions and points associated with live trees all have zero elevation values. The algorithm is most efficient when the size of the area being examined at a time is relatively small (≤ ½ ha). Due to this trait, when applying the algorithm to larger areas, the area should be partitioned into smaller areas or tiles (gridding) and the algorithm applied to them individually. After the algorithm has been applied to the partitioned areas, they can easily be melded back together for further analysis. In the following, the algorithm's stages and their corresponding filters are explained in more detail following the order of utilization.

To run the algorithm, upper and lower threshold values for intensity must first be determined for each area being examined. These threshold values serve as the cut-offs between points likely representing a solid wood surface (e.g., branches, bole, etc.), and points likely representing live vegetation (e.g., needles, leaves). Intensity values above the upper or below the lower intensity threshold are most likely associated with solid wood, while intensity values between the lower and upper threshold values are likely to be from live vegetation. The threshold values are determined on the individual plot level to help account for local effects associated

with lidar acquisition. For each plot, the lower and upper thresholds were determined using simple multiplication factors:

(1)

(2)

Where, is the lower intensity threshold, is the upper intensity threshold, and is the maximum intensity value associated with individual plot point cloud being examined. The multiplication factors (0.35 & 0.65) were determined through visual inspection, and trial and error. Recalibration of these factors could be necessary for different lidar datasets; especially those collected using different sensors. Both lower and upper threshold values remained relatively stable at both sites. The lower thresholds ranged from 66 to 89 i with a mean of 74 i at BMEF, and from 64 to 89 i with a mean of 75 i at SF. Upper thresholds ranged from 123 to 165 i with a mean of 136 i at BMEF, and from 120 to 165 i with a mean of 139 i at SF.

Stage One – Live Tree Point Elimination

In the first stage, the primary focus is to eliminate all points associated with live trees using three 3D local-area filters. Points are eliminated by replacing their height values with zero, which retains the x and y information and removes them from the overstory. The filters are robust to ensure that all points associated with live

trees are eliminated. This trait resulted in some points associated with snags being eliminated, but the goal of the second reinstitution stage is to identify these points and restore them using the retained x and y information.

Elimination Filter 1: Robust 3D Local-Area

The first elimination filter loops through all points meeting the live vegetation intensity criteria (< i <), and eliminates all points located within close proximity (Figure 3.3). Close proximity was defined as a point located within ±1.5 m in both the x and y directions, and below 1.5 m above the height of the live vegetation point. The ±1.5 m x and y thresholds were developed to approximate half the average tree crown-width from field data. They were robust enough to ensure the majority of local-area points associated with live trees were eliminated, while also maintaining points associated with neighboring snags. The z-dimension 1.5 m 'above' threshold criteria was utilized to ensure that live tree points associated with smaller live trees growing under snag canopies did not eliminate snag points located above them. Once all the points in close proximity to the individual point being analyzed were eliminated, the point being analyzed was eliminated. Even with the robust local-area filter, it was sometimes possible for a small number of live tree points to remain. The second filter uses a 3D local-area point density threshold to eliminate the remaining points associated with live trees.

Elimination Filter 2: Point Density 3D Local-Area

The second filter individually looped through each point with an elevation above zero and evaluated their 3D local-areas to determine if there is an adequate density of local points. The 3D local-area was defined as ±1.5 m in all three directions (x, y, z), and adequate density was defined as ≥ 3 points. The premise is that the local 3.375 m^3 areas, which can be thought of as individual point-centered voxels, with point densities < 4 are associated with areas of live trees that were not eliminated during the first filter. If a point has a local point density < 4, then that point is eliminated. The individual point loop was repeated two iterations to help ensure that all points not meeting the point density requirement were eliminated.

Elimination Filter 3: Dead-Top 2D Local-Area

In the final elimination filter, individual points with elevations above zero were analyzed using a 2D (x, y) local-area filter to determine if they were associated with live trees containing dead tops. If there were ≥ 5 points with intensity values meeting live vegetation intensity criteria (< i <) located within ±1.5 m of the point, the point was eliminated. Since the first elimination filter only removed points located below 1.5 m above the live vegetation point's elevation value, it was possible for points associated with dead tops to remain. The filter criterion used for

this filter (≥ 5 live tree intensity value points) was intentionally designed to be highly discriminative, making it difficult for this filter to remove any points. If it was not highly discriminative, points associated with snags having live tree(s) growing underneath them would be eliminated as well, thus rendering the 1.5 m elevation threshold used in the first filter meaningless. Only live trees with dead tops containing an abundance of live vegetation underneath all areas of their dead top canopies had their corresponding points eliminated with this filter.

After the three live tree elimination filters were completed, the points with elevations above zero were classified as snag points and they could no longer be eliminated. In addition, all points with intensities meeting snag criteria located within ±0.5 m in the x and y directions of the classified snag points had their h-values restored and were also classified as snag points. The ±0.5 m local-area threshold restored local-area snag points while also helping to ensure live tree points were not improperly restored. These points were most often associated with isolated snags, or large snags with branches.

Stage Two – Snag Point Reinstitution

In the second reinstitution stage, the focus is on reinstituting snag points that were eliminated in the first stage. Local-area statistics were created for eliminated points meeting snag criteria (i ≤ or i ≥) and analyzed individually to determine if they were associated with snags and thus needed to be reinstituted. The

reinstitution filters must be very discriminative to ensure that points associated with live trees are not reinstituted. The stage uses two filters containing multiple steps to identify snag reinstitution points. The first filter uses coarse-scale local-area statistics, while the second uses fine-scale local-area statistics. Together these two filters reinstitute and evaluate reinstituted points to identify points associated with snags.

Reinstitution Filter 1: Coarse-Scale 2D & 3D Local-Area

The first filter in the reinstitution stage uses coarse-scale 2D local-area statistics and 3D local-area point counts to identify snag points that were eliminated in the first stage. Individual points with zero elevation values meeting snag criteria (i ≤ or i ≥) were analyzed by first calculating the snag point ratio (SPR) within ±2 m in the x and y directions using the following formula:

$$SPR \qquad (3)$$

where, is the number of points within the 2D local-area with snag criteria intensity values (i ≤ or i ≥), and is the number of points within the 2D local-area with live tree criteria intensity values (< i <). Points with the higher SPR values are more likely to be associated with snags. Points with SPR values ≥ 0.75 were sorted in descending SPR order. A SPR value ≥ 0.75 was determined to be an adequate cut-off threshold for SPR, as it reduced the number of candidates while also helped to ensure possible snag points would not be removed from

consideration. The five highest ranked points became possible reinstitution candidates. Five was used as a precaution to limit the number of reinstitution candidate points, while also providing the ability to capture more than one additional snag. The cut-off resulted in some snag points not being reinstituted with this filter; however, it was necessary to ensure live tree points were not reinstituted.

A precautionary step was applied next to help ensure the five highest ranked SPR points were associated with snags and not large old decadent trees. It was found on a number of occasions (5 for the entire study) that SPR candidate points were associated with large old decadent trees. These trees often exhibited low percentages of live crowns and high percentages of large branches, thus lidar points intersecting these trees often exhibited higher than normal ratios of snag criteria points compared to most live trees. Since these trees were always large, it resulted in an abnormally high number of points with high SPR values. This characteristic was used to remove them from consideration for reinstitution. If one of the five candidate SPR points had more than 40 points located within ±2 m in the x and y directions with SPR values ≥ 0.75, all of the points located within an area of ±5 m in the x and y directions had their SPR values set to zero. A value of 40 was used as the threshold, because it was determined to adequately differentiate between the large old decadent trees and snags. The area of ±5 m (100 m^2) was used to eliminate SPR values, because it helped to ensure all point SPR values associated with large old

decadent trees would be removed since these trees never exhibited tree crowns greater than 72 m^2 based on field samples. After the large decadent tree step was completed the SPR values were sorted again in descending order and the five highest ranked values with SPR values ≥ 0.75 had their h-values restored. In addition, all points with intensity values meeting the snag criteria located within ±1 m in the x and y directions of these points had their h-values restored to their original values.

In the last step, the restored points were assessed with a 3D local-area filter to determine if they were associated with areas where the edges of multiple live tree crowns came together. It was found that live tree crown edges often contained points with intensity values below the lower intensity threshold. They were typically not enough to cause snag detection errors, but when multiple live tree crowns were oriented in such a way where they slightly overlapped, it was possible for the filter to falsely identify them as snags. This occurred eight different times for the entire study, with no obvious link to any particular strata. The restored point cloud pattern associated with these occurrences was characterized by having one small tightly grouped area of points with similar heights, and no points located beneath them. This trait was used to remove the incorrectly restored points. Each restored point's 3D local-area was assessed by counting the number of points located within ±1 m in the x and y directions and under 75% of the point's height (h-value). If the number of

counted points was ≤ 2, the point was flagged for elimination; however points were not eliminated in this step until all points had been analyzed.

Restored points were considered to be associated with snags and permanently reinstituted. In addition, all points with intensity values meeting the snag criteria located within ±1 m in the x and y directions of these points had their h-values restored to their original values. While multiple snags can be reinstituted using this filter, no more than two snags were reinstituted for any plot. The majority of plots (~71%) did not contain any points with SPR values meeting the filter's threshold value of ≥ 0.75.

Reinstitution Filter 2: Fine-Scale 2D Local-Area

The second reinstitution filter utilized fine-scale 2D local-area statistics to identify points most likely associated with snags that were eliminated in the first stage. Individual points with zero elevation values meeting snag criteria (i ≤ or i ≥) were analyzed by first calculating the SPR within ±0.5 m in the x and y directions. If a point had a SPR value ≥ 0.67 and at least 3 points were located within the local-area, additional 2D local-area statistics were calculated for that point. The SPR value threshold of ≥ 0.67 was used because it adequately distinguished between live tree and candidate snag points for the fine-scale local-areas. The 3-point minimum was applied to increase the efficiency of the algorithm without hampering its ability to identify candidate snag points. Points meeting the criteria had local-

areas surrounding them gridded into 0.5 x 0.5 m cells in multiple layers (Figure 3.4). For each grid cell, a SPR value was calculated by counting the number of points meeting snag criteria and live tree criteria, and then applying the SPR formula. The number of grid cells not containing any points were also summed in each layer. These statistics were then used to identify individual points that were most likely associated with snags. Three scenarios using the fine-scale local-area statistics were identified that adequately recognized the most likely snag points.

In the first scenario, small snags located in relatively open areas were targeted. It was found that the previous filters often did not capture smaller or shorter snags, even in relatively open areas, since these snags did not have sufficient point densities. For an individual point to be classified as a snag point under this scenario, it was required to meet three fine-scale local-area criteria. First, it required an initial SPR value ≥ 0.667 for the local-area surrounding the point (± 0.5 m). Next, ≤ 2 grid cells in both layers one and two surrounding the point could contain points. If it met these three criteria, the point was permanently reinstituted as a snag point.

The second and third scenarios targeted snags located adjacent to live trees that were often more difficult to identify. Both these scenarios were applied in areas with canopy cover values ≤ 70% (determined by the proportion of lidar points above the understory height threshold compared to all points), because it was found that in

areas with canopy covers > 70%, the algorithm incorrectly reinstituted live tree points.

In the second scenario, individual points were required to meet three fine-scale local-area criteria to be reinstituted. First, the SPR value was required to be ≥ 0.8 for the local-area within ± 0.5 m of the point. Next, ≥ 9 grid cells in the first layer and ≥ 14 grid cells in the second layer were required to either contain no points or have SPR values ≥ 0.5. In the third scenario, individual points were required to meet four fine-scale local-area criteria to be reinstituted. First, the SPR value was required to be ≥ 0.9 for the local-area within ± 0.5 m of the point. Next, ≥ 9 first layer grid cells, ≥ 13 second layer grid cells, and ≥ 20 third layer grid cells were required to either contain no points or have SPR values ≥ 0.5. If a point met all criteria under either the second or third scenarios, it was permanently reinstituted as a snag point.

After the three fine-scale local-area filter scenarios were completed, all points located within ±1 m of the reinstituted points with intensity values meeting snag criteria had their original h-values restored. At BMEF, one last step was used to remove points associated with mountain mahogany (*Cercocarpus ledifolius* Nutt. (Rosaceae)), whose growth characteristics (e.g., high ratio of exposed wood) often caused them to be misclassified as snag points. It occurred rarely (3 plots) and never grew above 2.5 m in height; therefore all points ≤ 2.5 m were eliminated. After this last step, the filter was completed.

After the reinstitution stage was applied, the entire snag filtering algorithm was completed. The result is a point cloud where only the most likely snag points have h-values above zero, while points with zero h-values are most likely associated with live trees. This final snag filtered point cloud was used to create the individual CHMs for each plot. These CHMs were then used to detect individual snags and measure their corresponding heights.

Individual-Snag Detection

Individual-snag detection was completed using a traditional airborne lidar individual-tree detection method. In the method, a CHM is first created using the snag filtered point cloud, and then individual-snags are located and measured using an automated local maxima detection algorithm. The method typically has problems identifying smaller understory trees because the CHM often incorporates smaller neighboring trees into larger tree canopies during the CHM smoothing process. This problem should be greatly reduced for this study, since snag-filtered point clouds and the sparse spatial arrangement associated with snags simplify the CHM creation process and reduce tree crown adjacency issues. The method produced an individual-snag list file containing location coordinates, and heights for each detected snag. These location coordinates were then compared to field-measured snag location coordinates to determine if individual snags were correctly detected.

The first step of the individual-snag detection method was to create a CHM using the snag filtered point cloud. CHMs can have various forms depending on how the surface is interpolated and smoothed. When the primary use for a CHM is to detect individual-trees or snags, it is crucial the CHM accurately represents individual trees or snags by providing single height maxima while following crown profiles. In this study, the CHM was created using the 'CanopyModel' command line utility processing program in the Fusion lidar software package (McGaughey, 2012). CanopyModel creates an interpolated canopy surface model using the lidar point cloud. The default setting assigns the elevation of the highest return within each grid cell to the grid cell center. The program provides additional smoothing of the generated surface using median or mean filters (McGaughey, 2012). It is also capable of preserving local maxima in the surface while smoothing to force the surface to adhere to the tops of trees.

Ground lidar points (h-values ≤ 0.1) were reinstituted into the snag filtered point clouds to support CHM creation. These points helped by filling open gaps in the point cloud. Using trial and error the following parameters where determined to create a CHM that adequately characterized individual snags. A grid cell size of 0.8 x 0.8 m was used, because it was large enough to ensure multiple maxima were not created for individual snags, while adequately adhering to crown profiles based on visual inspection. A 3 x 3 median smoothing filter was applied to the raster surface

model to smooth the CHM and also reduce the likelihood of multiple local maxima. The local maxima were also maintained through the surface smoothing process to help force the surface to adhere to the tops of trees.

Individual snags were located and measured from the lidar-derived CHM by using the automated command line utility processing program 'CanopyMaxima' in the Fusion lidar software package (McGaughey, 2012). In the program, the location of individual snags is estimated by searching for local height maxima in the CHM. Seeds are placed in every grid cell with a h-value greater than the understory height threshold (BMEF: 1.5 m & SF: 2 m) and allowed to climb in the direction of the steepest slope. When a seed reaches a position where all neighboring grid cells have lower h-values, a local maximum is found (see: Popescu & Wynne, 2004). At each local maxima the original x and y location of the highest point within the grid cell is designated as the snag location, and the h-value as the snag height. The program outputs a tree (snag) list with location coordinates and height values in comma separated file format.

Snag Detection & Error Rates

Each plot's CHM was analyzed with CanopyMaxima to produce individual plot snag lists. These snag lists were then compared with field-measured snag location data to determine snag detection and error rates. To determine if a snag was accurately detected, acceptable location distance errors had to be assigned. Taking

into account the positional accuracy of the differential GPS unit for determining the location of the subplot centers at SF and the permanent grid system accuracy at BMEF, individual snag locations errors are expected to be within 1.5 m for the field-measured locations. This error only refers to the position of the base of the tree, without considering the deviation of the tree top relative to the base. The CHM is expected to have a horizontal accuracy of approximately 0.5 m, given the estimated horizontal accuracy of the laser acquisition. It is also more likely for taller snags to have tops not aligned with the base of the snag. Given these characteristics, the thresholds for acceptable location distance errors were set as 2.5 m for snags < 9 m in total height and 4 m for trees with total heights ≥ 9 m. If a lidar detected snag location was within the acceptable distance of a field measured snag, it was classified as detected. Only one field measured snag could be associated with each lidar detected snag location. Lidar detected snags not within the acceptable distance of any field measured snags were classified as commission errors (e.g., a live tree or a portion of a live tree that was incorrectly classified as a snag). If a field measured snag was not detected using the lidar method it was classified as an omission error.

Detection and error rates were calculated for both grouped and individual strata in various DBH and height classes to assess the method's accuracy and applicability in different forest types and conditions. Commission and omission errors were summarized categorically to help understand error causes. Lidar derived snag

heights were also compared to field measurements to determine if the method produced accurate height estimates.

Results

Overall Snag Detection Rates

The overall snag detection rate for both study locations combined was 52.6% (± 1.7%) (Standard errors are given in parenthesis). Figure 3.5 depicts the overall detection rate trends for the various forest types. Snag detection rates increased as DBH and snag height increased in all strata. The average overall detection rate for snags in the smaller DBH classes (9-50 cm) was 46.4% (± 1.9%), while in larger DBH classes (51-90 cm) was 72.5% (± 3.3%). Overall detection rates were also calculated for greater than or equal DBH scenarios (e.g., number of snags over a specified DBH). The detection rate for snags with DBHs ≥ 25 cm was 65.7% (± 2.0%) and steadily increased to 79.3% (± 7.5%) for DBHs ≥ 90 cm. The detection rates for the various DBH scenarios were also calculated with different height thresholds (≥ 3, 6, 9, 12 m). The overall detection rates for the various DBH scenarios increased by an average of 3.9% for every 3 m increase in the height threshold, with the largest increases occurring between 3 and 6 m (6.0%).

Study Area and Forest Type Snag Detection Rates

The area sampled at BMEF was much higher than at SF (BMEF 30.8 ha vs. 10.5 ha). The two study areas produced similar detection rates for larger diameter snags, however smaller diameter snags were not detected as well at BMEF. Since the majority of snags at BMEF were small diameter snags the overall detection rates differed considerably between the two study locations (BMEF: 34.5% (±2.5%) vs. SF: 63.1% (±2.2%). The average detection rates for smaller and larger DBH classes were 30.8% (±2.5%) and 64.8% (±7.5%) respectively at BMEF versus 59.6% (±2.6%) and 70.7% (±7.0%) at SF (Figure 3.5). The detection rates at the two studies remained similar after DBHs reached the ≥ 51 cm threshold. At BMEF, the detection rate increased an average of 4.1% for every 3 m height threshold increase, while at SF it increased an average of 3.6% for every 3 m increase.

For BMEF and the interior ponderosa pine forest type, the majority of snags had DBHs ≤ 37 cm with an overall detection rate of 32.6% (±2.6%) for these snags. The method produced higher overall detection rates for snags with DBH > 37 cm (55.4% (±6.2%)), and DBH > 49 cm (65.0% (±7.5%)). There were four different snag species sampled at BMEF; white fir (ABCO), ponderosa pine (PIPO), Jeffrey pine (PIJE), and incense-cedar (CADE). The detection rates for the individual species are summarized in Table 3.3. PIPO and PIJE were grouped together since they have very similar growth characteristics. ABCOs made up 50.6% of the snags and had an overall

detection rate of 33.5% (±3.8%). PIPO/PIJE made up 43.3% of the snags, with the majority of these being PIPO, and had an overall detection rate of 47.0% (±4.3%). CADE had an overall detection rate of 55.6% (±11.7%) making up the remainder of the snags at BMEF (6.1%).

At SF, the detection rates remained above 60% for all ≥ DBH and height scenarios, steadily increasing from 63 to 81% as the ≥ DBH threshold increased from ≥ 9 to ≥ 90 cm. The majority of snags had DBHs between 12 and 63 cm with an overall detection rate of 64.1% (±2.5%). Snags with DBHs > 63 cm had an average detection rate of 70.8% (±3.9%). There were nine different snag species sampled at SF; white fir (ABCO), red fir (ABMA), incense-cedar (CADE), lodgepole pine (PICO), ponderosa pine (PIPO), Jeffrey pine (PIJE), sugar pine (PILA), Douglas-fir (PSME), and California black oak (QUKE). The true firs (ABCO & ABMA) made up 74.2% of all snags sampled, with ABCO being detected 63.5% (±3.4%) of the time and ABMA 56.8% (±4.0%). All other species had detection rates above 70.5% with the exception of QUKE, which had a detection rate of 46.2% (±6.5%).

The mixed conifer forest type had the lowest snag sample size and the most variable detection rates compared to all other forest types. Even with this increased variability the ≥ DBH snag detection rate remained above 60% in all DBH and height scenarios. As expected, mixed conifer had the most species diversity with seven

species being found within the strata. In order of abundance the species were: ABCO, CADE, PSME, PIPO, QUKE, PILA, PIJE.

The high fir forest type had the most stable overall ≥ DBH detection rate increasing steadily from 58.4% to 66.7% as the DBH threshold increased. The forest type also had the lowest species diversity, containing (in order of abundance): ABMA, ABCO, PICO (3 total), and PIJE (1 total). It had the highest snag DBH variability, with the majority of snags located between 12 and 76 cm (average detection rate of 57.7% (±3.4%)). With a height threshold ≥ 9 m the ≥ DBH detection rates ranged from 77% to 100%. The sample sizes for the two ≥ DBH scenarios with 100% detection rates were relatively small (≥ 77 DBH: 13, ≥90 DBH: 5).

The low fir forest type had the best overall results, with an overall detection rate of 67.6% (±3.6%) which increased to 90.0% (±8.7%) for DBHs ≥ 62 cm. This forest type had the highest percentage of larger DBH (≥ 62 cm) snags relative to snag sample size with an overall detection rate of 85.2% (±6.8%) for these larger snags. Six species were found in this forest type, with the majority of the snags being ABCO (81%). In order of abundance they were: ABCO, CADE, PIPO, QUKE, PSME, PILA.

BMEF Treatment Detection Rates

The detection rates were only calculated for snag height ≥ 3 m scenarios (all snags) due to the smaller sample sizes in the LoD and RNA treatments. The detection rates are summarized in Figure 3.6. The LoD treatment performed the best overall

and had the highest detection rates (42.6% (±6.1%)) for smaller snags (DBH < 38 cm). The HiD and RNA treatments had the lowest small snag detection rates for the entire study, but both still performed well for larger snags with detection rates > 60%. The RNA treatment had higher variability as would be expected with the low snag sample sizes. The ≥ DBH detection rates for LoD, HiD, and RNA treatments ranged from 42 to 100%, 34 to 68%, and 30 to 100% respectively.

Storrie Fire Severity Detection Rates

The detection rates for fire severity strata were grouped into two categories: High/Medium (HMS) and Low/Unchanged (LUS). This was done for two reasons: 1) to increase snag sample sizes to more meaningful levels, and 2) because there were no noteworthy differences within the grouped strata. The overall detection rate was higher for the HMS stratum (69.7% (±2.8%)) when compared to the LUS stratum (55.7% (±3.2%)) (Figure 3.7). In the two highest ≥ DBH scenarios (DBH ≥ 77 and 90 cm), LUS performed better than HMS when the height threshold was ≥ 3 m. This was due to decay condition 7 snags not being detected in the HMS. When the height threshold was set at ≥ 6 m, the HMS stratum performed better than the LUS stratum for the same DBH scenarios. The ≥ DBH detection rates ranged from 62.5% to 100% for all height scenarios in the HMS stratum, and from 55.7% to 100% for the LUS stratum.

Individual Species Detection Rates

Overall detection rates by species are presented in Table 3.3. ABCO was the most prevalent snag species in both BMEF and SF, with very different overall detection rates for the two areas (BMEF: 33.5% (±3.8%) vs. SF: 63.5% (±3.4%)). QUKE, the only deciduous species had the lowest detection rate of all species at SF, with an overall detection rate of 46.2% (±6.5%). QUKE also had the lowest average DBH and height. Only three PICO snags were sampled at SF. All three were large snags (DBH > 36 cm, heights > 18 m) and were detected using the lidar method. The overall detection rate for PILA was 88.9% (±10.5%) and all twelve of these snags were also larger in size. The overall detection rates were lower at BMEF for all three species compared to SF.

Snag Condition Detection Rates

Detection rates for the individual snag decay conditions at both study location are presented in Table 3.4 with all species grouped together. Overall detection rates generally decreased with increasing snag decay conditions at both study locations. Condition 3 and 4 snags with broken tops had lower rates of detection compared to condition 3 and 4 snags with intact tops. At BMEF, the condition 7 snags did have a higher detection rate compared to condition 5 and 6 snags, but the sample size was relatively low (n = 10). Condition 3 and 4 snags were detected more often at BMEF compared to condition class 5, 6 and 7 snags with an average detection rate increase > 20%. This trend was not present at SF, where detection rates were more stable

across all decay conditions. Detection rates were much higher at SF for all condition classes.

Detection Rate Trends

There were four trends identified that affected detection rates in all scenarios and strata. The first two were related to tree size. Detection rates increased as snag DBH and height increased. The amount of the increase varied for the different strata. On average the overall detection rate increased 0.4% for every 1 cm increase in DBH. For height, the overall average detection rate increased 1.3% for every meter increase in the height threshold.

The other two trends were associated with overstory canopy cover and lidar point density (Figures 3.8 & 3.9). Canopy cover was calculated for each plot as the proportion of first return lidar points in the canopy layer versus all lidar first return points. As canopy cover increased the detection rate decreased (Figure 3.8). The trend became less pronounced as the ≥ DBH threshold was increased. For snags with DBHs ≥ 64 cm, canopy cover had little effect on the detection rates. Detection rates increased as the plot-level point densities increased (Figure 3.9). The trend became less pronounced as the ≥ DBH threshold was increased.

Omission Errors

Omission errors occurred when snags were not detected using the lidar method. The reasons for these errors were explored and broken into seven categories: 1) low point densities, 2) adjacent to a live tree, 3) high canopy cover, 4) needles retained, 5) canopy height model, 6) live vegetation intensity values, and 7) unknown. The proportion of the errors falling into each category is presented in Table 3.5. There is some overlap between the categories, so the values should be viewed as general trends. High canopy cover was the largest source for omission errors (35.5%), followed by low point density (20.6%), and adjacent to live tree (16.3%). The 'high canopy cover' and 'adjacent to live tree' categories are caused when snags intermix with live tree crowns. This makes them difficult to detect with the filtering algorithm, because the local-areas associated with these snags have live vegetation intensity values associated with them as well. The canopy height model smoothing method caused 11% of the snags to be missed. This error occurred when two snags were located directly adjacent to each other. During the CHM creation process their individual canopies were smoothed into one snag surface, which caused only one snag to be detected. Snags with dead needles still attached were almost always missed and they constituted 6.3% of the omission errors. Dead attached needles caused lidar point intensity values to be categorized as live vegetation, and made them difficult to detect. Some snags that did not have dead needles were also found

to have too many live vegetation points associated with them and were not located adjacent to any live trees. These live vegetation criteria intensity values are hypothesized to be associated with fine branches, witches broom (i.e., small localized clump of branches caused by disease), or other finer material in the canopy. Some omission error snags could not be associated with any of the categories directly (7.2%), so they were classified as unknown. They are likely caused by either a combination of the identified factors or by another unidentified factor.

Commission Errors

Commission errors occurred when the lidar snag detection method falsely identified a live tree or a portion of a live tree as a snag (Table 3.6). All falsely created snags were either small to medium live trees (DBH < 38 cm) or comprised of a small portion of a large tree (DBH ≥ 38 cm). Many of the live trees classified as snags had either dead tops or had high risk ratings (3 or 4 rating) (~33%). The mixed conifer forest type had the highest commission error rate with 5.40 falsely created snags per hectare. The other forest types all had similar error rates between 0.64 to 1.37 snags per hectare.

Snag Height Comparison

Snag heights estimated using the automated lidar individual-snag detection method were compared to field measured heights. A simple ordinary least squares

(OLS) regression analysis was used to compare heights. The OLS scatterplot is presented in Figure 3.10, with values categorized by snag condition. The lidar method produced negatively-biased results for height estimation (Bias = -2.07 m), but displayed an overall good relationship with the lidar heights explaining a large amount of the variation associated with field measured heights (R^2 = 0.965). Snag condition 3 snags had a smaller negative bias (condition 3 bias = -0.96).

Discussion

Detection of Snags

The method presented in this study was able to accurately detect and locate a large proportion of snags in all strata. Snag detection rates increased as the size of snags increased (DBH & height) and decreased as snag conditions decayed. Most forest management snag stocking guidelines and standards are focused on larger snags, as they provide more wildlife habitat potential. For the areas in this study, a common snag size threshold for stocking guidelines is DBH ≥ 38 cm. The method presented in this paper provided an overall detection rate of 70.6% (±2.7%) for snags meeting this requirement.

The different strata provided an opportunity to explore the method's performance in various forest conditions and types. At SF, the datasets were relatively small for the individual forest types and had some unique characteristics, which likely caused these forest types to have inflated detection rates. Most of the

sampled snags at SF were located within the HS and LS strata (56%). These strata have very low canopy covers (0-25%) and live tree percentages (0-20%), which resulted in higher detection rates than would be expected in natural forest conditions for these forest types (e.g., higher live canopy covers). Thus, the interpretation of SF individual forest type detection rates should take this into account. More samples from each SF forest type need to be tested with the method to determine how it would perform in more natural conditions. The SF detection rates did however demonstrate the ability of the method to successfully detect individual snags post-wildfire (~ 9 years) in all three forest types with various fire severities. This could be useful for post-fire severity, wildlife habitat, or volume assessments. Even with the sample size limitations at SF, the method performed similar to BMEF in regards to overall trends.

At BMEF, there were a large number of samples in a wide range of natural conditions. Thus, more weight should be given to the results at BMEF in regards to how the method would perform in more natural forest conditions. Detection rates will likely be similar to the results at BMEF, with smaller snags (DBH < 38 cm, height < 9 m) being detected between 30-60% of the time, and larger snags being detected between 60-80% of the time.

Detection rates using this method were affected by a number of uncontrollable and controllable factors. Uncontrollable factors were associated with

forest stand and individual snag characteristics, while controllable factors were associated with the quality of the lidar data and the individual-snag detection methods. Canopy cover was an uncontrollable factor that significantly affected snag detection rates (Figure 3.7). As canopy cover increases the likelihood of snags intermixing with live tree crowns also increases. When intermixing occurs, lidar points meeting live tree intensity criteria are more likely to be located within snag point local-areas, making snag points more difficult to identify with the snag detection algorithm. The same problem occurs in lower canopy cover areas when a live tree is located directly adjacent to a snag. These stand characteristics occur normally in all forested environments, thus the method used in this study will be limited in these situations. The development of new snag detection lidar filtering methods or higher lidar point densities could help reduce or overcome this problem, but this is left for future work.

Snag detection was also influenced by individual snag characteristics using the method in this study. Four individual characteristics were found to adversely affect snag detection. First, snags with dead needles attached often had a large proportion of their lidar points with intensity values meeting live tree criteria, which caused them to be eliminated during the first stage of the filtering algorithm. This means that for this lidar dataset, the surface characteristics of intersected objects had more influence on intensity values compared to color. Overcoming this problem will be

difficult only using discrete-return lidar data, even with better intensity calibration. If the method is coupled with other remote sensing variables, such as those derived from airborne multispectral imagery, detection of these snags might be feasible. This also means there is a temporal component to snag detection; as time since mortality passes, snag detection rates should initially increase as the amount of dead needles and fine branches decrease, and then slowly decrease as decay conditions mature. In the instance of a large-scale disturbance, such as wildfire or insect outbreak, acquisition of lidar data for snag detection should be timed in consideration of the timing of needle- or leaf- cast.

The second characteristic found to affect detection rates was associated with QUKE, the only deciduous tree species in the study. All QUKE snags sampled in this study were located on four plots in SF, three in MC and one in LF (the LF plot containing only one QUKE). The growth characteristics associated with these snags in the MC plots produced a unique situation which adversely affected their detection rates and increased commission errors. In all cases, these snags were associated with multiple stems generating from one tree base. Due to the sampling protocol each stem with a DBH ≥ 9 cm was treated as a separate snag, and while one of them was successful detected in each case the other stems were treated as undetected snags. Making matters even more troublesome for these snags was the fact that they did not follow a simple vertical growth pattern. They grew with spread out dome-shaped

crowns. This caused the CHM for these snags to have multiple maxima, which in turn caused an increase in commission errors. This was the primary reason why the MC stratum had the highest commission error rate. Changing the CHM smoothing parameters would help to alleviate this problem, but identifying each individual snag stem will be difficult.

The other two uncontrollable individual tree characteristics that adversely affected the study's method were associated with trees declining in vigor or containing dead tops. Many of the commission errors were caused by live trees with large dead tops (e.g., dead tops constituting > 20% of the tree's total height) or trees that were showing signs of declining vigor (e.g., risk rating 3 and 4 trees). The error effects of both these factors might be reduced with increased lidar point densities, better intensity calibration, or modified filtering methods. While these trees caused commission errors, they also highlight the ability of the method to identify live trees displaying unique physical health characteristics. Trees with large dead tops and decreasing vigor often provide valuable wildlife habitat as well (Bull et al., 1997). In the future, modifications to the lidar filtering algorithm and the addition of new remote sensing variables might provide the ability to detect and classify trees with these characteristics, as well.

Controllable factors affecting the overall ability of the method to detect snags can be partitioned into three categories: 1) lidar acquisition and intensity calibration,

2) snag filtering algorithm, and 3) individual-snag detection methods. Adjustments to these could help improve overall detection rates. Lidar acquisition parameters determine the usefulness of the lidar data. The acquisitions in this study used a narrow beam divergence setting which resulted in a high percentage of first and single returns (BMEF: 90.2%, SF: 89.9%). These returns have been shown to provide better intensity information when compared to multiple returns and were the only returns used in this study (Morsdorf et al. 2010). The vendor also used the automatic variable gain setting during acquisition in both study areas which helped to provide more useful intensity information. Post-acquisition intensity calibration was not completed for the lidar data in this study. Doing so would likely improve the results. Lidar point densities need to be high enough to ensure there are enough lidar points to characterize individual snags and for the filtering algorithm to successfully identify individual snag points. Based on the lidar point density trends found in this study (Figure 3.8) and the results of the filtering algorithm, point densities ≥ 4 first or single return points m^{-2} should provide an adequate amount of data to successfully detect a majority of large snags (> 50%), although higher densities should improve results. Identifying the optimal lidar point density for snag detection will vary depending on the quality of the intensity information, forest stand characteristics (e.g., forest type, tree density, crown structure, etc.), and snag detection algorithm parameters.

The snag detection filtering algorithm displayed great potential in its ability to identify individual snag points. The two reinstitution filters successfully identified snag points that were removed during the elimination stage. The coarse-scale reinstitution filter reinstituted a total of 46 possible snags, all of which were larger in size (DBH > 38 cm), while the fine-scale reinstitution filter reinstituted a total of 163 possible snags. The majority of snags reinstituted using the fine-scale filter were small or broken snags identified under the first scenario (67%), and most often occurred in the high and medium fire severity strata at SF. The filtering method will likely perform better for species with denser foliage characteristics since the difference in intensity values between live and dead trees should be more pronounced for these species. Increasing point density and calibrating intensity information should also improve filtering results.

This is the first time this unique filtering method has been used for snag detection, thus improvements can likely be made. Using fine-scale 3D voxel-based filtering earlier in the algorithm might improve results by providing more detailed 3D local-area information. Another possibility warranting investigation is the use of small-footprint full-waveform airborne lidar (SFFW). SFFW provides more than just discrete-return coordinate and intensity information, it also provides laser pulse echo width information. Echo width information has proven to be useful for classifying ground and vegetation returns, thus it may provide more information for

differentiating between live and dead tree points (Ducic et al., 2006; Wagner et al., 2008). Costs associated with SFFW acquisition are still relatively high at the time of this study, making its use prohibitive for most broad-scale forest inventory applications. These costs are likely to decrease over the next decade. Incorporating different remote sensing technologies into the filtering framework could also provide improved filtering results.

The individual-snag detection method was able to correctly identify and locate snags in all strata. Having live tree points removed from the point clouds used to create the CHM made it easier differentiate individual snag canopies. The input parameters (e.g., grid cell size, smoothing factors, and size of the median filter) involved in the CHM creation and smoothing process ensure the CHM accurately represents individual snag canopies and ultimately how well individual snags are detected. Identifying proper CHM input parameters required a trial and error process, where multiple CHM were created and tested. This important process will be necessary for each individual lidar dataset. Even with the positive results, the CHM creation method still had two downfalls. First, snags located directly adjacent to each other were sometimes reduced to one snag canopy during CHM creation. This can be overcome by using a smaller grid cell size during CHM creation; however this could also result in more commission errors. Second, in areas where deciduous trees intermix with coniferous species the CHM will likely have problems characterizing

one or the other. A method that treats them separately might help, but this would be more difficult to implement. Higher point densities would help alleviate both problems by providing more information for canopy characterizations, but the problems would still likely remain in some capacity.

The CanopyMaxima individual-tree detection algorithm provided relatively accurate height information, even though it was negatively biased. Negative biases have been found in many lidar studies for tree heights, although they are typically smaller than the one found in this study (Stereńczak & Zasada, 2011). The larger negative bias was likely a function of the physical characteristics associated with snags (e.g., small target surface area at the top). Higher point densities would likely help reduce the height bias. A bias correction factor can also be applied, since the bias remained relatively stable, slightly decreasing with increasing snag height (Figure 3.9). The individual-snag detection method might be improved by using a different individual-tree segmentation method. Voxel-based methods utilizing 3D information to reconstruct individual snags from the ground upward are one possibility. It could also be possible to classify individual snags into decay condition stages based on information collected during an individual-snag detection algorithm (e.g., crown widths, heights, etc.).

The method presented had very similar snag detection results compared to Bütler & Schlaepfer (2004) and overcomes many of limitations associated with their

method (e.g., time, user bias). Their study was conducted in a spruce-dominated forest in Switzerland and produced detection rates of 27% for snags with DBHs ≥ 10 cm (n = 633), and 67% for snags with DBHs ≥ 25 cm (n = 211). They found detection rates increased as snag sizes increased and decreased as canopy closure increased, which this study also found. The biggest difference between the studies is associated with the individual snag detection methods. They used a manual segmentation method that coupled color infrared aerial photographs and a geographic information system, which introduced operator interpretation bias and subjectivity errors. These limitations are overcome using this study's method, while also improving time efficiency.

The extension of the method to different airborne lidar datasets, forest types and stand structures warrants further investigation. A number of the filtering algorithm parameters will likely need adjustment for lidar datasets with different point densities or intensity calibrations (e.g., SPR, local-area sizes, point density requirements). The current parameters should work well for lidar datasets acquired using similar methods (e.g., scan angle of $\pm 15^{o}$ from nadir, point densities > 4 points m^{-2}, automatic variable gain setting, narrow beam divergence). Filtering algorithm parameters can be adjusted for individual lidar datasets using a simple trial and error process. Useful detection parameters could also be standardized in the future for

various lidar datasets and forest types. Applications for the method should overcome a number of the traditional problems associated with the quantification of snags.

Applications

Extensive literature exists on the structural and functional characteristics of snags and their importance for wildlife habitat, biodiversity and overall forest health (Bull et al., 1997; Caza, 1993; Laudenslayer, 2002). Minimum stocking standards have been developed that require certain densities or volumes of snags to be maintained over time to provide continuous habitat and ecosystem sustainability. Both the development of and the assurance in meeting these requirements are based on field sampling and modeling methods, which often produce highly variable results due to sampling difficulties associated with irregular and sparsely distributed snags. The method presented in this study provides the ability to estimate snag densities while also providing the spatial location and arrangement of individual snags over a landscape. The method can provide useful snag density estimates using the following formula which applies corrections for undetected snags and commission errors.

(4)

where, is the snag density, is the number of snags detected from the lidar method, is the lidar detection rate determined from either a comparison with

field sampled snags or estimated based on prior performance, is the total area sampled, and is the commission error rate correction factor in the same area units as sampled (i.e., number of commission errors per hectare) and is also determined from either a comparison with field sampled snags or estimated based on prior performance. The formula can be applied to any DBH or height threshold scenario.

The efficient field sampling method used in this study can be incorporated into a traditional fixed-area plot forest inventory sampling design without much additional effort, but other sampling designs could also be utilized to sample individual snags and develop lidar detection rates. Once detection rates are known for various forest types and situations, snag density estimates could be determined using only airborne lidar data.

The other application and major benefit of the method is the creation of accurate snag distribution maps across the landscape. The ability to create snag stem maps across a landscape has never been available without costly intensive sampling. These maps can help with many forest management activities and decisions, some uses include: 1) identification of areas with high and low snag densities, 2) assessment of the spatial arrangement of snags and coordinating wildlife species interactions, and 3) monitoring snag spatial changes over time. Both applications should increase our understanding of snag dynamics in forest ecosystems, while also

helping to develop more accurate stocking standards. Additional uses for this type of dataset are likely to surface in the future.

The method also produced a by-product that could prove useful in the estimation and prediction of many live tree characteristics. The points eliminated during the filtering algorithm are most likely associated with live-trees. By taking another simple step, live-tree point clouds can be obtained. Live-tree points that were eliminated during the snag filtering algorithm can be reinstituted while identified snag points can be eliminated. This new live-tree point cloud should produce better lidar metrics for characterizing live-tree attributes (e.g., biomass, tree density, height attributes, basal area, etc.), since these point clouds are more representative of the live trees.

Conclusions

This study presented a new semi-automated airborne lidar-based method to identify and locate individual snags across forested landscapes. The method used both 2D and 3D local-area lidar point filtration focused on intensity values to identify individual lidar points associated with snags and eliminate lidar points associated with live trees. While the detection of smaller snags was somewhat limited, detection of larger snags was promising. Given the difficulties associated with the quantification of snags across the landscape, the method presented should provide a safer, simpler and more accurate alternative. The method has many promising

attributes: 1) it provides the ability to obtain less variable snag density estimates for forest stands; 2) it produces an accurate snag stem map for larger snags; 3) it is semi-automated; 4) it could become a standardized procedure and bring more clarity to snag stocking requirements.

The method's detection rates could be improved by using new lidar point filtering and detection methods, or by coupling the lidar information with other airborne remote sensing products. The method could also be extended to classify individual snags into snag decay condition classes and possibly identify individual live trees exhibiting unique health characteristics (e.g., dead tops, decadence ratings, etc.). Given the promising results, the method warrants further investigation in other forest types and conditions.

Acknowledgements

This study was funded through a cooperative agreement between Oregon State University and the U.S. Forest Service Pacific Southwest Research Station. The author gratefully acknowledges the field work and additional help of Thomas Fisher, David McClung and Travis Springer.

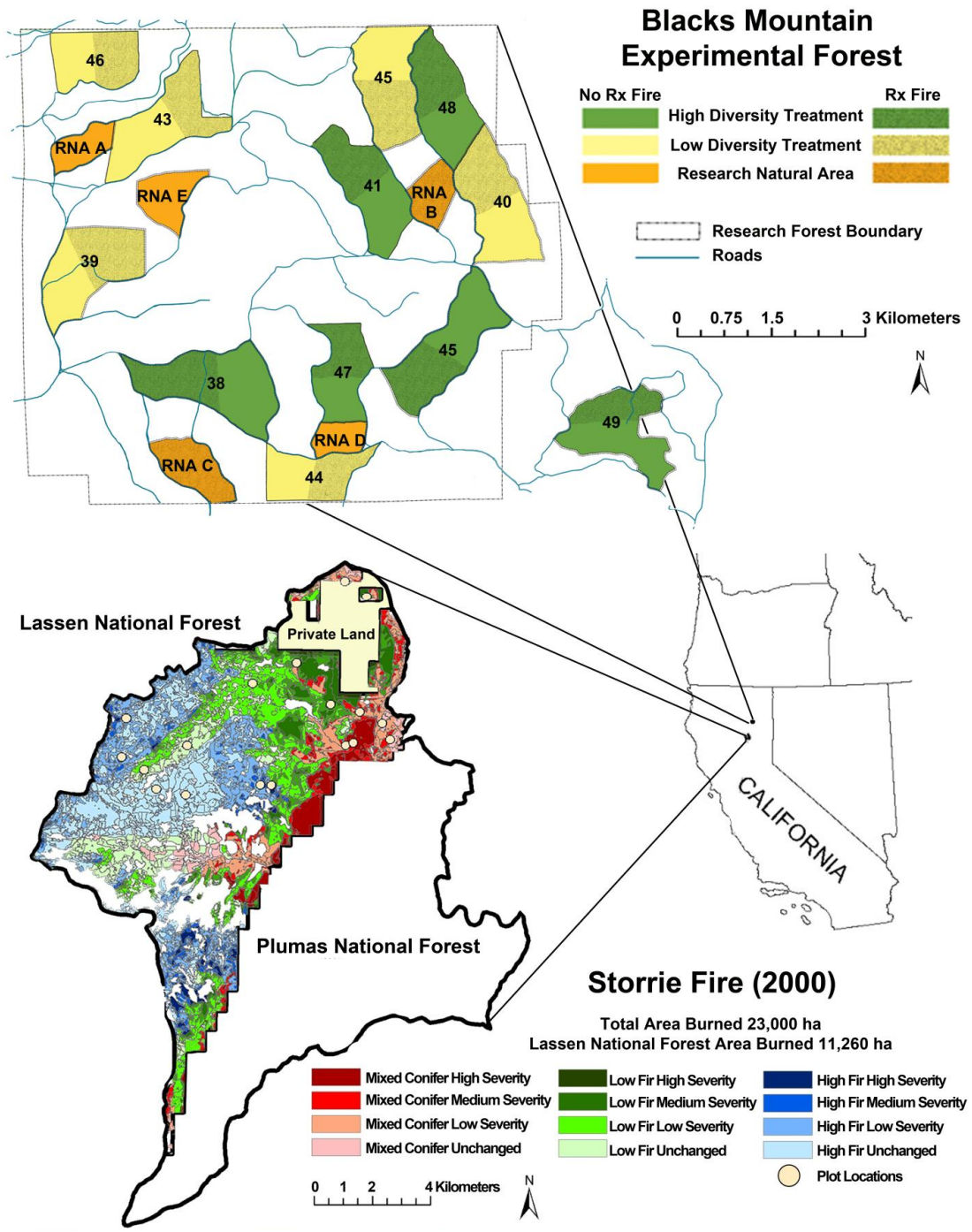

Figure 3.1: Geographic location of the Blacks Mountain Experimental Forest and the Storrie Fire with study design depictions.

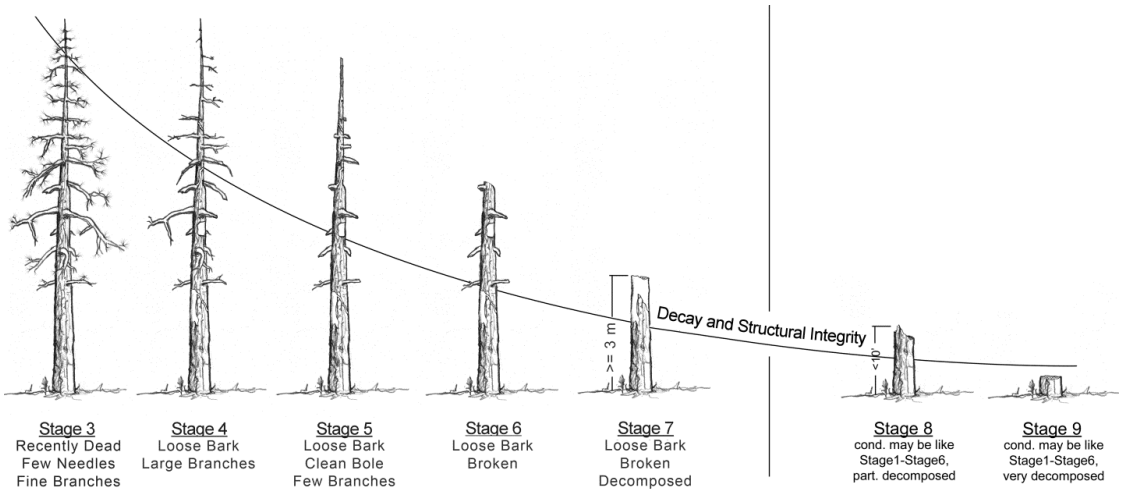

Figure 3.2: Visual depiction of snag condition stages used for the study. Derived from Thomas et al. (1979). Stage 8 and 9 snags were not sampled in the study.

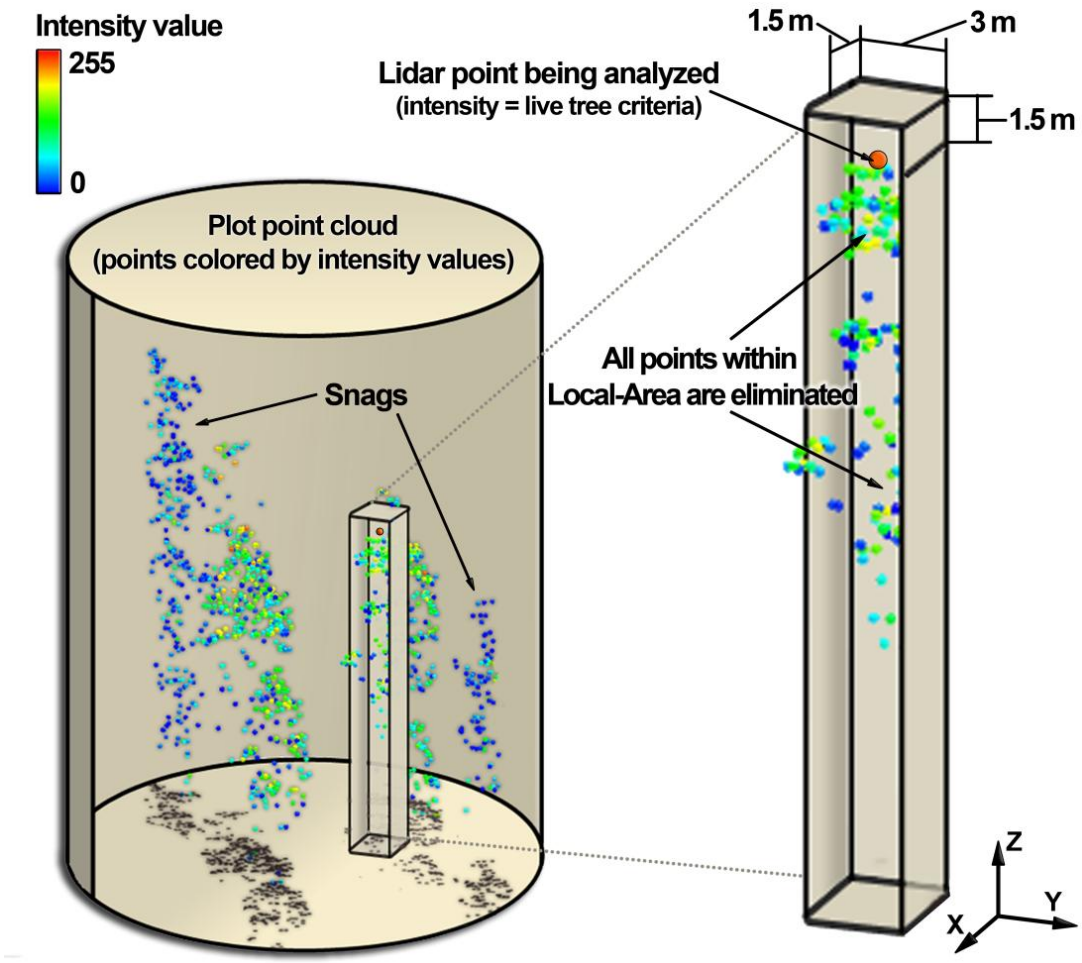

Figure 3.3: Depiction of a individual plot lidar cloud and the stage one 3D local-area robust elimination filter. Lidar points are colored by intensity values.

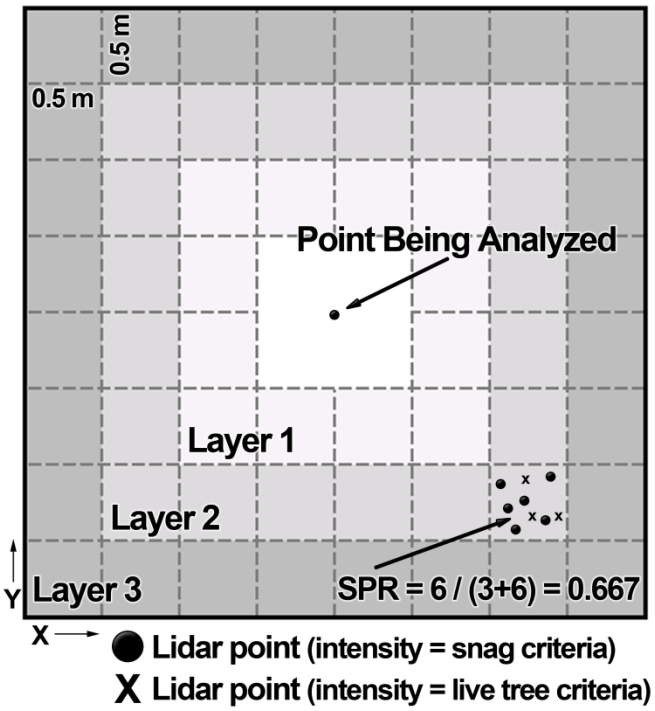

Figure 3.4: Depiction of a fine-scale 2D local-area used in the second reinstitution filter and how SPR was calculated for each grid cell.

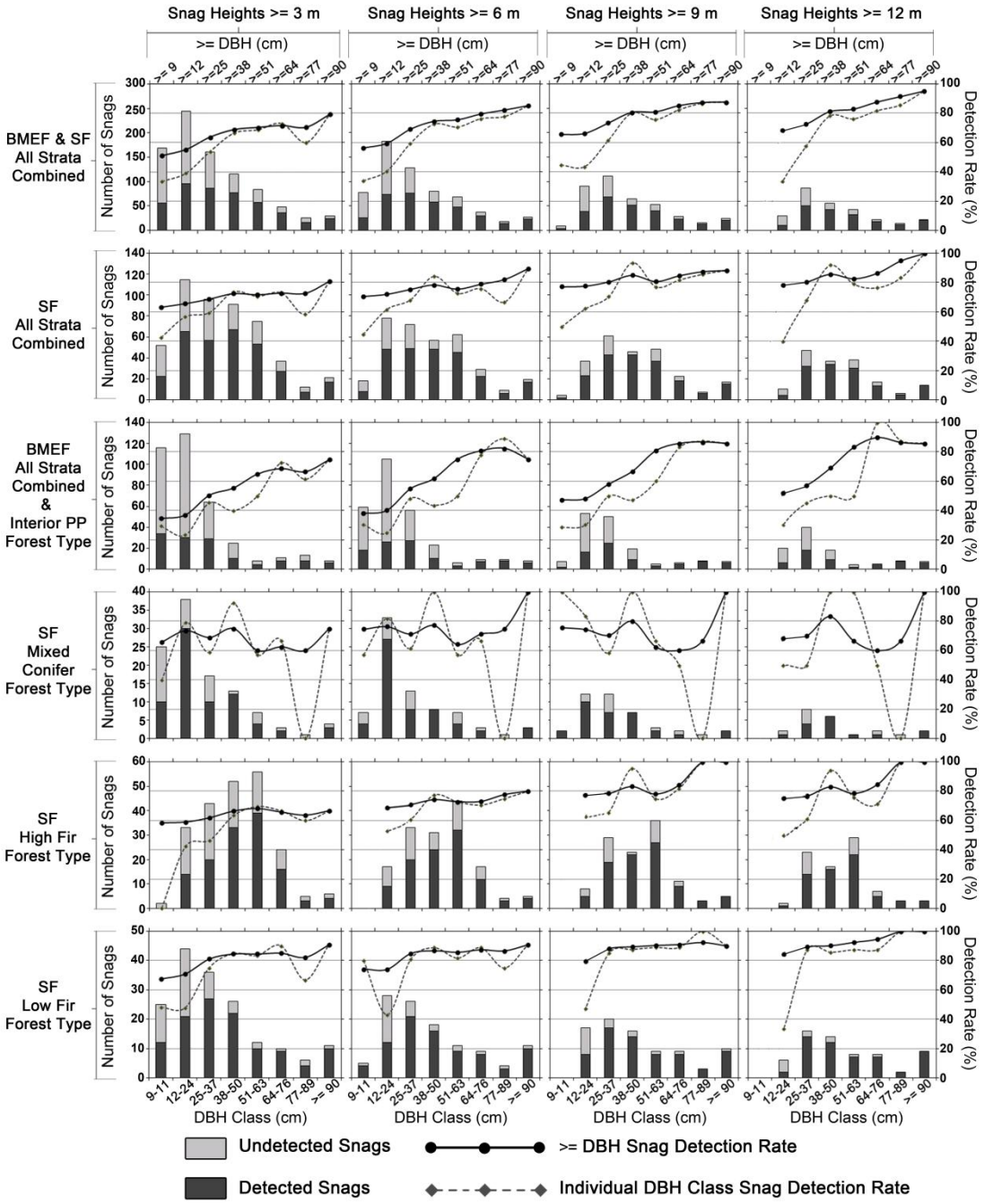

Figure 3.5: Overall detection rate summaries and trends for the various forest types at BMEF and SF under different DBH and height scenarios. >= DBH snag detection rates are defined as all snags with DBHs greater than or equal to the DBH listed (i.e., >= DBH 25 cm = detection rate for all trees with DBHs ≥ 25 cm).

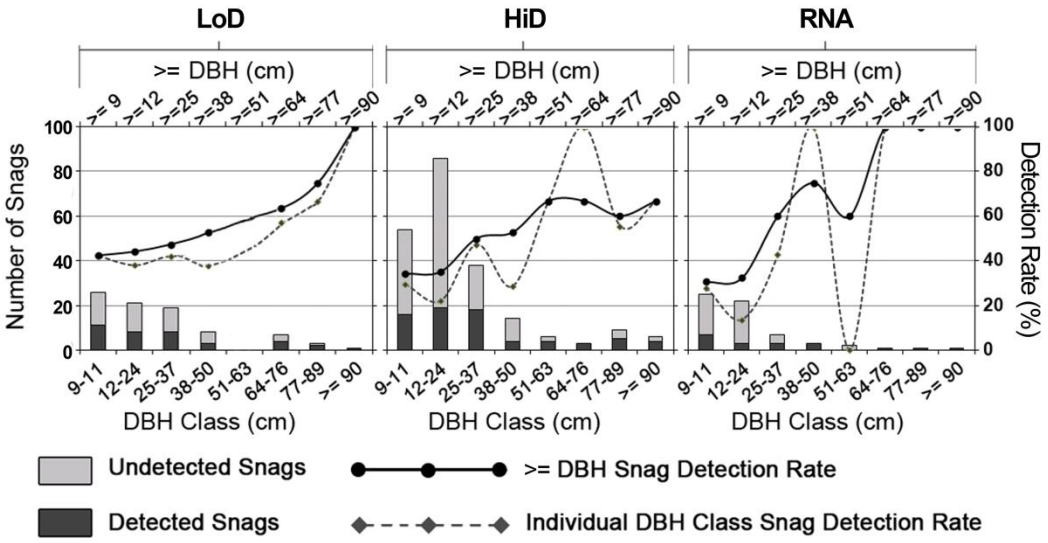

Figure 3.6: Detection rate summaries and trends for the three treatment groups at BMEF under different DBH scenarios (LoD = low diversity; HiD = high diversity; RNA = research natural area). All summaries are for the height ≥ 3 m scenario. >= DBH snag detection rates are defined as all snags with DBHs greater than or equal to the DBH listed (i.e., >= DBH 25 cm = detection rate for all trees with DBHs ≥ 25 cm).

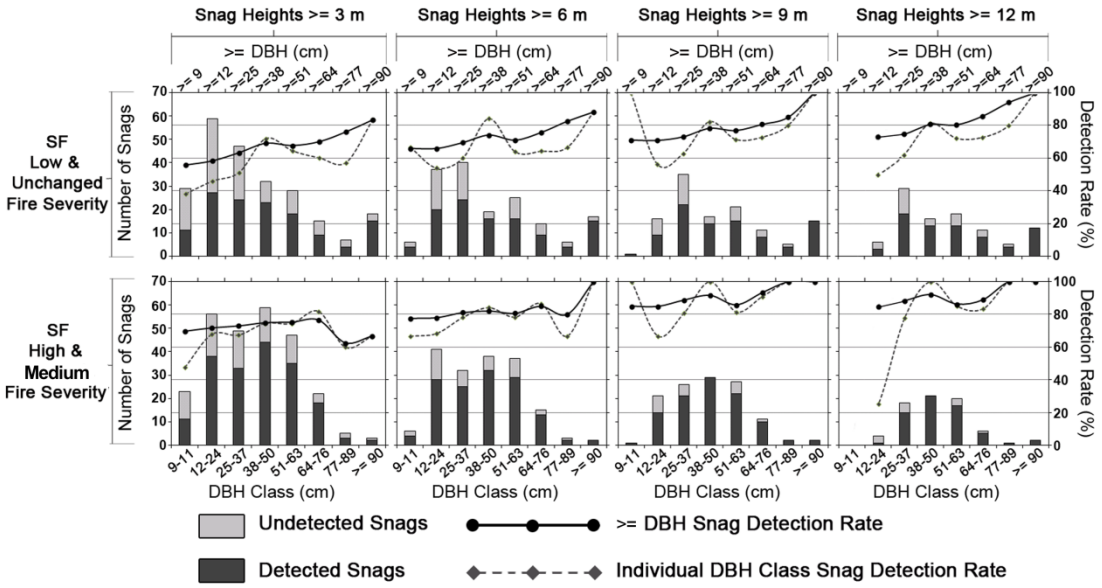

Figure 3.7: Overall detection rate summaries and trends for the two grouped fire severity strata at SF under different DBH and height scenarios. >= DBH snag detection rates are defined as all snags with DBHs greater than or equal to the DBH listed (i.e., >= DBH 25 cm = detection rate for all trees with DBHs ≥ 25 cm).

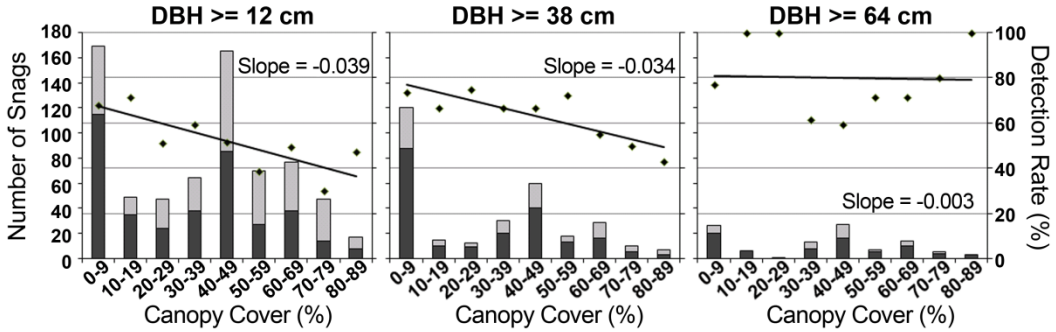

Figure 3.8: Canopy cover snag detection rate trends for different >= DBH scenarios combining data from both study locations (≥ 3 m height threshold). Data points represent the detection rates for the various canopy cover classes. Trend lines are based on the detection rate data points.

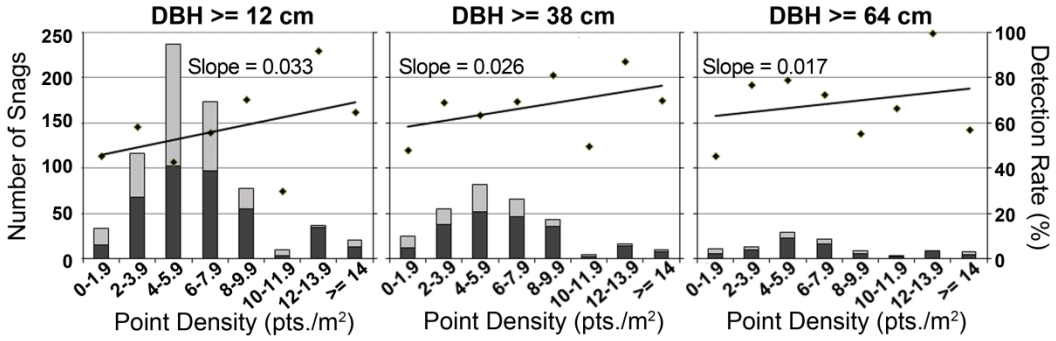

Figure 3.9: Lidar point density snag detection rate trends for different >= DBH scenarios combining data from both study locations (≥ 3 m height threshold). Data points represent the detection rates for the various canopy cover classes. Trend lines are based on the detection rate data points.

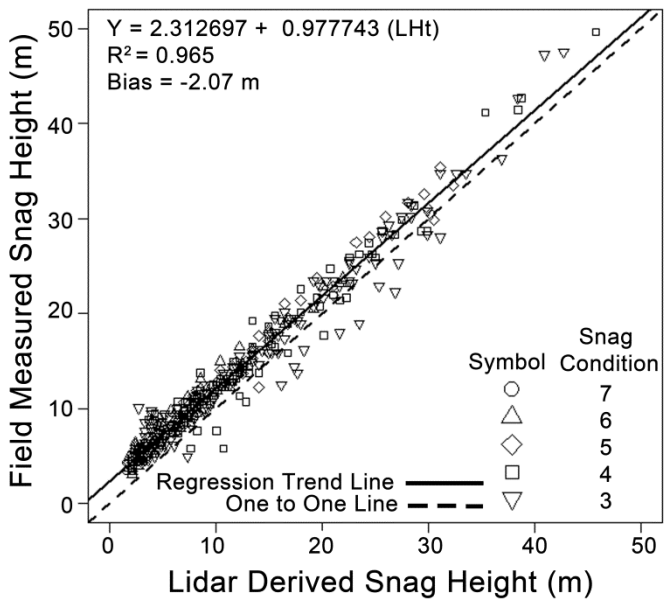

Figure 3.10:. Lidar derived snag heights versus field measured snag heights, categorized by snag condition.

Table 3.1: Standing live tree (DBH ≥ 9 cm; Heights ≥ 3 m) attributes from all plots per strata at SF and treatment type (LoD, HiD, RNA) at BMEF (n_s = number of snags; n_p = number of plots; sd = standard deviation).

		DBH (cm)			Live Tree Height (m)				Live Trees per Hectare		
Stratum	n_s	Range	Mean	sd	Range	Mean	sd	n_p[a]	Range	Mean	sd
BMEF											
Interior PP - Overall	3819	(9.0 - 135.1)	25.6	15.4	(1.8 - 41.4)	12.4	6.3	154	(24.7 - 1469.7)	306.3	238.6
Interior PP - LD	1081	(9.0 - 83.1)	26.6	9.4	(2.1 - 26.2)	11.9	4.4	65	(24.7 - 432.3)	205.4	81.9
Interior PP - HD	2183	(9.0 - 135.1)	26.4	18.0	(1.8 - 41.5)	12.9	7.1	79	(86.5 - 1469.7)	341.3	259.6
Interior PP - RNA	555	(9.1 - 88.9)	20.8	12.8	(2.4 - 37.2)	11.1	5.9	10	(358.2 - 1222.7)	685.4	302.5
SF											
Overall	767	(9.1 - 160.3)	38.5	24.6	(3.1 - 55.2)	18.6	11.0	52 (18)	(0.0 - 667.0)	182.2	171.9
Mixed Conifer	299	(9.1 - 128.8)	33.7	25.2	(3.1 - 55.2)	17.1	12.0	16 (6)	(0.0 - 568.1)	161.9	179.6
High Fir	236	(9.4 - 124.2)	39.0	21.6	(3.1 - 44.8)	17.8	9.1	18 (6)	(0.0 - 457.0)	191.0	132.1
Low Fir	232	(9.4 - 160.3)	44.1	25.3	(3.4 - 49.1)	21.4	10.9	18 (6)	(0.0 - 667.0)	230.8	194.7
High Severity	0	-	-	-	-	-	-	9 (3)	-	-	-
Medium Severity	92	(13.2 - 105.7)	50.0	22.4	(4.0 - 44.2)	24.1	9.5	12 (4)	(0.0 - 94.7)	94.7	88.8
Low Severity	280	(9.4 - 160.3)	40.0	25.3	(3.1 - 55.2)	19.3	11.1	16 (6)	(37.1 - 667.0)	216.1	155.0
Unchanged	395	(9.1 - 128.8)	34.9	23.7	(3.1 - 50.0)	16.8	10.8	15 (5)	(74.1 - 506.4)	307.7	152.7

a - number of clusters in parenthesis.

Table 3.2: Standing dead tree (DBH ≥ 9 cm; Heights ≥ 3 m) attributes from all plots per strata at SF and treatment type (LoD, HiD, RNA) at BMEF (n_s = number of snags; n_p = number of plots; sd = standard deviation).

		DBH (cm)			Snag Height (m)				Snags per Hectare		
Stratum	n_s	Range	Mean	sd	Range	Mean	sd	n_p[a]	Range	Mean	sd
BMEF											
Interior PP - Overall	344	(9.0 - 122.2)	27.2	21.2	(3.0 - 42.7)	10.5	6.6	154	(0.0 - 284.1)	27.6	41.2
Interior PP - LD	73	(9.0 - 94.7)	31.1	22.0	(4 - 31.4)	10.8	5.5	65	(0.0 - 86.45)	13.9	20.5
Interior PP - HD	216	(9.0 - 95.8)	26.7	21.3	(3.0 - 42.7)	10.3	6.7	79	(0.0 - 284.1)	33.8	50.4
Interior PP - RNA	55	(9.0 - 122.2)	23.6	21.4	(3.05 - 34.8)	10.8	7.7	10	(24.7 - 111.2)	67.9	31.4
SF											
Overall	499	(9.0- 137.4)	39.1	23.6	(3.0 - 49.7)	11.4	8.3	52 (18)	(0.0 - 358.2)	118.5	89.3
Mixed Conifer	98	(9.0 - 106.9)	26.9	20.9	(3.1 - 28.0)	9.1	5.0	16 (6)	(0.0 - 284.1)	75.6	186.8
High Fir	231	(9.1 - 121.4)	44.9	19.6	(3.0 - 41.5)	11.7	8.2	18 (6)	(37.1 - 370.1)	158.5	109.9
Low Fir	170	(9.0 - 137.4)	38.4	27.2	(3.1 - 49.7)	12.4	9.9	18 (6)	(24.5 - 197.6)	116.6	62.0
High Severity	128	(9.4 - 87.6)	42.3	18.6	(3.1 - 42.7)	10.5	7.2	9 (3)	(31.0 - 345.8)	175.6	105.0
Medium Severity	145	(9.0 - 110.0)	36.1	20.3	(3.1 - 34.8)	10.7	7.1	12 (4)	(25.0 - 358.2)	149.2	95.0
Low Severity	170	(9.1 - 137.4)	36.3	25.4	(3.0 - 47.2)	11.7	8.8	16 (6)	(37.1 - 296.4)	131.2	78.3
Unchanged	56	(9.0 - 131.3)	48.3	31.4	(3.0 - 50.0)	14.8	11.1	15 (5)	(0.0 - 160.6)	46.1	41.6

a - number of clusters in parenthesis.

Table 3.3: Snag species detection rates and summary for BMEF and SF (n = number of snags; sd = standard deviation).

Tree Species	Proportion of Snags (%)	Detection Rate (%)	DBH (cm) Range	DBH (cm) Mean	DBH (cm) sd	Height (m) Range	Height (m) Mean	Height (m) sd
BMEF (n = 344)								
ABCO	50.6	33.5	(9.0 - 92.7)	27.0	17.8	(3.1 - 36.3)	10.1	4.8
CADE	6.1	55.6	(9.0 - 95.8)	35.3	31.0	(3.1 - 26.2)	8.8	6.2
PIPO/PIJE	43.3	47	(9.0 - 122.2)	26.3	24.1	(3.0 - 42.7)	11.0	8.2
SF (n = 499)								
ABCO	41.7	63.5	(9.0 - 131.3)	36.9	24.4	(3.0 - 49.7)	11.1	8.9
ABMA	32.9	56.8	(9.1 - 102.9)	46.9	17.9	(3.0 - 34.7)	12.0	8.1
CADE	10.0	70.5	(9.1 - 137.4)	29.7	27.3	(3.1 - 30.8)	10.4	7.0
PICO	0.6	100	(36.8 - 52.8)	45.0	8.0	(18.9 - 31.4)	26.3	6.6
PIPO/PIJE	6.0	86.4	(7.6 - 106.9)	39.2	27.5	(3.4 - 29.9)	14.1	8.6
PILA	2.4	88.9	(37.8 - 84.8)	60.8	19.1	(3.7 - 27.4)	13.9	9.3
PSME	3.6	81.3	(7.6 - 106.9)	38.3	28.8	(3.4 - 29.9)	13.7	9.4
QUKE	2.8	46.2	(9.9 - 27.4)	14.3	3.7	(4.9 - 11.5)	8.3	1.7

Table 3.4: Snag detection rates for snag decay conditions for all snags combined (n = number of snags). Standard errors are given in parenthesis. Some snags were missing snag conditon information and were excluded from the table analysis.

Snag Decay Condition	Overall Detection Rate (%)	Intact Top Detection Rate (%)	Broken Top Detection Rate (%)	Proportion Broken Tops (%)	n
BMEF					
3	48.4 (4.0)	49.0 (4.0)	33.3 (19.2)	3.8	159
4	43.4 (5.7)	44.8 (6.5)	38.9 (11.5)	23.6	76
5	23.1 (6.7)	21.7 (8.2)	25.0 (10.8)	41.0	39
6	19.2 (7.7)	-	-	100.0	26
7	30.0 (14.5)	-	-	100.0	10
SF					
3	75.0 (4.1)	77.9 (4.3)	58.9 (11.9)	15.2	112
4	60.7 (4.4)	65.2 (5.7)	54.7 (6.8)	43.4	122
5	65.4 (4.6)	65.2 (9.9)	65.5 (5.2)	78.5	107
6	66.7 (5.1)	-	-	100.0	87
7	53.3 (12.9)	-	-	100.0	15

Table 3.5: Categorized omission error summary combining both study locations. Standard errors are given in parenthesis.

	Low Point Density[a]	Adjacent to Live Tree[b]	High Canopy Cover[c]	Retained Needles[d]	Canopy Height Model[e]	Live Vegetation Intensity Values[f]	Unknown[g]	Total Undetected (n)
Proportion of Undetected Snags (%)	20.6 (4.5)	16.3 (4.6)	35.3 (4.0)	6.3 (4.9)	11 (4.7)	3.3 (5.0)	7.2 (4.8)	399

a - Point density on the plot was < 3 points/m^2, causing problems with lidar snag filtering.
b - Located adjacent to one or more live trees with crowns intermixing.
c - Canopy cover for the plot was > 60%, likely crowns intermixing.
d - Snag is recently dead and still has dead needles attached, causing live vegetation intensity returns.
e - Smoothing error during CHM creation caused the snag to be missed.
f - Contained too many intensity values meeting live vegetation criteria.
g - Unknown reason, likely a combination of the identified factors.

Table 3.6: Summary of commission error rates for each forest type. Standard errors are given in parenthesis.

	Interior Ponderosa Pine	Mixed Conifer	High Fir	Low Fir
Number of Commission Errors	8	7	1	2
Area Sampled (ha)	12.5	1.3	1.5	1.5
Commission Error Rate (#/ha)	0.64	5.40	0.69	1.37

CHAPTER 4: IMPROVING PLOT-BASED PREDICTION OF LIVE ABOVE GROUND BIOMASS USING POINT-FILTERED AIRBORNE LIDAR DATA.

Brian M. Wing

Martin W. Ritchie

Kevin Boston

Warren B. Cohen

Alix Gitelman

Abstract

Live above ground biomass (AGB) assessments are used in a myriad of forest management applications. Airborne lidar remote sensing has been used successfully to predict live AGB at both the individual tree and the plot level, with the latter being more common in practice. Thus far, most plot-level assessments utilize lidar-derived metrics created using the entire plot's lidar point cloud to predict live AGB. While these metrics have produced promising results, many of the points located within these plot-point clouds are associated with dead trees introducing variability into the modeling framework. In this study, live AGB prediction models are created using three separate sets of plot-level lidar-derived metrics and compared using both model selection statistics and cross-validation statistics. The three sets of lidar-metrics used in the study were; 1) a 'traditional' set created using the entire plot lidar point cloud, 2) a 'live-tree' set created using a lidar point filtering algorithm that attempts to remove points associated with dead trees from the plot point clouds, and 3) a 'vegetation-intensity' set created by filtering and removing lidar points not meeting intensity value thresholds associated with live vegetation. The live-tree lidar metric set produced the best results, reducing prediction variability by 4.3% over the traditional set in plots containing filtered dead tree points. The study highlights the ability of filtering lidar point cloud data to create more useful and accurate

explanatory variables for prediction of live AGB. The method should also extend into the prediction of other live tree attributes with similar results.

Introduction

Accurate prediction of above-ground biomass (AGB) is important for multi-scale forest assessment. AGB is used to evaluate carbon stocks (Boudreau et al., 2008), measure carbon fluxes after natural and human disturbance (Turner et al., 1995), help characterize fuel loading and model fire behavior (Riaño et al. 2004; Rothermel, 1983), and quantify carbon exchanges between terrestrial and atmospheric sinks (Kimes et al., 2005). AGB has traditionally been estimated using extensive in-field inventory methods or aerial photography (Avery & Burkhart, 1994). These methods are relatively unbiased, but are also time consuming and expensive. More recently, the use of airborne lidar has been used to successfully estimate and predict live AGB.

Airborne lidar is an active remote sensing technology employing an aircraft mounted laser capable of simultaneously mapping terrain and vegetation heights with sub-meter accuracy. It has proven to be a very promising remote-sensing technology for increasing the accuracy and efficiency of large-scale forest inventories for a myriad of important forest inventory and wildlife habitat variables (Næsset, 2002; Maltamo et al., 2006; Martinuzzi et al., 2009). Airborne lidar can be used to directly measure the three-dimensional structure of terrestrial and aquatic

ecosystems across large spatial extents (Lefsky et al., 2002a). They provide a superior choice for remote-sensing of AGB compared to passive optical sensors that suffer from saturation in spectral response to dense canopies with high biomass. Discrete-return airborne lidar data produce three-dimensional characterizations of objects in the form of point clouds that are defined by precise x, y and z coordinates. They also help characterize the reflectance and surface properties of intersected objects by providing intensity values, which are a measure of return-signal strength, for each point.

The use of airborne discrete-return lidar to predict AGB, both live and dead, has received much attention. The methods can be separated into individual-tree and plot-based assessment (Reutebuch et al., 2005). Individual-tree AGB assessments seek to delineate individual trees and then estimate their biomass based on lidar-derived metrics (e.g., tree height, crown width, diameter at breast height (DBH)) (Bortolot & Wynne, 2005; Popescu et al., 2007; Zhao et al., 2009). The use of individual-tree methods has been restricted due to limitations. A significant limitation is associated with individual-tree segmentation and location algorithms. These algorithms are generally limited in their ability to locate intermediate and suppressed trees, trees in tight clusters, and trees located in stands with dense canopies (Maltamo et al. 2000). Additionally, stem identification algorithms are difficult to parameterize and are complicated by scale and adjacency effects (Holmgren, 2004,

Bortolot & Wynne, 2005; Zhao et al., 2009). Until these limitations can be overcome the use of the individual-tree based assessments will continue to be limited.

Plot-based AGB lidar assessments have been more common, because they have proven to accurately estimate and predict plot-level biomass in variable conditions. These methods derive a myriad of plot-level lidar point cloud metrics, which quantify canopy characteristics of individual point clouds (e.g., canopy point density above certain height thresholds, canopy point height percentiles, variability of canopy point heights). These metrics are then used as explanatory variables in linear and nonlinear regression analysis settings to estimate field measured AGB (Lim et al., 2003). Results have been promising in all cases using this method (Kim et al., 2009; Lefsky et al., 1999; Lim & Treitz, 2004; Means et al., 2000; Nelson et al., 2004). After model validation, the regression models are applied to the rest of the lidar dataset to predict AGB across the landscape using the two-stage procedure outline in Næsset (2002).

Most studies using the plot-based method to estimate AGB have combined live and dead tree biomass. Few studies have focused on separating the two, even though they play different roles in the carbon cycle (Siccama et al., 2007). Kim et al. (2009) successfully differentiated and estimated live and dead AGB using commonly used lidar canopy metrics derived from intensity stratified lidar point clouds. They found that point clouds containing only first-return lower intensity values estimated

dead AGB better than point clouds containing only high intensity values or point clouds containing both (i.e., all points included). The opposite was true for live AGB estimation were high intensity value point clouds performed the best. All other studies using the plot-based lidar method to estimate live, dead or combined AGB used the entire plot-level point cloud without any intensity or other stratification (Lefsky et al., 1999, Nelson et al., 2004).

Intensity values are an often underexploited feature of lidar data, due to difficulty and variability associated with acquisition settings and calibration (Wing et al., in review (a)). It is primarily a measure of surface reflectance and is a function of the wavelength of the source energy, path distance, and the composition and orientation of the surface or object which the laser pulse intersects (Boyd & Hill, 2007). The quality of the intensity value data is dependent upon lidar acquisition parameters and calibration techniques, which has resulted in a broad range of qualities and limited its use. Even with the difficulties, intensity has been used successfully in many forestry applications to differentiate between tree species, estimate live and dead biomass, and predict basal area (Donoghue et al., 2007; Holmgren & Persson, 2004; Hudak et al., 2006; Kim et al., 2009; Lim et al., 2003; Wing et al., in review (b)). Most recently, Wing et al. (in review (b)) utilized intensity values to filter and identify individual lidar points associated with dead trees and remove points associated with live trees from point clouds, with promising results. The

filtered point cloud was then used to identify and measure individual snags with an overall detection rate of 70.6% (±2.7%) for dead trees ≥ 38 cm in DBH. The study cited the possibility of reversing the filters results to create a live-tree point cloud by removing the dead-tree identified points and restoring points that were eliminated during the filtration algorithm. Canopy lidar metrics derived using this live-tree point cloud should, in theory, predict live tree attributes (e.g., live AGB) more accurately than traditional plot-level derived metrics that use the entire point cloud, since most points associated with dead trees are removed.

This study tests this theory by comparing the prediction and explanatory power of traditional lidar-derived canopy metrics created using three different point clouds to predict live ABG. The three point clouds used to create the metrics were as follows: one containing all first-return points (traditional), one containing filtered first-return live-tree points using the algorithm described in Wing et al. (in review (b)) (live-tree), and one containing only first-return points meeting live vegetation criteria intensity values (vegetation-intensity). The objectives of this study were to: 1) develop regression equations to predict live AGB from discrete return lidar data using the three different point cloud metric sets, and 2) examine and compare the results of the three point cloud metric set models in their ability to predict live AGB.

Materials and Methods

Study Area

The study was conducted at Blacks Mountain Experimental Forest (BMEF) located in northeastern California (Figure 4.1). BMEF (40°40´N, 10 121°10´W), managed by the USDA Forest Service Pacific Southwest Research Station, is located approximately 35 km northeast of Mount Lassen Volcanic National Park and ranges between 1700 and 2100 m elevation. Stands are dominated by ponderosa pine (*Pinus ponderosa* Dougl. ex P. & C. Laws) with some white fir (*Abies concolor* (Gord. & Glend.) Lindl.) and incense-cedar (*Calocedrus decurrens* (Torr.) Florin) at higher elevations. At lower elevations, Jeffrey pine (*Pinus jeffreyi* Grev. & Balf.; Oliver, 2000) can also be found in some stands. Classified as an interior ponderosa pine forest type (Forest Cover Type 237) (Eyre 1980), the 4,358 ha forest has a wide range of stand conditions as a result of past research and management activities, as well as disturbance events (Ritchie et al., 2007).

As part of a large-scale, long-term interdisciplinary experimental design at BMEF initiated in 1991, two contrasting stand structures were created: low structural diversity (LoD) and high structural diversity (HiD) (Oliver, 2000). LoD stands were thinned to maintain a single canopy layer of intermediate trees, with the goal of simplifying forest tree structure. At the time of treatment implementation, stands were thinned to a uniformly spaced density of approximately 40 trees ha^{-1},

maintaining trees with heights ranging between 12 to 30 m and crown ratios generally greater than 50%. At the time of the study, LoD stand densities ranged from 25 to 430 trees ha^{-1} based on plot-level data (DBH > 9cm). In contrast, the HiD units retained all canopy layers, which resulted in stands that feature multiple age classes and varying crown structures (Oliver, 2000). All large old trees were maintained with one smaller tree retained within the larger tree's crown circumference. Tree densities ranged from 60 to 95 trees ha^{-1} at initial implementation and ranged from 90 to 1400 trees ha^{-1} at the time of our study based on plot-level data (DBH > 9 cm). Plots with higher tree densities are associated with a few spatially scattered dense thickets (0.4-0.8 ha) containing smaller trees that were left as part of the HiD prescription.

Six research units each were randomly assigned from both the LoD and HiD treatments ranging in size from 77 to 144 ha. Each unit was then split in half with one randomly assigned half receiving prescribed fire treatments (Figure 4.1). Due to the large unit size, treatment implementation took several years. The three individual treatment blocks, each with four units, were created in 1996, 1997, and 1998, respectively.

Also included at BMEF, are four research natural areas (RNA) each approximately 40 ha in size (RA, RB, RC, RD). The RNAs were set aside to serve as unmanaged, qualitative controls representative of the interior ponderosa pine type.

They have never received mechanical treatment, but fire exclusion has greatly increased their understory tree densities. Two of the four RNAs (RB & RC) received one application of prescribed fire in the late 1990's. RNA stand densities ranged from 420 to 1220 trees ha^{-1} for trees ≥ 9 cm DBH at the time of the study.

As part of the experimental design all 16 research units at BMEF have permanently monumented grid markers located within them on a 100 x 100 m lattice pattern. The permanent grid markers serve as the center points for most all of the plot level research being conducted on the forest. Each grid was located by conventional survey methods using the High Precision Geodetic Network along with survey grade GPS (location error: ±15 cm) (Oliver, 2000). These provide a solid foundation to conduct aerial lidar research, because plot location errors are minimized.

Field Data

At BMEF, five of the LoD units, six of the HiD units and 2 randomly selected RNAs (RC & RD) were sampled in July 2009. Standing live and dead tree (DBH ≥ 9 cm) stand attributes for all three structure types at the time of the study are summarized in Table 4.1. Using the BMEF permanent grid system, plot locations were assigned systematically with a random start within each unit on every other grid point in all intercardinal directions (282 m spacing). At each selected grid point location an 805 m^2 circular plot was established. All trees with a DBH ≥ 9 cm were mapped from plot

center and measured for height, DBH, crown width, and height to live and dead crown. The stem map data were used for verification of plot locations. Trees were also assigned codes for various tree conditions (i.e., broken, dead or forked top, branching anomalies, mistletoe presence, etc.). Trees having DBH ≥ 60 cm were also assigned vigor condition class ratings using the systems developed by Ferrell (1989) for fir and cedar species, and Salman and Bongberg (1942) for pine species. The classification systems resulted in individual tree vigor risk ratings ranging from 1 to 3 for the fir and cedar species and 1 to 4 for pine species, with higher risk ratings associated with declining tree vigor.

Field Derived Biomass

The generalized national allometric equation of Jenkins et al. (2003) was used to calculate live tree biomass (dry weight) for individual trees and then expanded to plot-level. The Jenkins et al. (2003) equation (1) has separate parameter values for ten tree species groups (5 softwood, 4 hardwood, and 1 woodland) (Table 4.2).

(1)

where, is the individual tree biomass in kg for trees 2.5 cm and larger, and are species specific parameters for estimating biomass (Table 4.2), and is the individual tree's diameter at breast height (cm). Individual tree biomass corrections were applied to trees with broken or dead tops, raked off branches, and sparse

crowns. Plot-level live tree biomass was computed in Mg ha^{-1}. Live AGB for the three different treatments (i.e., LoD, HiD, RNA) is summarized in Figure 4.2.

Lidar Data

Discrete multiple return airborne lidar data were provided by Watershed Sciences Inc. in LAS file format (version 1.1). The lidar data was acquired in late July 2009 using a Leica ALS50 Phase II laser system mounted on a fixed wing aircraft. The aircraft was flown at 900 m above ground level following topography. Data were acquired using an opposing flight line side-lap of ≥ 50% and a sensor scan angle ± 14-degrees from nadir to provide good penetration of laser shots through the canopy layers. On-ground laser beam diameter was approximately 25 cm (narrow beam divergence setting), which resulted in a very low percentage of multiple returns (9.2%) and a very high percentage of single returns (81.4%). The high ratio of first and single returns (90.8%) helped provide better quality intensity information, because calibration problems associated with laser pulse energy are reduced for these returns (see: Morsdorf et al., 2010). An average of 6.9 points m^{-2} was obtained for the entire study area, with a standard deviation of 5.6 points m^{-2}. Ground survey data were collected to enable the geo-spatial correction of the aircraft positional coordinate data collected throughout the flight, and to allow for quality assurance checks on final LiDAR data products. Simultaneous with the airborne data collection mission, multiple static (1 Hz recording frequency) ground surveys were conducted over

monuments with known coordinates to enable geo-spatial data correction. Indexed by time, these GPS data were used to correct the continuous onboard measurements of aircraft position. To enable assessment of LiDAR data accuracy, ground truth points were collected using GPS based real-time kinematic (RTK) surveying.

The vendor post-processed lidar data using automated methods that utilized proprietary software (TerraScan) coupled with manual methods to identify ground points for development of the digital terrain model (DTM). Fundamental vertical DTM accuracy for BMEF was approximately 15 cm at a 95% confidence level. The vendor used an automatic variable gain setting during acquisition and did not calibrate the intensity values post-acquisition. Point clouds corresponding to the 805 m^2 circular plots were extracted and their heights were normalized using the DTM. All plot locations were manually inspected using the field-based stem map and the plot lidar point clouds. Only one plot needed a location adjustment (less than 1.5 m).

The individual plot lidar data was then used to create the three different point clouds used in the analysis. Only first and single returns were used in all three point clouds for three reasons: 1) these returns have been employed to predict biomass in previous studies (Kim et al., 2009, Lim et al., 2004), 2) the intensity filtering method used to create the live-tree point cloud needed to use these returns to ensure good results, and 3) the proportion of multiple returns for this lidar acquisition was very low due to the small laser footprint size (9.2 %). The first point cloud (traditional) was

created by extracting all first and single return points with no stratification based on intensity. This point cloud is traditionally the one utilized to derive lidar plot-level metrics in most previous studies for estimation of numerous forest attributes including biomass. The second point cloud (live-tree) was created using the individual-point local-area intensity filtering algorithm developed by Wing et al. (in review (b)). In the method, individual first- and single- return points are evaluated using a series of filtration steps that identify individual points associated with dead trees. As a by-product of the method individual points associated with live trees were also identified and removed from the point cloud by forcing their individual height values (h-values) to zero. To create the live-tree point cloud, the removed live-tree points were restored to the point cloud by restoring their original height values (h-values) and the identified dead-tree points were removed by forcing their h-values to zero. The end result is a plot-level point cloud containing points that are more than likely associated with live trees along with understory and ground points (heights < 2 m). The third point cloud (vegetation-intensity) was created using the live vegetation intensity value thresholds identified in Wing et al. (in review (b)). These are points that have intensity values more than likely associated with live vegetation (e.g., leaves and needles). Points with intensity values greater than or equal to the lower intensity threshold and less than or equal to the upper intensity threshold using equations (2) and (3) were kept, while all values not meeting these criteria were

removed. The final results were three separate point clouds for each plot that were then used to derive plot-level lidar metrics.

(2)

(3)

Where, is the lower intensity threshold, is the upper intensity threshold, and is the maximum intensity value associated with individual plot point cloud being examined. The multiplication factors (0.35 & 0.65) were determined through visual inspection, and trial and error.

Lidar-Derived Metrics

Various lidar-derived metrics were created from each plot-level point cloud to estimate plot-level biomass (Table 4.3). Lidar point height distributions were created using all first- and single- return points > 2 m for each plot-level point cloud. The 2 m threshold was used to ensure no understory points would be included in the analysis. A large number of metrics were derived from these distributions. From previous studies the following distributional metrics were created; 1) the height quantiles corresponding to the 0, 10, 20, 25, 30, …, 99 percentiles of the distributions, 2) the minimum, maximum and mean heights; and 3) the standard deviation and coefficient of variation for the heights. Furthermore, several canopy density metrics were derived, calculated as the proportion of points above certain height thresholds. The

following canopy density metrics were created: 1) the proportion of points > 5, 10, 15, and 20 m, 2) the proportion of points above the mean and mode values, and 3) the proportion of points above the understory layer (> 2 m), also referred to as canopy cover. One last metric was created which has shown promise in previous studies in the estimation of biomass. Often referred to as lidar canopy volume, it was created by multiplying the canopy cover value by the mean height.

Model Formation and Comparison

A multiple linear regression analysis was used to assess relationships between the lidar-derived metrics and field measured biomass estimates. In the multiple regression analysis, multiplicative models were estimated as linear regressions in the natural logarithmic scale, because such models were found to be suitable based on preliminary analysis and from previous studies estimating volume and biomass using the same or similar variables (Næsset, 1997; Næsset, 2002). The linear regression model was formulated as:

(4)

where, ABG is above ground biomass (Mg ha^{-1}), are parameter regression coefficients, and the individual parameters are the lidar derived metrics.

Stepwise selection was used to identify final model variables for each lidar-derived metric dataset. No predictor variable was included in the model with a partial *F* statistic with a significance level greater than 0.05. Since all variables are related to point height, the likelihood of variable correlation is high. All variables were assessed for multicollinearity using variance inflation factors (VIF). VIFs quantify how much the variance of the estimated regression coefficient is inflated by the existence of correlation among the remaining predictor variables in the model (Marquardt, 1970). A VIF of 1 means that there is no correlation among the predictor and the remaining predictor variables, and hence the variance of is not inflated at all. The general rule of thumb is that VIFs exceeding 4 warrant further investigation, while VIFs exceeding 10 are signs of serious multicollinearity requiring correction. Models containing multiple predictor variables were required to have VIFs less than 4.

In addition to the multivariate models, a single predictor variable model was identified for each of three lidar-derived datasets. It was found in preliminary analysis that all models selected the same variable as the most significant predictor; therefore these single models were added to the analysis to simplify the comparison between the three sets of lidar-derived metrics.

All BMEF treatment plots were combined for the regression analysis (n = 154). Models were fit to the entire dataset using each set of lidar-derived metrics individually (i.e., traditional, live-tree, vegetation-intensity). In addition, a secondary dataset was constructed to aid with comparison between the three different lidar-derived metric sets. Plots containing dead trees that were detected using the filtering method outlined in Wing et al. (in review (b)) and meeting specific snag criteria were used as a secondary model dataset (henceforth referred to as: detected snag dataset). Plots meeting either one of the following snag criteria were utilized in the detected snag dataset: 1) at least one detected dead tree with a DBH ≥ 25 cm, or 2) a cumulative detected dead tree plot biomass ≥ 0.3 Mg ha^{-1}. There were 53 plots meeting these criteria. This dataset aided the comparison by focusing the model analysis on plots where the three lidar-derived metric sets should vary the most.

The above criteria resulted in twelve models used for comparison, six each for the two datasets. Models were compared using traditional model fit and selection statistics, as well as a cross validation procedure. Traditional model fit statistics included the coefficient of determination (R^2), root mean square error (RMSE), Akaike's information criterion (AIC), and the Bayesian information criterion (BIC). No independent data were available to assess the prediction accuracy of the estimated regression equations. A leave-one-out cross validation procedure was therefore used to assess prediction accuracy. In the procedure, one of the sampled plots was

removed from the dataset at a time, and the selected models were fit to the data from the remaining sample plots. Biomass was then estimated for the removed plot using these models. When converting log-linear equations back to the original scale a bias will be introduced (Goldberger, 1968). Therefore, it was essential to apply a bias correction when converting the values back into the original scale. An approximate and simple correction that will introduce an error of less than 1% is to add half the model variance to the regression intercept before conversion (Flewelling & Pienaar, 1981). This correction factor was used to reduce the conversion bias. The cross validation statistics used for comparison were absolute bias (AB) and root mean squared error (RMSE) calculated using the following formulas:

(5)

(6)

Results

Final Models

The final twelve models are summarized in Table 4.4, with coordinating fit and selection statistics. All models performed well in the estimation live AGB (R^2 > 0.85). All model fits found the lidar canopy volume metric (VolCov) to be the most

significant variable in estimation of live AGB biomass. No multiple variable models were identified for either the traditional or live-tree metric sets due to significant variable interactions (VIF > 4). Differences between single predictor variable models using VolCov and multiple variable models were low for all lidar-derived metric sets. The RMSE ranged from 24.3 to 30.7 Mg ha^{-1} for the all plot model fits and 16.0 to 22.1 Mg ha^{-1} for the detected snag model fits. Multiple variable models contained no more than three significant predictor variables, which were often associated with either the lower or upper portion of the canopy distribution.

The live-tree lidar-derived metric models had the highest coefficient of determination, and lowest RMSE, AIC, and BIC values compared to all other models for both datasets ($LT1_{ab}$, $LT2_a$, $LT2_b$). Model fit statistics can only be compared using identical datasets (i.e., the all plots dataset models cannot be compared with the detected snag dataset models). Traditional models ($T1_{ab}$, $T2_a$, $T2_b$) performed similar to the vegetation-intensity models ($V1_a$, $V1_b$, $V2_a$, $V2_b$) for both datasets. In terms of RMSE the traditional models outperformed the vegetation-intensity models, while the vegetation-intensity models had lower overall AIC and BIC values for both datasets. The vegetation-intensity models also had the highest RMSE for both datasets.

The most significant differences between models were found for the detected snag dataset. The AIC and BIC decreased by -36.8 and -18.1 respectively when

switching from the traditional to the live-tree lidar-derived metric models, while RMSE decreased by more than 3 Mg ha^{-1}. For the all plots dataset the relationship was also prevalent, with AIC and BIC value reductions of 43.4 and 39.7 respectively and a RMSE reduction of 0.8 Mg ha^{-1}.

Scatter plots for all six single variable models are presented in Figure 4.3. Errors located below the trend lines were typically associated with the presence of dead tree biomass. These errors were reduced for both the live-tree and vegetation-intensity models compared to the traditional models, with the former performing the best. Three of the four largest errors below the trend line for the $LT1_{ab}$ model were associated with plots that had dead trees that were undetected using the filtering algorithm. The remaining error seemed to be caused by a large number of trees located directly outside that plot's boundary, with their crowns extending into the plot. Errors occurring above the trend line were typically associated with denser areas where biomass was over predicted.

Cross Validation

The leave-one-out cross validation results are summarized in Table 4.5. All models performed well in the prediction of live AGB (RMSE < 9% of the estimated biomass). The live-tree models performed the best overall, with an overall RMSE of 7.3% for the all plots dataset ($LT1_{ab}$) and a RMSE of 5.4% for the detected dead tree (snag) dataset ($LT2_a$). The difference between the traditional models and the live-tree

models was negligible for the dataset using all plots (RMSE $LT1_{ab}$: 7.3% versus $T1_{ab}$: 7.5%), while much more pronounced for the detected snag dataset (RMSE $LT2_a$: 5.4% versus $T2_a$: 6.8%). The vegetation-intensity models performed the poorest overall for both datasets.

Absolute bias was similar for the all plot models, and higher for the traditional and vegetation-intensity models using the snag detection dataset. The traditional and vegetation-intensity models both had a negative AB greater than 1 Mg ha^{-1} for the detected dead tree dataset, while the live-tree models had AB values closer to zero.

Discussion

Model Comparison

The live-tree lidar metric models successfully reduced prediction model variation for live AGB compared to models based on traditional point cloud lidar metrics. This confirms that filtering and removing dead tree points from plot-level point clouds can provide more accurate lidar metrics for prediction of live AGB. The results will likely extend into the prediction of other live tree attributes, as well. While differences between the live-tree and traditional lidar metric models were less significant when all plots were analyzed, the live-tree model still performed better based on the model selection statistics and the cross validation results. The differences between the two sets of lidar metrics will depend upon dead tree

density. In areas with higher densities of dead trees the difference will become more pronounced, with the live-tree metrics performing better.

Vegetation-intensity metrics performed similar to the traditional metrics, although variability came from different sources. The vegetation-intensity metrics were able to reduce the variability associated with dead trees, but overall variability was not reduced. Live trees have a significant number of points meeting the live vegetation intensity criteria used for stratification, but they also have a large proportion of low intensity points resulting from lidar pulses intersecting branches or other solid wood surfaces. These points were often removed using the live vegetation intensity thresholds, which likely caused the extra variation. If the lower intensity value threshold was relaxed it might perform better, since fewer live tree points would be eliminated. The vegetation-intensity metrics are easier to create compared to the live-tree metrics, so if new threshold values can be identified that produce similar results, the vegetation-intensity metrics would increase the method's efficiency.

According to both AIC and BIC model selection criteria, the live-tree models provided the strongest evidence for selection for both datasets. According to Raferty (1995) and Kass and Raferty (1995), a difference in BIC values (ΔBIC) of ≤ 2 between models is "not worth more than a bare mention" and a ΔBIC > 10 implies very strong evidence that the models are different. The same general trend holds for the

difference in AIC values according to Burnham and Anderson (2002). AIC and BIC values are not directly comparable since they have different target models (Reschenhofer, 1996). With this in mind, both AIC and BIC model selection criteria provided strong support for the live-tree models, with both AIC and BIC value decreases of > 10 when compared to the other two model types.

This study adds to the growing research highlighting the ability of canopy lidar-derived metrics to accurately predict standing tree forest attributes. The most significant variable in all but one model was lidar canopy volume (VolCov), demonstrating the strong relationship between VolCov and AGB (Figure 4.3). This relationship has been found in previous studies estimating AGB as well (Kim et al., 2009; Lefsky et al., 2002b). The metric has the ability to accurately characterize and summarize the unique attributes associated the canopy layer. When the variable was removed from the model selection process, it was typically replaced by a combination of a canopy density and height metrics, most often by the two variables used in the creation of the VolCov metric (e.g., canopy cover and mean height).

Future Developments

In the future, new point cloud filtering techniques are likely to improve lidar-derived prediction models. Filtering individual points will aid in the creation of more accurate lidar explanatory metrics for a myriad of forest attributes. The filtering algorithm used to create the live-tree point cloud utilized lidar point location and

intensity value attributes to identify points associated with dead trees. As such, the usefulness of intensity information to help characterize forest attributes is dependent upon the quality of the intensity information. The intensity data in this study did not receive post-acquisition calibration, which should improve filtering results. Incorporating airborne lidar with other remote sensing techniques such as aerial photography, or utilizing small-footprint full-waveform (SFFW) airborne lidar could also enhance the ability to filter lidar points. SFFW airborne lidar provides more than just coordinate and intensity information, it also provides echo width information. Echo width information has proven to be useful for classifying ground and vegetation returns and warrants investigation (Ducic et al., 2006; Wagner et al., 2008).

The filtering algorithm attempted to identify live tree lidar points and remove dead tree points. Not all dead trees points were removed using the filtering method, which likely caused some of the variability in the live-tree models. Another identified source of variability was found when trees located just outside plot boundaries had crowns overlapping into the plot-level point cloud. In these cases points not associated with measured trees are used when deriving the lidar metrics. These instances are always likely to occur, but their impact could be reduced by developing a filtering algorithm that identifies and eliminates them, or by using a weighted point

structure that gives less weight to points located near plot boundaries. If either of these is successfully implemented, variability should be reduced further.

Applications

Application of a prediction model to forest stands can be completed following the traditional airborne lidar two-stage plot-based gridding procedure outlined in Næsset (2002). In this procedure, stands of interest meeting the model criteria are first divided into grid cells that match the prediction model's plot size. Then significant independent variable values are obtained for each grid cell and the prediction model is applied using weights for each grid cell to minimize edge bias associated with the smaller boundary-edge grid cells. Upon completion a raster dataset is created where every 805 m^2 grid cell contains a live AGB prediction. These can be used to obtain accurate predictions of live AGB across entire landscapes, while also providing the ability to assess the spatial arrangement of the biomass.

Extension of the method to different forest types warrants further investigation. The results will depend on the filtering algorithms ability to identify live and dead trees points. Three key components affecting the algorithms ability to do so are: 1) the quality of the intensity information, 2) lidar point density, and 3) canopy cover. The quality of intensity information directly affects the ability of the algorithm to distinguish between live and dead tree points. Currently, most airborne lidar acquisitions use the automatic variable gain setting to compensate for changes in

ground reflectance and do not apply any post acquisition calibration. This type of acquisition should provide adequate intensity calibration for accurate differentiation between live and dead tree points. The algorithm also does not perform as well when lidar point densities are less than 4 points m^{-2} or in forests with dense canopy covers (> 70%). Filtering becomes more difficult in these situations because it is harder to distinguish unique forest structures. A number of parameters used in the filtering algorithm also might need adjustment for different lidar datasets (Wing et al., in review (b)).

Conclusions

This study highlights the ability of filtered lidar point clouds to produce higher quality lidar-derived explanatory variables for the prediction of live AGB. The method should also extend into the prediction of other live tree attributes with similar results. While the filtering method used to identify individual live tree points was successful and provided a more accurate prediction model, it can likely be improved by developing more accurate point filtering methods. Filtering methods in the future should focus on identifying live and dead tree points more accurately and removing points associated with tree crowns originating from trees outside the plot. This should result in even more accurate predictions.

The results from this study can be used to create accurate live AGB maps for the interior ponderosa pine forest type. Extension of the method to additional forest

types warrants further investigation and the results will likely depend on tree density (i.e., canopy cover) and the quality of the lidar data (i.e., point density and intensity calibration). Filtering lidar points to help estimate and predict forest attributes warrants further investigation.

Acknowledgements

This study was funded through a cooperative agreement between Oregon State University and the U.S. Forest Service Pacific Southwest Research Station. The author gratefully acknowledges the field work and additional help of Thomas Fisher, David McClung and Travis Springer.

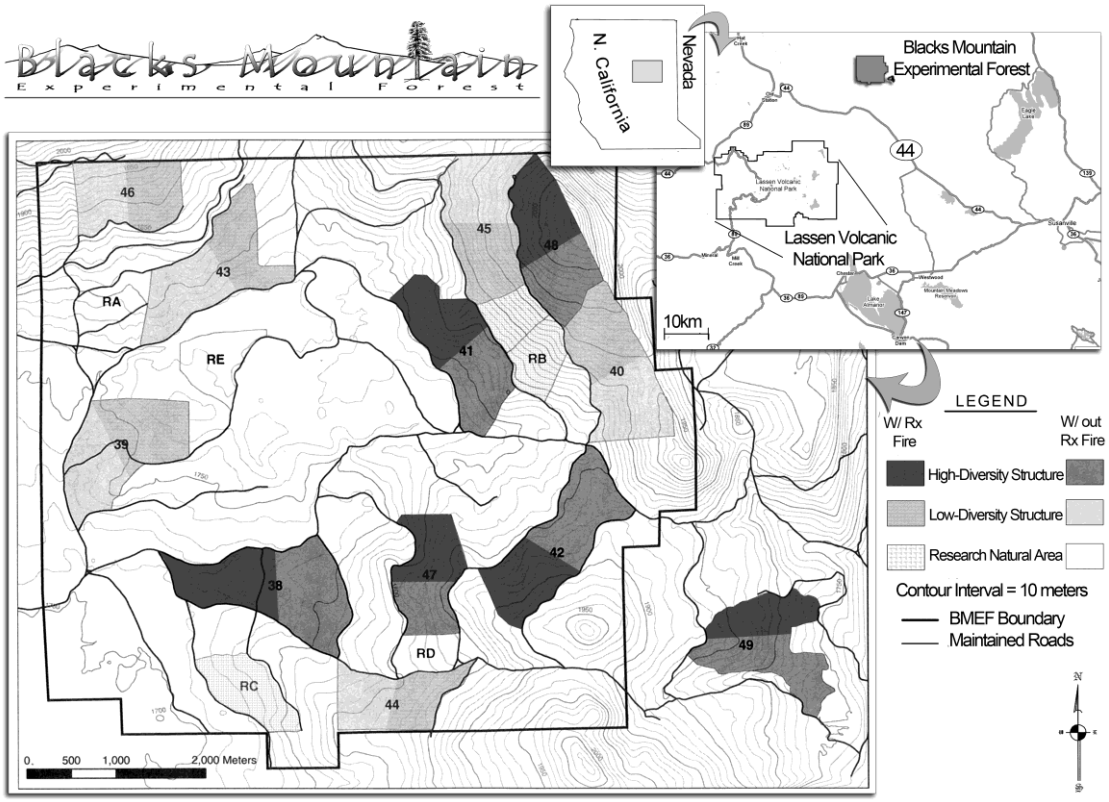

Figure 4.1: Geographic location of the Blacks Mountain Experimental Forest and layout of the Blacks Mountain Long-Term Ecological Research Project in northeastern California.

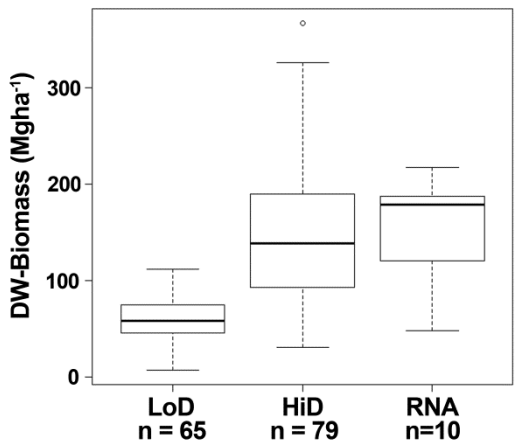

Figure 4.2: Live tree (DBH > 9 cm) oven dry weight above ground biomass summary from all plots per treatment type (LoD, HiD, RNA) at BMEF.

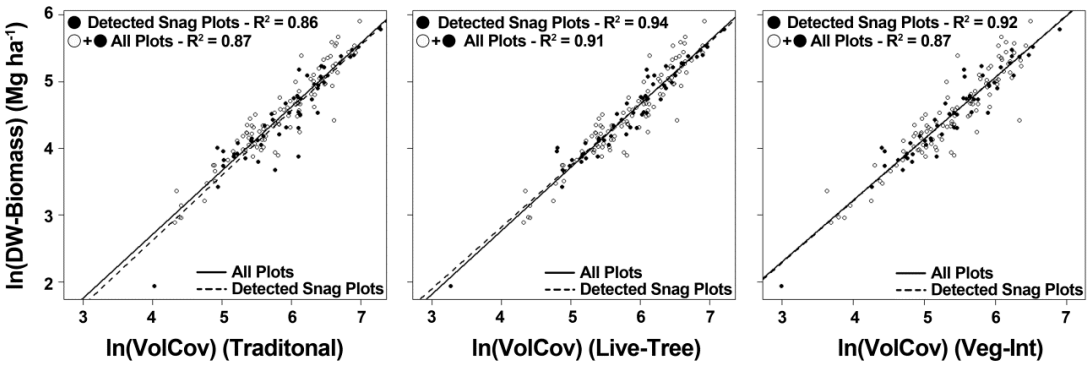

Figure 4.3: Lidar canopy volume (VolCov) versus field estimated live above ground biomass for the three different sets of lidar-derived metrics (Traditional, Live-Tree, and Vegetation-Intensity).

Table 4.1: Standing live and dead tree (DBH ≥ 9 cm; Heights ≥ 3 m) attributes from all plots per treatment type (LoD, HiD, RNA) at BMEF (n_s = number of snags; n_p = number of plots; sd = standard deviation).

		DBH (cm)			Tree Height (m)				Trees per Hectare		
	n_s	Range	Mean	sd	Range	Mean	sd	n_p	Range	Mean	sd
Live											
Overall	3819	(9.0 - 135.1)	25.6	15.4	(1.8 - 41.4)	12.4	6.3	154	(24.7 - 1469.7)	306.3	238.6
LoD	1081	(9.0 - 83.1)	26.6	9.4	(2.1 - 26.2)	11.9	4.4	65	(24.7 - 432.3)	205.4	81.9
HiD	2183	(9.0 - 135.1)	26.4	18.0	(1.8 - 41.5)	12.9	7.1	79	(86.5 - 1469.7)	341.3	259.6
RNA	555	(9.1 - 88.9)	20.8	12.8	(2.4 - 37.2)	11.1	5.9	10	(358.2 - 1222.7)	685.4	302.5
Dead											
Overall	344	(9.0 - 122.2)	27.2	21.2	(3.0 - 42.7)	10.5	6.6	154	(0.0 - 284.1)	27.6	41.2
LoD	73	(9.0 - 94.7)	31.1	22.0	(4 - 31.4)	10.8	5.5	65	(0.0 - 86.45)	13.9	20.5
HiD	216	(9.0 - 95.8)	26.7	21.3	(3.0 - 42.7)	10.3	6.7	79	(0.0 - 284.1)	33.8	50.4
RNA	55	(9.0 - 122.2)	23.6	21.4	(3.05 - 34.8)	10.8	7.7	10	(24.7 - 111.2)	67.9	31.4

Table 4.2: Parameter values used for the biomass equation (Jenkins et al., 2003). R^2 is the coefficient of variation model statistic calculated using the number of data points generated from the published equations for parameter estimation.

Species Name	β_0	β_1	R^2
Abies concolor	-2.5384	24814	0.992
Pinus ponderosa	-2.5356	2.4349	0.987
Pinus jeffreyi	-2.5356	2.4349	0.987
Calocedrus decurrens	-2.0336	2.2592	0.981

Table 4.3: Plot-level lidar-derived explanatory variables (metrics) used in regression analysis (h subscript stands for height).

Variables	Description
$P01_h$	1st percentile height (m)
$P05_h$	5th percentile height (m)
$P10_h$	10th percentile height (m)
$P20_h$	20th percentile height (m)
$P25_h$	25th percentile height (m)
$P30_h$	30th percentile height (m)
…	…
$P99_h$	99th percentile height (m)
Min_h	minimum height (m)
Max_h	maximum height (m)
$Mean_h$	mean height (m)
$Mode_h$	mode height (m)
SD_h	standard deviation of heights (m)
CV_h	coefficient of variation of heights (m)
$D5_h$	proportion of points above 5 m (%)
$D10_h$	proportion of points above 10 m (%)
$D15_h$	proportion of points above 15 m (%)
$D20_h$	proportion of points above 20 m (%)
DM_h	proportion of points above the mean height (%)
DMd_h	proportion of points above the mode height m (%)
CC_h	proportion of points above 2 m (%)
VolCov	lidar canopy density (CC_h x $Mean_h$)

Table 4.4: Final regression model parameters with fit and selection statistics for the two datasets (all plots and detected snag plots). Model T = traditional lidar point cloud metrics; Model LT = live-tree point cloud metrics; Model V = vegetation-intensity point cloud metrics; a = final model; b = single variable model; VIF = variance inflation factor.

	Model	Parameters	β	SE	VIF	R^2	RMSE (Mg ha^{-1})	AIC	BIC
All Plots (n = 154)	$T1_{ab}$	Intercept	-1.12	0.17	-	0.874	26.9	-7.3	1.8
		VolCov	0.96	0.03	-				
	$LT1_{ab}$	Intercept	-1.04	0.15	-	0.905	26.1	-50.7	-41.5
		VolCov	0.95	0.02	-				
	$V1_a$	Intercept	-0.81	0.17	-	0.885	28.0	-18.6	-6.4
		VolCov	0.80	0.04	2.09				
		$P90_h$	0.33	0.08	2.09				
	$V1_b$	Intercept	-0.46	0.16	-	0.870	30.7	-4.3	4.9
		VolCov	0.92	0.03	-				
Detected Snag Plots (n =53)	$T2_a$	Intercept	-0.85	0.32		0.888	20.3	-0.5	7.4
		VolCov	1.19	0.08	2.46				
		$P95_h$	-0.56	0.15	2.46				
	$T2_b$	Intercept	-1.28	0.33		0.859	20.9	10.1	16.0
		VolCov	0.97	0.06					
	$LT2_a$	Intercept	-0.21	0.37		0.942	17.0	-34.6	-26.8
		VolCov	0.89	0.04	1.37				
		Min_h	-0.57	0.27	1.37				
	$LT2_b$	Intercept	-0.88	0.20		0.936	17.3	-32.1	-26.2
		VolCov	0.92	0.03					
	$V2_a$	Intercept	-0.15	0.25		0.924	21.7	-18.8	-9.0
		DM_h	0.97	0.06	1.29				
		$P95_h$	0.67	0.10	1.59				
		$P25_h$	0.18	0.08	1.31				
	$V2_b$	Intercept	-0.50	0.21		0.916	22.1	-17.2	-11.3
		VolCov	0.93	0.04					

Table 4.5: Live above ground biomass leave-one-out cross validation summary statistics for all models using both datasets (all plots (n = 154), and detected snag plots (n = 53)). Model T = traditional lidar point cloud metrics; Model LT = live-tree point cloud metrics; Model V = vegetation-intensity point cloud metrics; a = final model; b = single variable model; RMSE (%) = normalized root mean square for plot estimated biomass.

	Model	RMSE (Mg ha^{-1})	RMSE (%)	Bias (Mg ha^{-1})
All Plots (n = 154)	$T1_{ab}$	27.1	7.5	-0.20
	$LT1_{ab}$	26.2	7.3	0.27
	$V1_a$	28.6	7.9	-0.19
	$V1_b$	31.0	8.6	0.12
Detected Snag Plots (n = 53)	$T2_a$	21.8	6.8	-1.65
	$T2_b$	21.7	6.8	-1.72
	$LT2_a$	17.3	5.4	0.16
	$LT2_b$	17.8	5.6	-0.54
	$V2_a$	22.7	7.2	-1.30
	$V2_b$	23.2	7.3	-1.31

CHAPTER 5: CONCLUSIONS

The overall goal of this dissertation was to explore the use of airborne discrete-return lidar to both predict and identify important forest attributes. Chapter 2 presented a new method to predict understory vegetation cover; increasing model explanatory power compared to traditional models (R^2 value increases of ~0.35 to the 0.7-0.8 range). Chapter 3 presented a new method to identify and quantify snags which overcomes many common difficulties associated with snag quantification and also provides information on their spatial arrangement. Chapter 4 presented a method to reduce model variability for the prediction of plot-level live above ground biomass. All three chapters demonstrate the ability of airborne lidar data to accurately predict and identify important forest attributes. Intensity information proved to be extremely useful for filtering point clouds and identifying individual lidar points associated with unique forest attributes in all three chapters. The intensity filtering methods described in this dissertation are new to the literature, and provide an enhanced framework for analyzing lidar data.

The primary objectives of Chapter 2 were to: 1) analyze the potential of airborne lidar-derived metrics to estimate and predict understory vegetation cover; 2) explore the use intensity values to filter understory component lidar points, 3) compare two modeling approaches for prediction of understory vegetation cover using the airborne lidar-derived metrics, and 4) develop a practical method that

utilizes airborne lidar-derived metrics to predict understory vegetation cover. Understory vegetation cover has been difficult to estimate and predict, especially over large spatial extents. The method presented in Chapter 2 increased the ability to predict understory vegetation cover in interior ponderosa pine forests considerably (R^2 values increasing from 0.2-0.45 to 0.7-0.8). The new lidar-derived variable understory vegetation cover density (ULCD), created by filtering the plot-level understory lidar point cloud using intensity values, had a very strong relationship with understory vegetation cover. The intensity filter successfully removed a portion of the understory lidar points associated with non-vegetation understory components, which made the metric more accurate in the prediction of understory vegetation cover.

Both modeling approaches had similar results, and provided accurate predictions without introducing bias. The method worked well under different forest conditions in the interior ponderosa pine forest type. Results will likely be diminished in areas where understory vegetation grows underneath high canopy densities or in forests where the understory and overstory layers intermix. Extension of the method to other forest types and conditions warrants further investigation.

The primary objectives of Chapter 3 were to: 1) create an individual point-based local-area filtering algorithm that removed points associated with live trees, 2) apply an individual-snag detection method to the filtered point cloud and test the

detection and error rates associated with the method, and 3) test the method in various forest types and structures to determine applicability in different forest conditions. This was the first individual point-based local-area filtering algorithm used to identify individual points associated with snags and eliminate individual points associated with live trees. It demonstrated the potential to use intensity values and local-area statistics to characterize individual lidar points. Given that this was the first attempt at this type of point filtering algorithm, the method can likely be improved. The method presented in this study was able to accurately detect and locate a large proportion of snags in various forest types and conditions, with smaller snags (DBH < 38 cm, height < 9 m) being detected between 30-60% of the time, and larger snags (DBH > 38 cm, height > 9 m) being detected between 60-80% of the time. Snag detection rates increased as snag DBH and height increased and decreased as snag conditions decayed.

Detection rates were affected by a number of uncontrollable and controllable factors. Uncontrollable factors were associated with forest stand and individual snag characteristics, while controllable factors were associated with the quality of the lidar data and the individual-snag detection methods. The two primary outputs from this research are: 1) the ability to derive accurate snag density estimates in a practical and relatively simple manner, and 2) the ability to map individual snags across entire

landscapes. Both these outputs should provide useful tools for many forest management applications.

The primary objectives of Chapter 4 were to: 1) develop regression equations to predict live above ground biomass (AGB) using airborne discrete-return lidar-derived metrics from three separate plot-level point clouds, and 2) examine and compare the results of the three point cloud metric set models in their ability to predict live AGB. Models containing lidar metrics developed using the live-tree filtered point cloud provided the most accurate prediction of live AGB. The live-tree lidar metric models reduced prediction model variation compared to models based on traditional plot-level point cloud metrics. This result demonstrates the ability of filtered point clouds to produce more accurate lidar-derived explanatory variables when specific attributes are targeted. When predicting live AGB, the differences between the live-tree and traditional lidar metric sets will depend upon the dead tree density within the stand. In stands with higher densities of dead trees the difference will become more pronounced, with the live-tree metrics performing better.

All three chapters successfully utilized lidar point location and intensity values to filter points associated with targeted forest attributes (e.g., understory vegetation, live and dead trees). Thus, successful extension of these methods will be predicated on the quality of the intensity value information. The intensity values used in all three chapters did not receive post-acquisition radiometric calibration. If they had, the

results would likely improve. The lidar acquisitions used narrow laser beam divergence and automatic variable gain settings, which provided a large proportion of first- and single-returns and better calibrated intensity values. First- and single returns provide better quality intensity information and therefore should be used when filtering lidar points with intensity values. In the future, intensity calibration will likely become more common, which should increase the usefulness of intensity information. Even without post-acquisition calibration the intensity values used in this dissertation were able to adequately differentiate between points associated with solid wood and finer materials, such as photosynthetic vegetation and small branches.

While all three studies were successful in meeting their individual objectives, the results could be improved. In terms of lidar acquisition, increasing lidar point densities and calibrating intensity information should provide better results for all three studies. Higher point densities would provide more detailed information and increase the ability to develop more accurate lidar point filters. Lidar point filters can also be improved for all three chapters. Utilizing fine-scale local-area 3D voxels could provide the ability to more accurately filter lidar points and characterize forest attributes. Incorporating other remote sensing technology metrics, such as those produced from hyper- or multispectral imagery, might also enhance results. Another possibility warranting investigation is the use of small-footprint full-waveform

airborne lidar (SFFW). SFFW provides more than just discrete-return coordinate and intensity information, it also provides laser pulse echo width information. Echo width information has proven to be useful for classifying ground and vegetation returns, thus it could provide more information for differentiating between unique forest attributes.

This dissertation focused on the ability of airborne discrete-return lidar to characterize important forest attributes in both the overstory and understory with promising results. The innovative intensity based filtering techniques, demonstrated the ability of lidar intensity information to adequately differentiate between unique forest attributes. In the future, it is expected that airborne lidar data will continue to provide more useful tools and information for forest management and assessment. The technology provides the ability to accurately quantify many important forest attributes at fine-resolutions across large areas. This information can be used to enhance forest management decisions by providing more accurate and detailed information on the spatial arrangement of forest attributes. In the future, this information could also be used to assess achievement of forest management goals and objectives, and optimize forest planning to meet multiple objectives over time. It is expected that the use of airborne lidar for forestry applications will continue to accelerate in the future as the technology continues to evolve.

BIBLIOGRAPHY

Andersen, H-E., McGaughey, R.J., & Reutebuch, S.E. (2005). Estimating forest canopy fuel parameters using Lidar data. Remote Sensing of Environment, 94, 441-449.

Avery, T.E., & Burkhart, H.E. (1995). Forest measurements (4th ed.). New York: McGraw-Hill (pp.408).

Bate, L.J. (1995). Monitoring woodpecker abundance and habitat in the central Oregon Cascades. Moscow, ID: University of Idaho. M.S. thesis (pp. 116).

Bate, L.J., Garton, E.O., & Wisdom, M.J. (1999). Estimating snag and large tree densities and distributions on a landscape for wildlife management. Pacific Northwest Research Station, Portland, OR: US. USDA Forest Service General Technical Report PNW-GTR-425.

Bater, C.W., Coops, N.C., Gergel, S.E., LeMay, V., & Collins, D. (2009). Estimation of standing dead tree class distributions in northwest coastal forests using lidar remote sensing. Canadian Journal of Forest Resources, 39, 1080-1091.

Boddy, L., Frankland, J.C., & van West, P. (2008). Ecology of Saprotrophic Basidiomycetes. Amsterdam: Elsevier (pp. 386).

Bonham, C.D. (1989). Measurements for terrestrial vegetation. New York: John Wiley & Sons (pp.338).

Bortolot, Z., & Wynne, R.H. (2005). Estimating forest biomass using small footprint LiDAR data: An individual tree-based approach that incorporates training data. ISPRS Journal of Photogrammetry & Remote Sensing, 59(6), 342-360.

Boudreau, J., Nelson, R., Margolis, H., Beaudoin, A., Guindon, L., & Kimes, D. (2008). Regional aboveground forest biomass using airborne and spaceborne LiDAR in Québec. Remote Sensing of Environment, 112 (10), 3876-3890.

Boyd, D.S., & Hill, R.A. (2007). Validation of airborne lidar intensity values from a forested landscape using Hymap data: Preliminary analysis. IAPRS, XXXVI, Part 3/ W52.

Bull, E.L., Holthausen, R.S., & Marx, D.B. (1990). How to determine snag density. Western Journal of Applied Forestry, 5(2), 56-58.

Bull, E.L, Parks, C.G., & Torgersen, T.R. (1997). Trees and logs important to wildlife in the interior Columbia River basin. Pacific Northwest Research Station, Portland, OR: US. USDA Forest Service General Technical Report PNW-GTR-391.

Burnham, K.P., & Anderson, D.R. (1998). Model Selection and Inference: A Practical Information-Theoretical Approach. New York: Springer-Verlag (pp.353).

Bütler, R., & Schlaepfer, R. (2004). Spruce snag quantification by coupling colour infrared aerial photos and a GIS. Forest Ecology and Management, 195, 325-339.

Chen, J., Shiyomi, M., Yamamura, Y., & Hori, Y. (2006). Distribution model and spatial variation of cover in grassland vegetation. Grassland Science, 52, 167-173.

Chen, J., Shiyomi, M., Hori, Y., & Yamamura, Y. (2008a). Frequency distribution models for spatial patterns of vegetation abundance. Ecological Modelling, 211, 403-410.

Chen, J., Shiyomi, M., Bonham, C.D., Yasuda, T., Hori, Y., & Yamamura, Y. (2008b). Plant cover estimation based on the beta distribution in grassland vegetation. Ecological Research, 23, 813-819.

Clawges, R., Vierling, K., Vierling, L., & Rowell, E. (2008). The use of airborne lidar to assess avian species diversity, density, and occurrence in a pine/aspen forest. Remote Sensing of Environment, 112, 2064-2073.

Cohen, W.B., & Goward, S.N. (2004). Landsat's role in ecological applications of remote sensing. Bioscience, 54(6), 535-545.

Coops, N. C., Hilker, T., Wulder,W.A., St-Onge, B., Newnham, G., Siggins, A., & Trofymow, J.A. (2007). Estimating Canopy Structure of Douglas-Fir Forest Stands from Discrete-Return Lidar. Trees-Structure and Function, 21(3), 295-310.

Croft, F.C., Heller, R.C., & Hamilton, D.A. (1982). How to interpret tree mortality on large-scale color aerial photographs. Intermountain Forest and Range Experiment Station, Ogden, UT: US. USDA Forest Service General Technical Report INT-GTR-124.

Crotteau, J.S. (2011). Natural Tree Regeneration dynamics a decade after the Storrie Fire in the Lassen National Forest. Arcata, CA: Humboldt State University. M.S. thesis (pp. 108).

Damgaard, C. (2009). On the distribution of plant abundance data. Ecological Informatics, 4, 76-82.

Donoghue, D.N.M., Watt, P.J., Cox, N.J., & Wilson, J. (2007). Remote sensing of species mixtures in conifer plantations using Lidar height and intensity data. Remote Sensing of Environment, 110(4), 509-522.

Ducey, M.J., Jordan, G.J., Gove, J.H., & Valentine, H.T. (2002). A practical modification of horizontal line sampling for snag and cavity tree inventory. Canadian Journal of Forest Research, 32, 1217-1224.

Ducic, V., Hollaus, M., Ullrich, A., Wagner, W., & Melze, T. (2006). 3D vegetation mapping and classification using full-waveform laser scanning. International workshop 3D remote sensing in forestry, Vienna, Feb. 14-15, 2006, 211-217.

Dunning, D. (1928). A tree classification for the selection forests of the Sierra Nevada. Journal of Agricultural Research. 36(9), 755-771.

Eskelson, B.N.I., Madsen, L., Hagar, J.C., & Temesgen, H. (2011). Estimating riparian understory vegetation cover with beta regression and copula models. Forest Science, 57(3), 212-221.

Espinheira, P.L., Ferrari, S.L., & Cribari-Neto, F. (2008). On beta regression residuals. Journal of Applied Statistics, 35(4), 407-419.

Eyre, F.H. (1980). Forest cover types of the United States and Canada. Washington, DC: Society of American Foresters (pp. 148).

Falkowski, M. J., Evans, J. S., Martinuzzi, S., Gessler, P. E., & Hudak, A. T. (2009). Characterizing forest succession with Lidar data: An evaluation for the inland Northwest USA. Remote Sensing of Environment, 113, 946-956.

Fan, Z., Shifley, S.R., Thompson, F.R., & Larsen, D.R. (2004). Simulated cavity tree dynamics under alternative timber harvest regimes. Forest Ecology and Management, 193, 399-412.

Ferrari, S.L., & Cribari-Neto, F. (2004). Beta regression modeling rates and proportions. Journal of Applied Statistics, 31(7), 799-815.

Ferrell, G.T. (1989). Ten-Year Risk-Rating Systems for California Red Fir and White Fir: Development and Use. Pacific Southwest Research Station, Berkeley, CA: US. USDA Forest Service General Technical Report PSW-GTR-115.

Flewelling, J.W., & Pienaar, L.V. (1981). Multiplicative regressions with lognormal errors. Forest Science, 27, 281-289.

Franklin, J.F., Berg, D.R., Thornburgh, D.A., & Tappeiner, J.C. (1997). Alternative silvicultural approaches to timber harvesting: variable retention harvest systems. In: Kohm, K.A., Franklin, J.F. (Eds.), Creating a Forestry for the 21st Century: The Science of Ecosystem Management. Washington, D.C.: Island Press (pp. 67-98).

Frescino, T.S., Edwards, & Moisen, G.G. (2001). Spatially explicit forest structural attributes using generalized additive models. Journal of Vegetation Science, 12, 15-26.

Goetz, S., Steinberg, D., Dubayah, R., & Blair, B. (2007). Laser remote sensing of canopy habitat heterogeneity as a predictor of bird species richness in an eastern temperate forest, USA. Remote Sensing of Environment, 108, 254-263.

Goldberger, A.S. (1968). The interpretation and estimation of Cobb-Douglas functions. Econometrica, 35, 464-472.

Goodwin, N. R., Coops, N. C., Bater, C., & Gergel, S. E. (2007). Assessment of sub-canopy structure in a complex coniferous forest. Proceedings of the ISPR Workshop "Laser Scanning 2007 and SilviLaser 2007", Espoo, September 12-14, 2007, Finland, Vol. XXXVI. (pp. 169−172) ISSN:1682-1777, P3/W52.

Gray, A. (2003). Monitoring stand structure in mature coastal Douglas-fir forests: effect of plot size. Forest Ecology and Management, 175, 1-16.

Guo, Q., Kelly, M., Gong, P., & Liu, D. (2007). An object-based classification approach in mapping tree mortality using high spatial resolution imagery. GIScience and Remote Sensing, 44 (1), 24-47.

Haara, A., & Nevalainen, S. (2002). Detection of dead or defoliated spruces using digital aerial data. Forest Ecology and Management, 160, 97-107.

Hamilton, R., Megown, K., Ellenwood, J. Lachowski, H., & Maus, P. (2010). Advances in threat assessment and their application to forest and rangeland management. Pacific Northwest Research Station, Portland, OR: US. USDA Forest Service General Technical Report PNW-GTR-802.

Harmon, M.E., & Sexton, J. (1996). Guidelines for measurements of woody detritus in forest ecosystems. Seattle, WA: U.S. Long-Term Ecological Research (LTER) Network Office, University of Washington. Publication No. 20 (pp. 73).

Harmon, M.E. (2002). Moving towards a new paradigm for woody detritus management. Pacific Northwest Research Station, Portland, OR: US. USDA Forest Service General Technical Report PNW-GTR-181.

Heurich, M., Persson, Å ., Holmgren, J., & Kennel, E. (2004). Detecting and measuring individual trees with laser scanning in mixed mountain forest of central Europe using an algorithm developed for Swedish boreal forest conditions. International Archives of Photogrammetry. Remote Sensing Spat. Inf. Sci. 36, 307-312.

Hill, R. A., & Broughton, R. K. (2009). Mapping the understorey of deciduous woodland from leaf-on and leaf-off airborne Lidar data: A case study in lowland Britain. ISPRS Journal of Photogrammetry and Remote Sensing, 64, 223-233.

Holloway, G.L., Caspersen, J.P., & Vanderwel, M.C., Naylor, B.J. (2007). Cavity tree occurrence in hardwood forests of central Ontario. Forest Ecology and Management, 239 (1-3), 191-199.

Holmgren, J., & Persson, Å. (2004). Identifying species of individual trees using airborne laser scanning. Remote Sensing of Environment, 90, 415-423.

Hopkinson, C., Chasmer, L., Lim, K., Treitz, P., & Creed, I. (2006). Towards a universal lidar canopy height indicator. Canadian Journal of Remote Sensing, 32, 139-152.

Hudak, A.T., Crookston, N.L., Evans, J.S., Falkowski, M.J., Smith, A.M.S, Gessler, P.E., & Morgan, P. (2006). Regression modeling and mapping of coniferous forest basal area and tree density from discrete-return lidar and multispectral satellite data. Canadian Journal of Remote Sensing, 32, 126-138.

Hudak, A. T., Crookston, N. L., Evans, J. S., Hall, D. E., & Falkowski, M. J. (2008). Nearest neighbor imputation modeling of species-level, plot-scale structural attributes from Lidar data. Remote Sensing of Environment, 112, 2232-2245.

Hyyppä, J., Kelle, O., Lehikoinen, M., & Inkinen, M., (2001). A segmentation based method to retrieve stem volume estimates from 3-dimensional tree height models produced by laser scanner. IEEE Trans. Geosci. Remote Sensing, 39, 969-975.

Jenkins, J. C., Chojnacky, D.C., Heath, L.S., & Birdsey, R.A. (2003). National-Scale Biomass Estimators for United States Tree Species. Forest Science, 49(1), 12-35.

Jonsson, B.G., Kruys, N., & Ranius, T. (2005). Ecology of species living on dead wood – lessons for dead wood management. Silva Fennica, 39, 289-309.

Kaartinen, H., & Hyyppä, J. (2008). EuroSDR / ISPRS Commission II project: "Tree Extraction" – final report. Frankfurt am Main: Germany. Official publication no. 53. EuroSDR (pp. 60).

Kaasalainen, S., Hyyppä, H., Kukko, A., Litkey, P., Ahokas, E., Hyyppä, J., Lehner, H., Jaakkola, A., Suomalainen, J., Akujärvi, A., Kaasalainen, M., & Pyysalo, U. (2009). Radiometric calibration of LiDAR intensity with commercially available reference targets. IEEE Transactions on Geoscience and Remote Sensing, 47(2), 588-598.

Kass, R.E., & Raferty, R.E. (1995). Bayes factors. Journal of American Statistical Association, 90(430), 773-795.

Kelly, M., Shaari, D., Guo, Q., & Liu, D. (2004). A comparison of standard and hybrid classifier methods for mapping hardwood mortality in areas affected by "sudden oak death". Photogrammetric Engineering and Remote Sensing, 70 (11), 1229-1239.

Kenning, R., Ducey, M., Brisette, J., & Gove, J. (2005). Field efficiency and bias of snag inventory methods. Canadian Journal of Forest Research, 35(12), 2900-2910.

Kerns, B.K., & Ohmann, J.L., (2004). Evaluation and prediction of shrub cover in coastal Oregon forests (USA). Ecological Indicators, 4, 83-98.

Kerr, J. T., & Ostrovsky, M. (2003). From space to species: Ecological applications for remote sensing. Trends in Ecology and Evolution, 18, 299-305.

Kieschnick, R., & McCullough, B.D. (2003). Regression analysis of variates observed on (0, 1): Percentages, proportions and fractions. Statistical Modelling, 3, 193-213.

Kim, Y., Yang, Z., Cohen, W.B., Pflugmacher, D., Lauver, C. L., & Vankat, J.L. (2009). Distinguishing between live and dead standing tree biomass on the North Rim of Grand Canyon National Park, USA using small-footprint lidar data. Remote Sensing of Environment, 113, 2499-2510.

Kimes, D.S., Ranson, K.J., Sun, G., & Blair, J.B. (2006). Predicting lidar measured forest vertical structure from multi-angle spectral data. Remote Sensing of Environment, 100(4), 503-511.

Kmenta, J. (1986). Elements of econometrics (2nd ed.). New York : Macmillan (pp.733).

Korhonen, L., Korhonen, K.T., Stenberg, P., Matlamo, M., & Rautianen, M. (2007). Local models for forest canopy cover with beta regression. Silva Fennica, 41(4), 671-685.

Krebs, C.J. (1989). Ecological methodology. New York: Harper Collins Publishers, Inc. (pp. 654).

Lämas, T., & Stahl, G. (1998). On the accuracy of line transect sampling of rare forest objects. In: Bachmann, P., Ko¨hl, M., Pa¨ivinen, R. (Eds.), Assessment of Biodiversity for Improved Forest Planning. Dordrecht: Kluwer Academic Publishers (pp. 273-281).

Laudenslayer, W.F., Jr. (2002). Cavity-nesting bird use of snags in eastside pine forests of northeastern California. Pacific Southwest Research Station, Fresno, CA: U.S. USDA Forest Service General Technical Report PSW-GTR-181.

Leckie, D.G., Jays, C., Gougeon, F.A., Sturrock, R.N., & Paradine, D. (2004). Detection and assessment of trees with Phellinus weirii (laminated root rot) using high resolution multi-spectral imagery. International Journal of Remote Sensing, 25 (4), 793-818.

Lefsky, M.A., Cohen, W.B., Acker, S.A., Parker, G.G., Spies, T.A., & Harding, D. (1999). Lidar Remote Sensing of the Canopy Structure and Biophysical Properties of Douglas-Fir Western Hemlock Forests. Remote Sensing of Environment, 70(3), 339-361.

Lefsky, M. A., Cohen, W. B., Harding, D. J., & Parker, G. G. (2002a). Lidar remote sensing for forest ecosystem studies. BioScience, 52, 19-30.

Lefsky, M. A., Cohen, W. B., Harding, D. J., & Parker, G. G., Acker, S.A., & Gower, S.T. (2002b). Lidar Remote Sensing of Above-Ground Biomass in Three Biomes. Global Ecology and Biogeography, 11(5), 393-399.

Legare, S., Bergeron, Y., & Pare, D. (2002). Influence of forest composition on understory cover in boreal mixed-wood forests of Western Quebec. Silva Fennica, 36, 353-365.

Lim, K., Treitz, P., Baldwin, K., Morrison, I., & Green, J. (2003). Lidar remote sensing of biophysical properties of tolerant northern hardwood forests. Canadian Journal of Remote Sensing, 29, 648-678.

Lim, K. S. & Trietz, P.M. (2004). Estimation of above ground forest biomass from airborne discrete return laser scanner data using canopy-based quantile estimators. Scandinavian Journal of Forest Research, 19(6), 558-570.

Maltamo, M., Kangas, A., Uuttera, J., Torniainen, T., & Saramäki, J. (2000). Comparison of percentile based prediction methods and Weibull distribution in describing diameter distribution of heterogenous Scots Pine stands. Forest Ecology and Management, 133, 263-274.

Maltamo, M., Eerikäinen, K., Pitkänen, J., Hyyppä, J., & Vehmas, M. (2004). Estimation of timber volume and stem density based on scanning laser altimetry and expected tree size distribution functions. Remote Sensing of Environment, 90 (3), 319-330.

Maltamo, M., Packalén, P., Yu, X., Eerikäinen, K., Hyyppä, J., & Pitkänen, J. (2005). Identifying and quantifying structural characteristics of heterogeneous boreal forests using laser scanner data. Forest Ecology and Management, 216, 41-50.

Maltamo, M., Malinen, J., Packalén, P., Suvanto, A., & Kangas, J. (2006). Nonparametric estimation of stem volume using airborne laser scanning, airborne photography, and stand-register data. Canadian Journal of Forest Research, 36(2), 426-436.

Marquardt, J. (1970). Generalized inverses, ridge regression and biased linear estimation. Technometrics, 12, 591-612.

Martinuzzi, S., Vierling, L.A., Gould, W.A., Falkowski, M.J., Evans, J.S., Hudak, A.T., & Veirling, K.T. (2009). Mapping snags and understory shrubs for a Lidar-based assessment of wildlife habitat suitability. Remote Sensing of Environment, 113, 2522-2546.

McCullagh, P., & Nelder, J.A. (1989). Generalized linear models. 2nd ed. Monographs on statistics and probability 37. London: Chapman & Hall (pp. 511).

McDermid, G. J., Franklin, S. E., & LeDrew, E. F. (2005). Remote sensing for large-area habitat mapping. Progress in Physical Geography, 29, 449-474.

McGaughey, R. J (2012). FUSION/LDV: Software for LiDAR Data Analysis and Visualization – V3.10. Pacific Northwest Research Station, Portland, OR: US. USDA Forest Service (pp. 168).

Means, J.E., Acker, S.A., Fitt, B.J., Renslow, M, Emerson, L., & Hendrix, C.J. (2000). Predicting Foreset Stand Characteristics with Airborne Scanning Lidar. Photogrammetric Engineering and Remote Sensing, 66(11), 1367-1371.

Mehtätalo, L. (2006). Eliminating the effect of overlapping crowns from aerial inventory estimates. Canadian Journal of Forest Research, 36 (7), 1649-1660.

Mellen, K., Marcot, B.G., Ohmann, J.L., Waddell, K., Livingston, S.A., Willhite, E.A., Hostetler, B.B., Ogden, C., & Dreisbach, T. (2006). DecAID, the decayed wood advisor for managing snags, partially dead trees, and down wood for biodiversity in forests of Washington and Oregon. Version 2.0. Portland, OR: USDA Forest Service, Pacific Northwest Region and Pacific Northwest Research Station; USDI Fish and Wildlife Service, Oregon State Office.

Miller, J. D., Knapp, E.E., Key, C.H., Skinner, C.N., Isbell, C.J., Creasy, R.M., & Sherlock, J.W. (2008). Calibration and validation of the relative differenced Normalized Burn Ratio (RdNBR) to three measures of fire severity in the Sierra Nevada and Klamath Mountains, California, USA. Remote Sensing of Environment, 113, 645-656.

Morsdorf, F., Mårell, A., Koetz, B., Cassagne, N., Pimont, F., Rigolot, E., & Allgöwer, B. (2010). Discrimination of vegetation strata in a multi-layered Mediterranean forest

ecosystem using height and intensity information derived from airborne laser scanning. Remote Sensing of Environment 114, 1404-1415.

Mutlu, M., Popescu, S., Stripling, C., & Spencer, T. (2008). Mapping surface fuel models using lidar and multispectral data fusion for fire behavior. Remote Sensing of Environment 112, 274-285.

Næsset, E. (1997). Estimating timber volume of forest stands using airborne laser scanner data. Remote Sensing of Environment, 61, 246-253.

Næsset, E., (2002). Predicting forest stand characteristics with airborne scanning laser using a practical two-stage procedure and field data. Remote Sensing of Environment, 80, 88-99.

Nelsen, R.B., (2006). An introduction to copulas. New York: Springer (pp. 239).

Nelson, R., Short, A. & Valenti, M. (2004). Measuring biomass and carbon in Delaware using airborne profiling Lidar. Scandinavian Journal of Forest Research, 19, 500-511.

Oliver, W.W. (2000). Ecological research at Blacks Mountain Experimental Forest in northeastern California. Pacific Southwest Research Station, Albany, Calif. USDA Forest Service General Technical Report. PSW-GTR-179.

Ospina, R., & Ferrari, S. (2012). A general class of zero-or-one inflated beta regression models. Computational Statistics and Data Analysis. Computational Statistics and Data Analysis,56(6),1609-1623.

Packalén, P., & Maltamo, M. (2006). Predicting the plot volume by tree species using airborne laser scanning and airborne photographs. Forest Science, 52(6), 611-622.

Pasher, J., & King, D.J. (2009). Mapping dead wood distribution in a temperate hardwood forest using high resolution airborne imagery. Forest Ecology and Management, 258, 1536-1548.

Pesonen, A., Maltamo, M., Eerikäinen, & Packalén, P. (2008). Airborne laser scanning based prediction of coarse woody debris volumes in a conservation area. Forest Ecology and Management, 255, 3288-3296.

Pielou, E.C. (1977). Mathematical ecology. New York: John Wiley & Sons (pp. 384).

Popescu, S.C., & Wynne R.H. (2004). Seeing the trees in the Forest: Using Lidar and Multispectral Data Fusion with Local Filtering and Variable Window Size for Estimating Tree Height, Photogrammteric Engineering & Remote Sensing, 70(5), 589-604.

Popescu, S. (2007). Estimating biomass of individual pine trees using airborne lidar. Biomass and Energy, 31(9), 646-655.

Raferty, A.E. (1995). Bayesian model selection in social research. Sociological Methodology, 25, 111-163.

Reitberger, J., Schörr, C.L., Krzystek, P., & Stilla, U. (2009). 3D segmentation of single trees exploiting full waveform LIDAR data. Journal of Photogrammetry and Remote Sensing, 64, 561-574.

Reschenhofer, E. (1996). Prediction with vague prior knowledge. Communications in Statistics - Theory and Methods, 25, 601-608.

Reutebuch, S.E., Andersen, H.-E., & McGaughey, R.J. (2005). Light detection and ranging (LIDAR): An emerging tool for multiple resource inventory. Journal of Forestry, 103(6), 286-292.

Riaňo, D., Meier, E., Allgöwer, B., Chuieco, E., & Ustin, S.L. (2003). Modeling airborne laser scanning data for the spatial generation of critical forest parameters in fire behavior modeling. Remote Sensing of Environment, 86, 177-186.

Riaño, D., Chuvieco, E., Condés, S., Gonzáles-Matesanz, J., & Ustin, S. (2004). Generation of crown bulk density for *Pinus sylvestris* L. from lidar. Remote Sensing of Environment, 92(3), 345-352.

Ritchie, M.W., Skinner, C.N., & Hamilton, T.A. (2007). Probability of wildfire-induced tree mortality in an interior pine forest: effects of thinning and prescribed fire. Forest Ecology &. Management, 247, 200-208.

Rose, C.L., Marcot, B.G., Mellen, T.K., Ohmann, J.L, Waddell, K.L., Lindley, D.L., & Schreiber, B. (2001). Decaying wood in Pacific Northwest forests: concepts and tools for habitat management. In: Johnson, D.H.; O'Neil, T.A., eds. Wildlife-habitat

relationships in Oregon and Washington. Corvallis, OR: Oregon State University Press (pp 580-623).

Rothermel, R.C. (1983). How to predict the spread and intensity of forest and range fires. Intermountain Experimental Station, Ogden, UT: US. USDA Forest Service General Technical Report INT-GTR-143.

Russell, R. E., Saab, V. A., & Dudley, J. (2007). Habitat suitability models for cavity-nesting birds in a postfire landscape. The Journal of Wildlife Management, 71, 2600-2611.

Salman, K.A., & Bongberg, J.W. (1942). Logging high risk trees to control insects in the pine stands of northeastern California. Journal of Forestry, 40(7), 533-539.

Schroeder, T.A., Cohen, W.B., & Yang, Z. (2007). Patterns of forest regrowth following clearcutting in western Oregon as determined from a Landsat time-series. Forest Ecology and Management, 243, 259-273.

Scott, J. H., & Reinhardt, E. D. (2001). Assessing crown fire potential by linking models of surface and crown fire behavior. Res. Pap. RMRS-RP-29. Fort Collins, CO: U. S. Department of Agriculture, Forest Service, Rocky Mountain Research Station. 59 p.

Seielstad, C.A., & Queen, L.P. (2003). Using airborne laser altimetry to determine fuel models for estimating fire behavior. Journal of Forestry, 101(4), 10-15.

Siccama, T.G., Fahey, T.J., Johnson, C.E., Sherry, T.W., Denny, E.G., Girdler, E.B., Likens, G.E., & Schwarz, P.A. (2007). Population and biomass dynamics of trees in a northern hardwood forest at Hubbard Brook. Canadian Journal of Forest Research, 37(4), 737-749.

Smithson, M., & Verkuilen, J. (2006). A better lemon squeezer? Maximum-likelihood regression with beta-distributed dependent variables. Psychological Methods, 11(1), 54 -71.

Stage, A.R., & Salas, C. (2007). Interactions of elevation, aspect, and slope in models of forest species composition and productivity. Forest Science, 53(4), 486-492.

Stereńczak, K., & Zasada, M. (2011). Accuracy of tree height estimation based on LIDAR data analysis. Folia Forestalia Polonica, Series A, 53(2), 123-129.

Suchar, V.A., & Crookston, N.L. (2010). Understory cover and biomass indices predictions for forest ecosystems of the Northwestern United States. Ecological Indicators, 10, 602-609.

Thomas, J.W., Anderson, R.G., Maser, C., & Bull, E.L. (1979). Wildlife habitats in managed forests; the Blue Mountains of Oregon and Washington. USDA Forest Service Ag. Handbook No. 553 (pp. 512).

Tremblay, N.O., & Larocque, G.R., (2001). Seasonal dynamics of understory vegetation in four eastern Canadian forest types. International Journal of Plant Sciences, 162, 271-286.

Turner, D.P., Koerper, G.J., Harmon, M.E., & Lee, J.J. (1995). A Carbon Budget for Forests of the Conterminous United States. Ecological Applications, 5(2), 421-436.

Vauhkonen, J., Ene, L., Gupta, S., Heinzel, J., Holmgren, J., Pitkänen, J., Solberg, S., Wang, Y., Weinacker, H., Hauglin, K.M., Lien, V., Packalén, P., Gobakken, T., Koch, B., Næsset, E., Tokola, T., & Maltamo, M. (2011). Comparative testing of single-tree detection algorithms under different types of forest. Forestry, International Journal of Forest Research, doi:10.1093/forestry/cpr051.

Venier, L. A., & Pearce, J. L. (2007). Boreal forest land birds in relation to forest composition, structure, and landscape: Implications for forest management. Canadian Journal of Forest Research, 37, 1214-1226.

Vierling, K. T., Vierling, L. A., Martinuzzi, S., Gould, W., & Clawges, R. (2008). Lidar: Shedding new light on habitat modeling. Frontiers in Ecology and the Environment, 6, 90-98.

Vosselman, G., Gorte, B.G.H., Sithole, G., & Rabbani, T. (2004). Recognizing structure in laser scanning point clouds. Information Science, 46(8), 1-6.

Wagner, W., Hollaus, M., Briese, C., & Ducic, V. (2008). 3d vegetation mapping using small-footprint full-waveform airborne laser scanners. International Journal of Remote Sensing, 29(5), 1433-1452.

Wang, Y., Weinacker, H., Koch, B., & Sterenczak, K. (2008). LIDAR point cloud based fully automatic 3D single tree modelling in forest and evaluations of the procedure.

International Archives of Photogrammetry, Remote Sensing and Spatial Information Sciences, 37 (Part B6b), 45-51.

Weisberg, S. (1985). Applied linear regression (2nd ed.). New York: Wiley (324 pp.).

Wing, B.M., Ritchie, M.W., Boston, K., Cohen, W.B., Gitelman, A., & Olsen, M.J. (in review (a)). Prediction of understory vegetation cover with airborne lidar in an interior ponderosa pine forest. Remote Sensing of Environment.

Wing, B.M., Ritchie, M.W., Boston, K., Cohen, W.B., & Olsen, M. (in review (b)). Individual snag detection using airborne lidar data and 3D local-area point-based intensity filtration. Forest Science.

Wulder, M., & Franklin, S. (2003). Remote sensing of forest environments: Concepts and case studies. Dordrecht / Boston / London: Kluwer Academic Publishers (pp. 519).

Yoccoz, N.G., Nichols, J.D., & Boulinier, T. (2001). Monitoring of biological diversity in space and time. Trends in Ecology and Evolution, 16(8), 446-453.

Zimble, D.A., Evans, D.L., Carlson, G.C., Parker, R.C., Grado, S.C., & Gerard, P.D. (2003). Characterizing vertical forest structure using small-footprint airborne LIDAR. Remote Sensing of Environment, 87, 171-182.

Zhao, K, Popescu, S., & Nelson, R. (2009). Lidar remote sensing of forest biomass: A scale-invariant estimation approach using airborne lasers. Remote Sensing of Environment, 113(1), 182-196.

APPENDIX A

LIST OF SYMBOLS USED IN TEXT

Symbol	Definition
3D	Three-dimensions
AB	Absolute bias
ABCO	White fir
ABMA	Red fir
AGB	Above ground biomass
AIC	Akaike's information criterion
BA	Basal area
BIC	Bayesian information criterion
ΔBIC	Change in Bayesian information criterion
BMEF	Blacks Mountain Experimental Forest
BR	Beta regression
CADE	Incense-cedar
CBI	Composite burn index
CC_h	Proportion of points above 2 m lidar metric
	Commission error rate correction factor
CHM	Canopy height model
CIR	Color-infrared
Cm	Centimeters
CV_h	Coefficient of variation height lidar metric
CWD	Coarse woody debris
	Snag density
$D5_h$ …$D20_h$	Proportion of points above height thresholds lidar metrics
DBH	Diameter at breast height (cm)
DM_h	Proportion of points above mean height lidar metric
DMd_h	Proportion of points above mode height lidar metric
	Lidar snag detection rate
DTM	Digital terrain model
DTS	Digital terrain synthesis
EPC	Effective plot coverage
EXP	Exponential function
GIS	Geographic information system
H	Height (m)
Ha	Hectare
HiD	High diversity treatment

HMS	High and medium fire severity strata
HS	High fire severity strata
I	Lidar intensity value
LAI	Leaf-area index
Lidar	Light Detection And Ranging
	Lower lidar intensity value threshold
Ln	Natural logarithm
LoD	Low diversity treatment
LS	Low fire severity strata
LT1, 2, 3, 4	Live-tree lidar metric models
	Local-area lidar points meeting live vegetation intensity criteria
LUS	Low and unchanged fire severity strata
M	Meters
Max_h	Maximum height lidar metric
	Maximum intensity value
Mg	Megagram
Min_h	Minimum height lidar metric
$Mode_h$	Mode height lidar metric
MS	Medium fire severity strata
N	Sample size
NF	National Forests
NIR	Near-infrared
	Density of overstory first return lidar points in the fifth strata
	Standard deviation of overstory lidar first return point heights
OLS	Ordinary least squares
$P01_h$...$P99_h$	Percentile height lidar metrics
PICO	Lodgepole pine
PIJE	Jeffrey pine
PILA	Sugar pine
PIMO	Western white pine
PIPO	Ponderosa pine
PSME	Douglas-fir
QUKE	California black oak
R	Pearson's correlation coefficient
R^2	Coefficient of determination
RA	Research Natural Area A

RB	Research Natural Area B
RC	Research Natural Area C
RD	Research Natural Area D
RdNBR	Relative differenced Normalized Burn Ratio
RGP	Relative ground points
RMSE	Root mean squared error
RMSPE	Root mean squared prediction error
RNA	Research Natural Area
RTK	Real-time kinetic
	Number of detected snags
	Local-area lidar points meeting snag intensity criteria
Sd	Standard deviation
SD_h	Standard deviation height lidar metric
SF	Storrie Fire
SPR	Snag point ratio
SFFW	Small-footprint full-waveform lidar
T1, 2, 3, 4	Traditional lidar metric models
U	Unchanged fire severity strata
	Upper lidar intensity value threshold
ULCD	Understory lidar cover density
UP_f	Filtered understory lidar points
UPD	Understory lidar point density
USDA	United States Department of Agriculture
V1, 2, 3, 4	Vegetation-intensity lidar metric models
	Variance
VolCov	Lidar canopy density lidar metric
WR	Weighted regression
X	Lidar point x coordinate
	Vector of explanatory variables
Y	Lidar point y coordinate
Z	Lidar point z coordinate
B	Vector of regression coefficients
	Residual model errors
	Link function
H	Vector of linear predictors
ω	Vector of weighted regression weights